Injury Mechanisms and Priorities for Cervical Spine Trauma Mitigation in Rollover Crashes: The development and analysis of *in vitro* testing of axial compressive cervical spine impacts

---

A Thesis Presented to the faculty of
The School of Engineering and Applied Science
University of Virginia

In Partial Fulfillment

of the Requirements for the Degree

Master of Science in Mechanical and Aerospace Engineering

by

Jonathan B. Foster

May 2013

APPROVAL SHEET

The thesis is submitted in partial fulfillment of the
requirements for the degree of
Master of Science (Mechanical and Aerospace Engineering)

_____
Jonathan B. Foster, Author

The thesis has been read and approved by the examining Committee:

_____
Jeff R. Crandall, Thesis Advisor

_____
Richard W. Kent, Committee Chair

_____
Mark R. Sochor, Committee Member

Accepted for the School of Engineering and Applied Science:

_____

Dean, School of Engineering and
Applied Science

May 2013

ACKNOWLEDGMENTS

There are several people who have supported me throughout my college career that I would like to thank. First I would like to thank my mentors and advisors at the Center for Applied Biomechanics for providing guidance and support during my undergraduate and graduate studies, namely, Jeff Crandall, Jason Kerrigan, and Rob Salzar. I would also like to thank the staff and students of the CAB who have helped me achieve my goals and kept me entertained along the way. Special thanks to Joe Ash, Jack Lockerby, Francisco J. Lopez-Valdez, Matt Panzer, Jason Forman, and Rich Kent. Additional thanks to Dennis Roethlisberger, Mark Sochor, Sara Heltzel, and Chris "The Intern" Sowers for their tireless work on the Drop Spine project.

I would also like to thank my parents, Rochelle and Steve, for their love and support. I would finally like to thank my friends who have made my time at the University of Virginia some of the best years of my life: Andrew, Andy, Brian, Chris, Macon, Russell, Sanders, and Zach. I look forward to enjoying their friendship for years to come.

ABSTRACT

Rollover crashes are a major public health concern, associated with over one-third of all passenger vehicle fatalities in the US. Of the injuries sustained by occupants in rollover crashes, cervical spine trauma is among the most frequent and life threatening. Occupant initial orientation and loading distribution has been shown to influence injury outcome in biomechanical testing with cadaveric subjects; however, these loading conditions have not been well characterized for rollover-involved occupants. Slight changes in boundary condition or eccentricity in axial compression (the loading mechanism most associated with cervical spine injury in this crash mode) have been shown to have enormous bearing on the injury tolerance and severity of injury. A thorough review of cadaveric injury mechanism literature and of clinically representative rollover cases (queried from a national trauma database) was conducted for the purpose of retrospectively linking injury with failure mechanism and reverse-engineering the loading environments experienced by rollover-involved occupants with cervical spine trauma. Data gathered from these analytical observations, such as the influence of laterally eccentric loading, passive musculature, and torso augmentation, help establish an *in vitro* test approach relevant to injurious rollover-type loading.

Cervical spine compression tests with full post-mortem human surrogates were performed at the Center for Applied Biomechanics with the goals of assessing 1) boundary condition influence on bony fracture in a full cadaver, 2) the effective mass of the human torso as it augments load to the base of the cervical column (the process believed by experts to be the greatest contributing factor to cervical spine injury in

rollovers), and 3) the subsequent buckling kinematics of the cervical spine during the initiation of an applied axial load. Dynamic high-speed x-ray was employed for this study, showing buckling of the spine within the first 12 milliseconds of axial loading, a phenomenon never before observed radiologically *in situ*. Bony fracture was produced in 3 of the 4 surrogates, all of which coincide with relevant rollover type fracture and compressive injury mechanism. Injury outcome differences, however, raise questions pertaining to the end conditions and effective torso mass employed by previous authors in simplified cervical spine studies, the same studies used for injury reference values in current neck injury criteria.

Kinematics data was ascertained to determine the amount of cephalocaudal translation that is required to initiate 2nd-order buckling of the neck, a value found to be lower than previously believed. Findings of this study can be used in the design of component level (head-neck complex) biomechanical tests of the human cervical spine, a significant experimentation cost reduction from full-scale cadaveric testing. This study illustrates the disparity between previous test approaches and this author's methodology which lays the groundwork for future studies in determining injury thresholds usable in a crash dummy or computational model to analyze injury risk.

TABLE OF CONTENTS

Chapter One

Cadaveric Experimentation Review and Analytical Observations of Cervical Spine Injury Mechanisms in Clinical Rollover Cases

INTRODUCTION

The Crash

Rollover crashes account for more than one-third of all passenger vehicle road traffic occupant fatalities in the United States. Using 2010 statistics, 27.5% of all traffic occupant fatalities, including those involving buses, motorcyclists, pedalcyclists, and pedestrians, involved the rollover of a vehicle (7,659 out of 27,805 fatalities). However, rollovers as a portion of motor vehicle crashes are far scarcer, accounting for only 3% of all crashes on roads in the US. Rollover fatalities are therefore grossly overrepresented on the national scale of roadway occupant fatality statistics.

National trauma databases are widely used by traffic engineers, biomechanists, crash reconstructionists, and emergency medicine physicians for ascertaining the injury mechanisms responsible in serious automotive crashes. Two such federally funded databases are the National Automotive Sampling System Crashworthiness Database System (NASS-CDS) and the Crash Investigation Research and Engineering Network (CIREN). Both are National Highway Traffic Safety Administration (NHTSA) resources sponsored by the US Department of Transportation and compile data from trauma centers throughout the US. Such databases have been extensively investigated for application in rollover crashes, which are not only rare and catastrophic when they occur, but have been growing with relevance in the past few decades with the popularity of SUVs and vehicles with higher centers of gravity (CG). Trauma databases show enormous potential for rollover crash injury mitigation by allowing researchers to evaluate vehicle countermeasure effectiveness and to evaluate occupant injury risk through *in vitro* and *in silico* reproduction of rollovers.

It has been shown that initial occupant positioning during roof-to-ground interaction can have a great bearing on the injury outcome sustained by an occupant. Small changes in a driver's posture during the initial phases of a rollover can greatly influence injury outcome. Nusholtz et al. (1983) reported that loading to heads with only slight lateral flexion compared to those oriented along the mid-sagittal plane result in vastly different injury outcomes to the cervical spine, the body region most severely affected in pure rollovers (Ridella et al., 2009).

Real-life case analysis also shows promise for improving standardized occupant conditions for full-scale rollover tests. For the purposes of positioning anthropomorphic test devices (ATD) or post-mortem human surrogates (PMHS) in realistic rollover testing environments, factors such as initial orientation or posture of the occupant are vital and can potentially be gleaned from the analysis of traffic trauma databases. Previous investigations into rollover injury and prevention have attempted to describe vehicle and occupant kinematics during the rollover's critical event (Bahling 1990, Raddin et al. 2009, Young et al. 2007, Moffatt and James 2005). Despite the importance of pre-crash occupant position and its effects on loading, current rollover testing methodologies, such as the controlled rollover impact system (CRIS) and the Jordan rollover system (JRS) have largely ignored the issue of occupant position (Cooper et al., 2001; Moffatt et al., 2003; Friedman et al., 2003). CRIS and JRS Tests have been previously performed in a nominal driving posture, which likely represents a very small minority of real rollover situations.

Justifications for ignoring occupant position changes due to the initiation of the rollover have included the desire for decreased test complexity, the use of standardized

conditions, improved repeatability, and lack of information on occupant conditions. Driving posture has been shown to change due to steering maneuvers, proposing a potential shortfall for testing in a nominal driving seating position. It is likely that corrective steering maneuvers are implemented by drivers anticipating an impending rollover crash, thus altering their seating posture. Adamec et al. (2005) showed that volunteers responded to 15-degree lateral rotations by activating abdominal, shoulder, and thigh muscles. The volunteers responded to the initial roll of their surface by changing their bodies' positions, done to maintain upright head and torso positions for visibility and protection.

Test Methods for Investigating Injuries and Injury Sources

The focus on body orientation becomes critical when considering existing cadaver literature for experimental comparison. Much literature exists over the past 40 years pertaining to the cervical spine's responses to compressive loading, the situation most closely associated with catastrophic injury in rollovers (Raddin et al., 2009). However, much of the existing biomechanical literature was intended for other uses, including diving injuries, injuries due to falls, sports, and other modes of automotive crashes (McElhaney et al., 1979; Bauze and Ardran, 1978; Hodgson and Thomas, 1980; Yoganandan et al., 1986; Pintar et al., 1989, 1990; Myers et al., 1991). Therefore, the experimental loading conditions of previous neck compression studies must be reviewed before such studies are used to assess dummy biofidelity or implemented in computer models of rollover-related events.

The current injury criteria used by NHTSA to evaluate restraint systems in automobiles was developed in the late 1990's and called Nij (Eppinger et al., 1999). The

biomechanical basis of Nij relies on the notion that cervical spine injuries are the result of an axial component (force) and a bending component (moment). Tolerance values for the human neck in flexion (forward neck rotation, the "yes" motion), extension (backward neck rotation), compression (cephalocaudal loading), and tension are based on experimental data.

$$N_{ij} = \frac{F_z}{F_{crit}} + \frac{M_y}{M_{crit}} \tag{1}$$

The Nij calculation (1) uses two of the four critical values depending on the type of loading incurred and designates injury if the intercept between the critical values in breached (Figure 1) (Kleinberger et al., 1998).

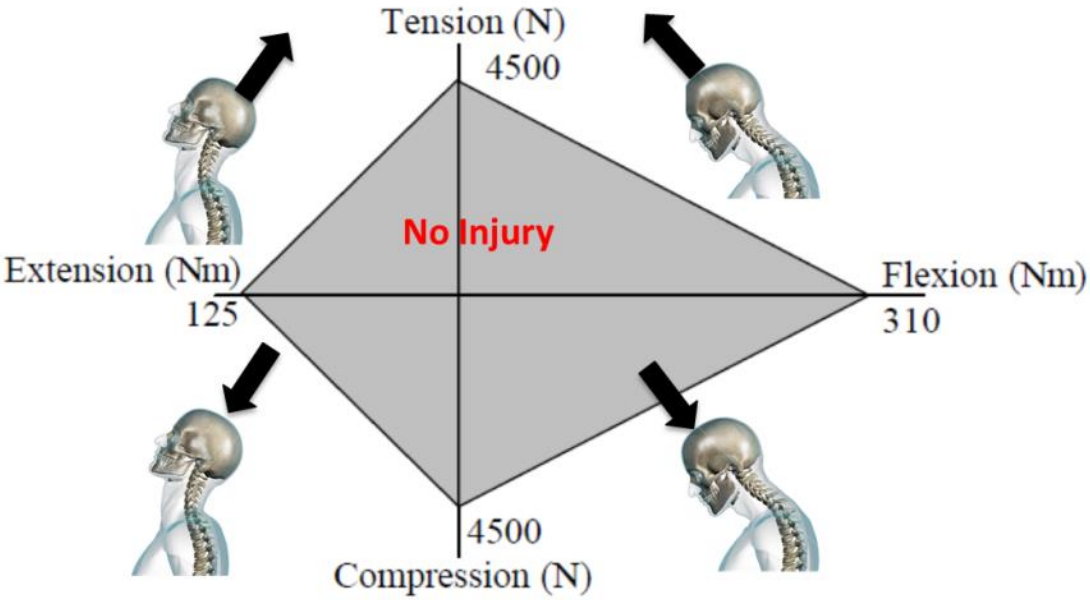

Figure 1: The criteria referred to as Nij, where "ij" represents indices for the mechanisms of compression or tension, and flexion or extension, respectively. N_{TE}, N_{TF}, N_{CF}, and N_{CE} are shown clockwise around the kite shape. The moment value is taken is the sagittal plane bending moment, M_y in Equation (1).

For compressive neck injury, which is most closely linked to rollover injury, the critical intercept value is taken from a pair of widely cited neck compression studies,

Pintar et al. (1995) and Nightingale et al. (1997). Both studies explore the effects of the head-neck complex subjected to head impact and subsequent compressive loading. Nightingale and other researchers at Duke University conducted testing of 22 head-neck complexes inverted and dropped onto an impact surface (Figure 2). They sought to address several questions in the growing cervical spine injury field, such as the effects of end conditions (padding, impact angle) and the relationship of head motion and neck injury.

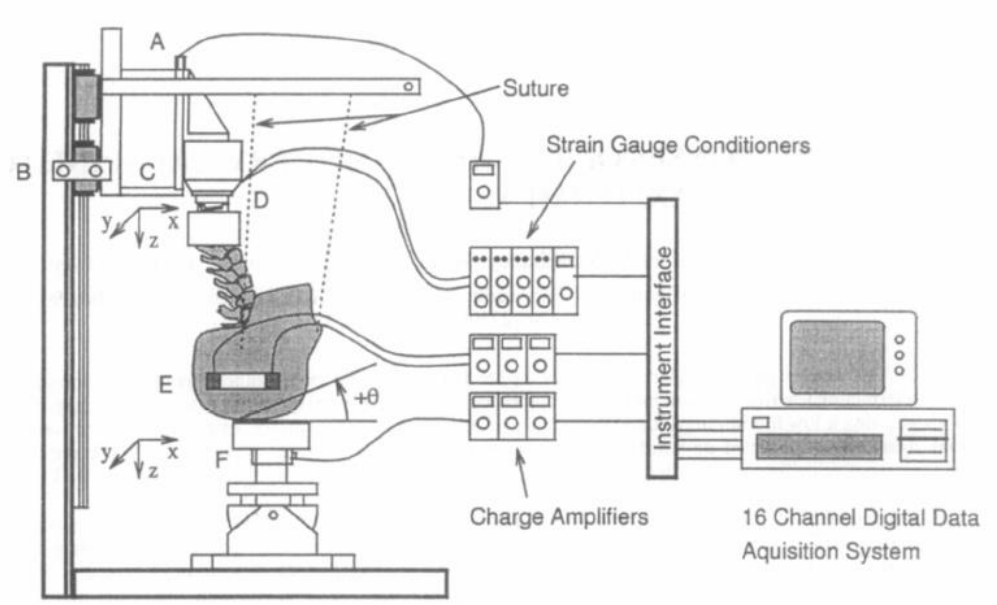

Figure 2: A diagram of the Duke test apparatus showing the accelerometer on the torso mass(A), the optical velocity sensor(B), the carriage and the torso mass(C), the six-axis load cell at T1(D), the head accelerometers(E), and the anvil and three-axis load cell(F).

The neck compression experiments by Nightingale et al. (1996, 1997) were performed using unembalmed cadaveric head and neck specimens transected at the top of the thoracic spine and rigidly potted at the base of the cervical spine. The potting fixture was mounted to a one degree-of-freedom track, allowing only vertical translation. The head hung below the potting fixture and was oriented with the Frankfurt Plane parallel to the ground, the anthropometric landmark measured at the auriculo-orbital plane

considered to be the position of the head when normally carried by a living person. The C7-T1 interface was potted into the fixed mount at a 25-degree angle to preserve the resting, nominal lordosis of the neck, a value measured by Matsushita et al. (1994) in living, volunteer drivers. The heads were dropped from heights of 52 cm to produce impact velocities of around 3.2 m/s. The orientations of the impact plate, as well as the compliance of the surface, were modified using foam and Teflon. Changing the orientation of the impact surface induced both flexion and extension attitudes. In addition, a 16 kg steel carriage was mounted to the drop track to simulate the effective weight of the absent torso. Multiaxis transduction recorded the head impact forces, head accelerations, and the reaction forces at T1.

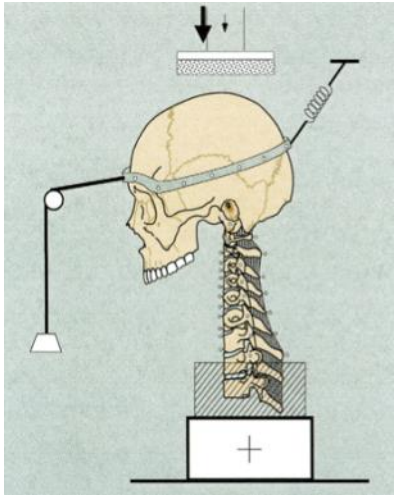

Figure 3: A diagram of the MCW test apparatus showing the cadaver ligamentous head-neck preparation and the cranial "halo". A pulley weight system that was implemented to simulate active anterior and posterior musculature and restrain some head motion. A six-axis load cell was mounted inferiorly.

Around the same time, a team of researchers at the Medical College of Wisconsin (MCW) performed component tests of 33 cadaveric head-cervical spine segments (Pintar et al., 1989, 1990, 1995). While Duke's tests incorporated the neutral curvature of the spine (slight lordosis), MCW researchers removed the natural resting lordosis of the cervical spine by preflexing the cervical column 15-degrees (Figure 3). This was done to

ensure compressive loading and induce spinal fracture by aligning the vertebral bodies of adjacent vertebrae into what they refer to as the "stiffest axis." The crowns of the cadaver heads were impacted in a superior-to-inferior direction with an electrohydraulic piston apparatus.

Loading rates were varied from 2.5 m/s to 8 m/s but the impact surface remained constant throughout the test series. MCW prepared specimens before impact with slight positive or negative eccentricities, or the sagittal distance between the occipital condyles and the T1 endplate (for the stiffest axis case, the eccentricity would equal zero). The injury mechanisms, such as flexion-compression, direct compression, and extension-compression, were therefore prescribed by the initial orientation of the head relative to the base of the cervical spine. A force-deformation tolerance curve was developed from 20 specimens (Figure 4).

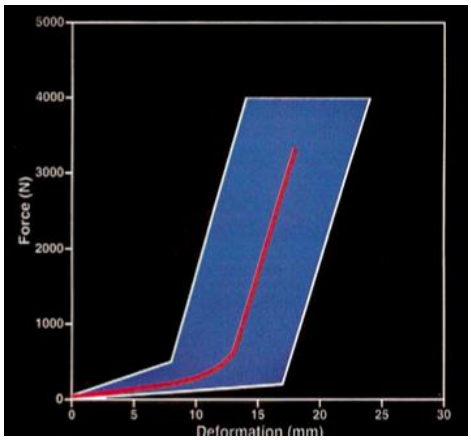

Figure 4: Plot from MCW's 1995 paper showing the derived dynamic force-deformation corridor, the mean force at failure (red) and the mean stiffness (slope of linear portion).

In both Pintar et al. and Nightingale et al., many assumptions are made to simplify testing procedures. Neither study used a full human body and each rigidly planted the base of the cervical spine into a potting fixture which restricts its horizontal motion. Pintar impacted the head with a piston which was terminated when the spine failed, thus

achieving injury in all 20 specimens. Nightingale tested at the same impact velocity allowing the torso-simulating mass to effectively load the spine, achieving neck injury in 16 of 22 cadaver spines.

The NHTSA-developed Nij proposes an axial limit of 4500N for the 50^{th} percentile male based on the experimental data from the Pintar force-deformation corridor (Eppinger et al., 1999). The authors claim that since Nightingale's study allows for a bending moment by preserving lordosis in the neck, the compressive force to failure were significantly lower and, thus, too low for the mid-sized male.

Aside from the force and moment-based injury criteria of Nij, velocity-based injury criteria have been colloquially used by cervical spine researchers and have become a matter of debate among experts in the field, particularly in the litigation arena (Friedman et al., 2007; Viano et al., 2008). A 3.2 m/s (7mph) injury assessment reference value is used by experts, claiming the head must reach this critical speed when interacting with the vehicle's roof to induce neck injury (Piziali, 2012, personal communication). Others believe head-to-roof impact speed can be far less to create neck fracture (Friedman et al., 2007), while others, still, believe a velocity-based approach is far too simplistic. The cadaver literature should be more extensively investigated by researchers developing neck injury criteria rather than choosing arbitrary values from cadaveric tests with experimental protocols that might not accurately apply to rollover-type loading. Until now, the lack of understanding of neck injury mechanism and tolerance levels during rollover crashes has hindered the design of vehicle countermeasures for this crash mode.

Perspective

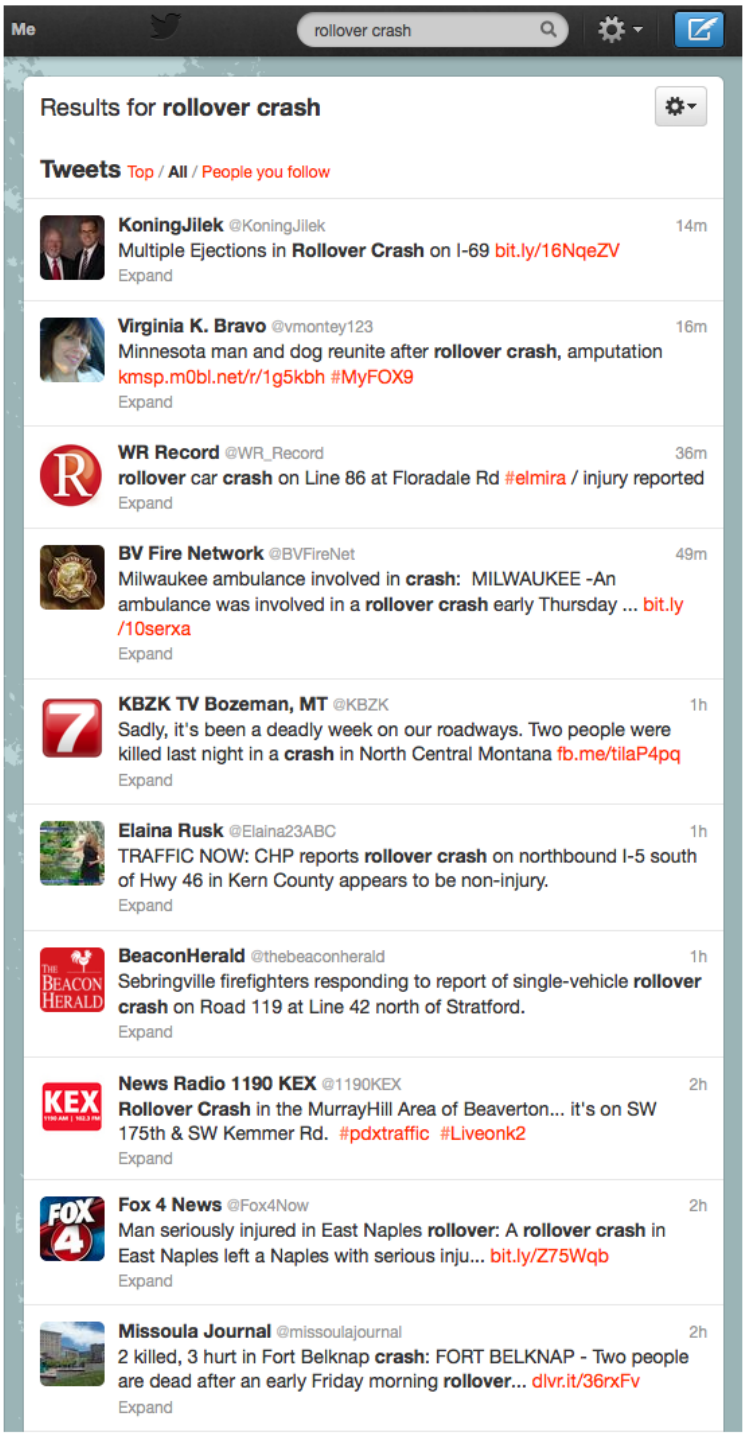

Twitter feed mentioning 'Rollover crash' over 2-hour segment between 10:00AM EST and noon on Friday, March 22, 2013 in the US.

SUMMARY OF PAPER

Materials and Methods

A literature review was performed of existing cadaver cervical spine compression studies. The injury outcomes were compared with the occupant injuries in a sample of real-life rollover victims queried from the CIREN database. The case occupants were involved in only pure rollovers and sustained cervical spine injuries. Injury outcomes between CIREN occupants and cadaver specimens were compared based on vertebral level of fracture (C1-C7), vertebral structure affected, and the symmetry of fractures.

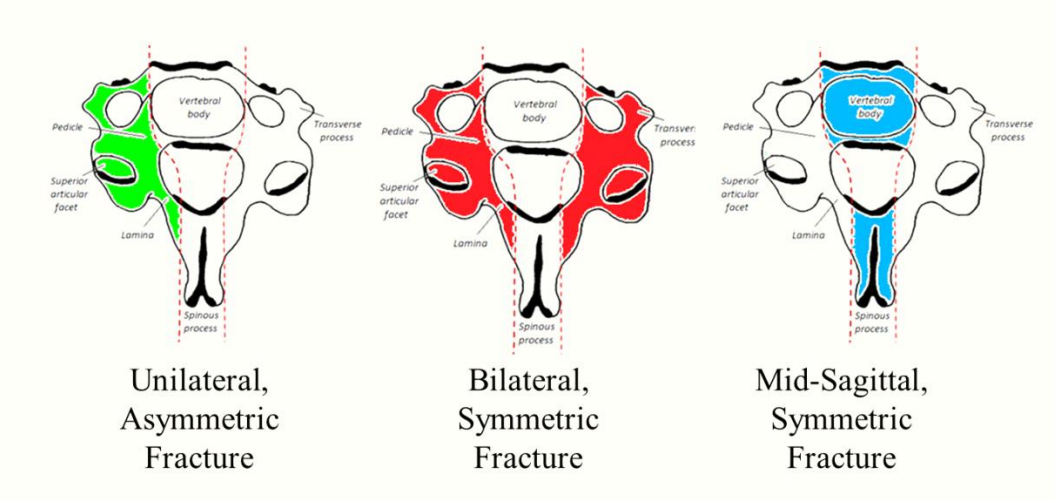

Unilateral fractures indicate a situation where compression or torsional force is greater on one side, while bilateral and mid-sagittal fractures indicate symmetrically dissipated loads (Maiman et al., 1983; Myers and Winkelstein, 1995).

Results

Twenty published studies containing 175 cadaver tests satisfied the inclusion criteria for the literature review. Cadaver specimens were divided into two subsets: cadavers loaded axially along the mid-sagittal or antero-posterior (AP) plane and cadavers loaded with laterally eccentric or non-sagittal out-of-plane loading. 205

fractures and 19 dislocations were tabulated from the cadaver specimens loaded mid-sagittally and 31 fractures and one dislocation were achieved in the cadaver spines loaded non-sagittally.

There were a substantially greater number of symmetric fractures than unilateral fractures produced in cadaver tests where mid-sagittal loading was employed. Cadaver tests employing laterally eccentric load vectors displayed greater incidence of unilateral fractures. This subset was more similar to the spectrum of injuries seen in the CIREN occupant group. Of the 23 case subjects reviewed from the CIREN database query, there were a total of 74 cervical spine fractures and 9 dislocations. Injury detail, head contact locations, and radiology are shown for each CIREN case occupant in Appendix A.

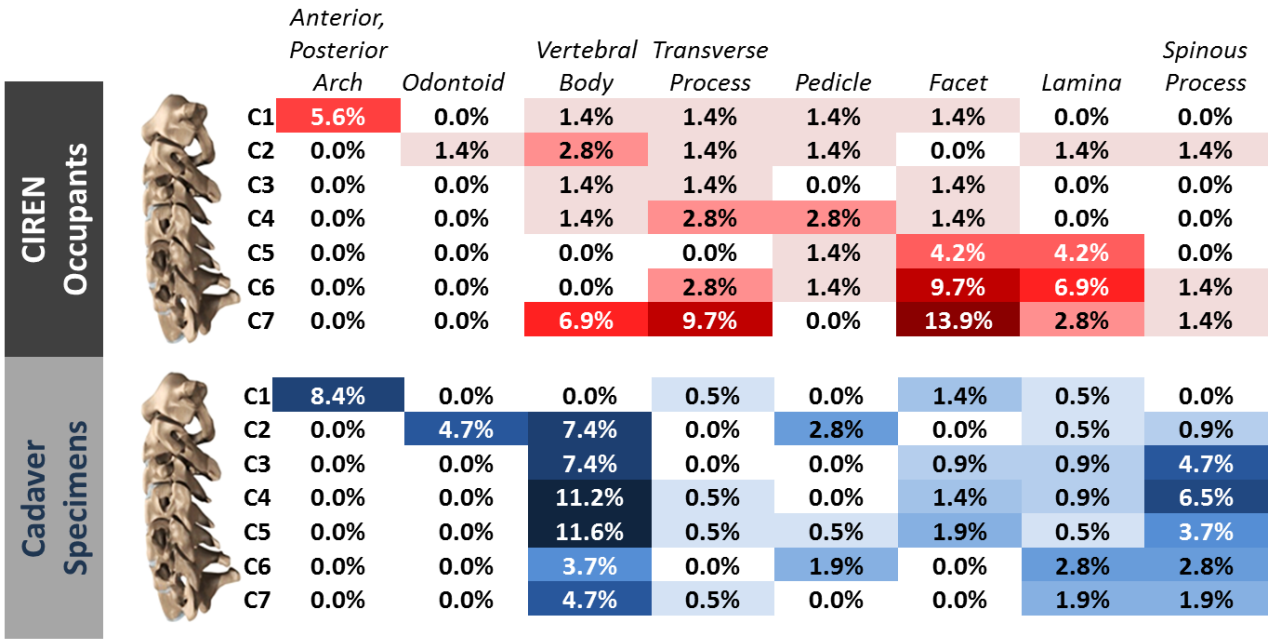

Figure 5: Color frequency plots for CIREN occupant fracture distribution and cadaver specimen fracture distribution, showing the anatomical features most affected with fracture by the darker shade of red or blue. The most common injury type seen clinically is fracture to the facet, transverse process and lamina. For *in vitro* subjects, the hotspots occur at the vertebral bodies and spinous processes especially of the mid and upper cervical spine.

CIREN occupants and cadaver specimens suffered fracture and dislocation patterns that were different based on symmetry of fracture, vertebral level affected, and vertebral structure affected. Overall, cadaver specimens sustained more vertebral body and spinous process fractures, especially to the upper and middle cervical spines, while CIREN occupants sustained lower cervical spine fractures to the transverse processes, facets, and laminae at higher rates of frequency (Figure 5). When the non-sagittally loaded specimen subset is isolated, however, better correlation with the CIREN occupant injuries occurs. Also, cadaver subjects loaded mid-sagittally show better association with AIS 3+ and AIS 4+ CIREN injuries, showing potentially greater efficacy for cadaver tests when used to assess severe and catastrophic injuries (Hangman's fractures, odontoid fractures, burst fractures, and unstable bilateral fractures).

Lastly, dislocation pathologies in the clinical CIREN cases contained impaction fractures, which are fractures to the adjoining lateral aspects of the vertebral level of interest. This is a phenomenon absent in the cadaveric dislocations produced *in vitro*. The findings from this study aid researchers in understanding the implications of test procedure parameters for occupant injury risk and provide rationale for expanding occupant parameters in current neck injury criteria to include lateral or coronal neck moment, M_x. Possible reasons for the injury outcome discrepancies between clinical cases and cadaver subjects are the absence of passive musculature and active muscle tensing, the ages of donated cadaver specimens, inherent deficiencies in post-mortem tissue, and unrealistic boundary conditions employed in many cadaveric compression studies.

PAPER MANUSCRIPT

Title

Cervical Spine Injury Patterns and Mechanisms for CIREN Rollover Crashes

Author Names and Affiliations

Corresponding Author: Jon B. Foster[a]
jbf3t@virginia.edu

Jason R. Kerrigan[a]
jrk3z@eservices.virginia.edu

Roger W. Nightingale[b]
rwn@duke.edu

James R. Funk[a]
jfunk@brconline.com

Joseph M. Cormier[a]
jcormier@brconline.com

Dipan Bose[a]
Dipan.bose@gmail.com

Mark R. Sochor[c]
msochor@virginia.edu

Stephen A. Ridella[d]
stephen.ridella@dot.gov

Jeff Crandall[a]
jrc2h@eservices.virginia.edu

[a]Center for Applied Biomechanics, University of Virginia
Address: 4040 Lewis N' Clark Drive, Charlottesville, VA, USA 22911

[b]Department of Biomedical Engineering, Duke University
Address: Room 136 Hudson Hall, Box 90281, Durham, NC, USA 27708

[c]Department of Emergency Medicine, University of Virginia
Address: P.O. Box 800699, Charlottesville, VA, USA 22908

[d]National Highway Traffic Safety Administration
Address: 1200 New Jersey Avenue, SE, West Building, Washington, DC, USA 20590

Abstract

Associated mechanisms of injuries sustained by rollover-involved occupants are absent from the existing literature, which restricts the applicability of existing studies on cervical spine injury tolerance in the development of injury criteria for rollover-induced injuries. The objective of this study was to analyze the pathologies and specific spinal injury mechanisms from rollover crash occupants using existing data from cadaver cervical spine compressive tests. Sampled cases (n=23) of single-vehicle, single-event rollovers from the Crash Injury Research and Engineering Network (CIREN) database were analyzed. A review of 20 experimental cervical spine loading studies from the literature was conducted to support the mechanism determination for occupant injuries. Axial loading was found to be the predominant loading component responsible for cervical spine injury in all of the CIREN occupants. Discrepancies between CIREN injuries and cadaver test pathologies exist, primarily with regard to asymmetry in AIS 2 fractures. Eighteen of the 23 CIREN occupants sustained asymmetric fracture, an injury type seldom produced in mid-sagittally loaded cadaver spines. The difference was less for experimental tests involving eccentric compressive loading. Differences between the field injuries and cadaver tests can be accounted for by inherent limitations of cadaver tissue and/or the paucity of non-sagittal cadaver tests, emphasizing the need for further investigation into non-sagittal cervical spine compression injury to improve the level of correlation between cadaver tests and the clinical outcomes seen in the field.

Keywords

Cervical spine, rollover, CIREN, bilateral facet dislocation (BFD)

Introduction

Vehicle rollovers result in over one-third of vehicle occupant fatalities in the United States; of the injuries sustained by rollover-involved occupants, trauma to the cervical spine is among the most frequent and life-threatening. From a National Automotive Sampling System (NASS) study of all adult, front row-seated, non-ejected occupants involved in rollovers between 2003 and 2007, over 55% of AIS3+ injuries suffered in pure rollovers were to the head or spine (Ridella et al. 2009). Head interaction with roof structures within the vehicle likely occurs during many rollover crashes, leaving the head and cervical spine vulnerable to compressive forces (Viano and Parenteau 2008). Countermeasure development aimed at mitigating cervical spine injury in rollover-involved occupants requires a biofidelic dummy and appropriate injury criteria, which are necessary to predict the onset of injury. The biomechanics literature contains numerous studies aimed at determining loading response and injury thresholds in cadaver cervical spines loaded in axial compression, which are appropriate starting points for the development of such injury criteria. However, much of the existing literature was not originally designed for rollover application; stated applications involve diving-related injuries (McElhaney et al. 1979, Bauze and Ardran 1978), contact sports (Hodgson and Thomas 1980), other modes of automotive crashes (Pintar et al. 1989, 1990, Myers et al. 1991) and injury due to falls (Yoganandan et al. 1986). Most studies state several of these potential applications without reference to vehicular rollover (Yoganandan et al. 1990).

Previous rollover testing series have shown lateral loads acting on the heads of anthropomorphic test devices (ATDs) during roof contact which also compresses the

neck (Raddin et al. 2009). Clinical injuries associated with these phenomena have been seldom explored in the cadaver literature. Toomey et al. (2009) performed tests on cadaver specimens in the same fashion as Nightingale et al. (1997), who tested cadaveric head-neck complexes in controlled drop tests. Instead of loading the specimen along the midline of the head, Toomey et al. studied the effects of lateral eccentricity and bending, laterally flexing two specimens and angling the impact plate 15-degrees from the horizontal for three specimens. The authors list rollover crashes as a reason for deviating from Nightingale's methods. The tests were performed to mimic events where either the neck maintains a vertically aligned posture and lateral flexion is produced by an angled impact, or the neck is initially laterally bent and compressed caudally. A study by Nusholtz and Kaiker (1986) examined the effects of rotation about the longitudinal axis of the neck during superior-to-inferior impact loading. These loading environments are justified by recent epidemiological findings; Bambach et al. (2013), through an analysis of the National Automotive Sampling System (NASS) Crashworthiness Data System, found a high rate of fractures to the cervical spine resulting from lateral bending or axial rotation. The authors note limits of the study including insufficient injury detail in the NASS database. An analysis of the National Highway Traffic Safety Administration (NHTSA) Crash Injury Research and Engineering Network (CIREN) database, which involves significantly more detailed injury resources, is therefore needed to evaluate complex injury mechanisms in real-world rollover crashes.

Nonetheless, existing cadaver studies exhibit potential application to rollover injury mechanism research since cervical spine injuries in rollover-involved occupants are hypothesized to be the result of compressive loading (Ridella et al. 2009, Raddin et al.

2009, Young et al. 2007). To evaluate the applicability of individual studies, injuries produced in cadavers are compared directly to injuries seen in the field data to determine their clinical relevance. Additionally, investigations of individual crash cases from the field data provide information regarding global and local loading modes and injury mechanisms that can be used to further evaluate existing biomechanical test results. Thus, the primary goal of this study is to assess the applicability of existing biomechanical data to rollover-involved occupants and, as a long-term goal, to determine clinical injury mechanisms in rollover-involved occupants for future investigations into dummy biofidelity and the use of a dummy to predict injury risk in dynamic rollover tests.

Methods

Cervical Spine Database Formulation

Biomechanics literature from the last 40 years was surveyed to identify studies with cervical spine loading tests on cadavers. The specimens from each test were included in a database if the following criteria were met: tests were performed on human cadavera (i.e., not involving non-human primates), test specimens contained no previous traumatic spine injuries or pathological spinal conditions, the specimen included no fewer than 5 consecutive cervical vertebrae (full head-neck complexes, full cadaver, full osteoligamentous cervical spine (C1-T1), or any five consecutive vertebrae were accepted), loading was directed to the crown of the head or to the most superior vertebra in a superior-to-inferior loading direction or other environments where axial loading was applied in a compressive nature (such as inferior-to-superior loading via T1), the authors' full test methodologies were provided (including initial orientations of the head and neck), complete injury detail of each specimen was provided, and the specimen was not

re-tested (i.e., single impact only). Cadaver pathology was separately tabulated to compare differences of the two loading orientations: studies with loading applied along the mid-sagittal or antero-posterior (AP) plane and studies involving laterally eccentric or non-sagittal loading.

In-Depth CIREN Analysis

The next portion of the study was performed using information drawn from the NHTSA-sponsored CIREN database. The database contains information collected from approximately 5,000 crashes where at least one serious (AIS => 3) or two moderate (AIS = 2) injuries occurred to one of the vehicle occupants. A complete list of CIREN inclusion criteria may be found in the United States Federal Register (CIREN, 2010).

The CIREN database was queried for cases that involved belted, non-ejected occupants in single-event rollover crashes involving 8-quarter turns or less that sustained an AIS 2+ injury to the cervical spine. The resulting case information was then used by the case review team along with the vehicle and occupant kinematics to identify the particular injury causation scenario for each of the AIS 3+ injuries and AIS 2 fractures to the cervical spine, including the perceived loading direction, injury mechanism, and rollover phase in which the injury was assumed to have occurred. Since many AIS codes provide limited injury description, each injury to the cervical spine was logged based on operating room transcripts, pathology reports and radiology.

Integrating CIREN and Cervical Spine Database

Injuries to the case occupants were compared with existing cadaver test specimens in an attempt to determine global and local injury mechanisms (i.e., kinematics and external loadings that lead to injury) for each case. To characterize the

location of individual vertebral fractures, a classification scheme was developed to determine the location of the fracture relative to the mid-sagittal plane of the vertebrae. Unilateral fractures, or fractures to only one lateral aspect (left or right) indicate situations where compressive force, shearing, or torsional force was greater on one side (Myers and Winkelstein, 1995). Bilateral fractures, or fractures to both laminae, pedicles, transverse processes or facets of a vertebra, indicate forces symmetrically dissipated in the sagittal plane (Maiman et al. 1983). Unilateral and bilateral fractures were recorded and tabulated for the CIREN occupants and cadaver specimens. Fractures occurring along the mid-sagittal plane, or AP axis, were also tabulated; these structures, such as the vertebral body and spinous processes, do not contain lateral elements and typically fracture close to the midline (Toomey et al. 2009).

Distributions of fractures based on vertebral level, type of fracture and lateral nature were compared between the CIREN occupants' injuries and the fractures sustained by cadavera in biomechanical testing. The presence or absence of interfacetal dislocation was also recorded. Once an injury seen in a case occupant was closely linked with an injury produced *in vitro*, the mechanism explained by the author of that study was determined to be a possible mechanism for the case occupant's injury.

Results

Cervical Spine Database Formulation

Of the current body of spine biomechanics, 20 published studies by eleven different corresponding authors spanning four decades of biomechanical literature satisfied the inclusion criteria, totaling 175 cadaver specimens. The orientation of the head and loading surface was often found to determine the global injury mechanism to

the neck, whether it was compression, flexion, extension or a combination thereof. Cadaver injuries were assigned local mechanisms as well, including compression or distraction, with or without flexion or extension. All specimens were loaded axially and all but ten were intended to be loaded along the mid-sagittal plane (Table 2) (Toomey et al. 2009, Nusholtz and Kaiker 1986, Nusholtz et al. 1983).

Authors used several methods to induce injury. Some studies provided an input displacement with either a controlled fixed displacement or displacement until failure. Other studies applied an input energy (e.g., drop tests from a specified height). Studies involved full cadavers loaded axially with a pneumatic piston (Nusholtz and Kaiker 1986, Maiman et al. 1983, Alem et al. 1984, Nusholtz et al. 1981, Culver et al. 1978, Yoganandan et al. 1989), full cadaver drop tests (Yoganandan et al. 1986, Nusholtz et al. 1983, Sances et al. 1986), head and cervical spine complexes loaded axially (Pintar et al. 1989, 1990,1995, Yoganandan et al. 1989, 1990, 1994, Toomey et al. 2009, Nightingale et al. 1996, 1997),, and isolated ligamentous cervical spine sections fixed in load frames and axially compressed (Myers et al. 1991, Maiman et al. 1983, Yoganandan et al. 1989, McElhaney et al. 1983, 1988).

A total of 205 fractures and 19 dislocations were produced in the 165 cadavers loaded along the mid-sagittal plane. The most commonly produced injuries in this subset were vertebral body fractures (including wedge, burst, compression and teardrop fractures) and spinous process fractures, together making up 68.8% of the total number of fractures (Figure 6). Fractures to the lateral aspects, which include the superior and inferior articular facets, pedicles, laminae and transverse processes, made up 33 of the 205 total fractures (16.1%) in the mid-sagittally loaded cadaver specimens. Thirty-one

fractures and one dislocation were produced in the 10 cadavers applied with laterally eccentric or non-sagittal out-of-plane loading. The most common fractures in this subset were to the laminae and facets, accounting for 48.4% of the total fractures (Figure 6).

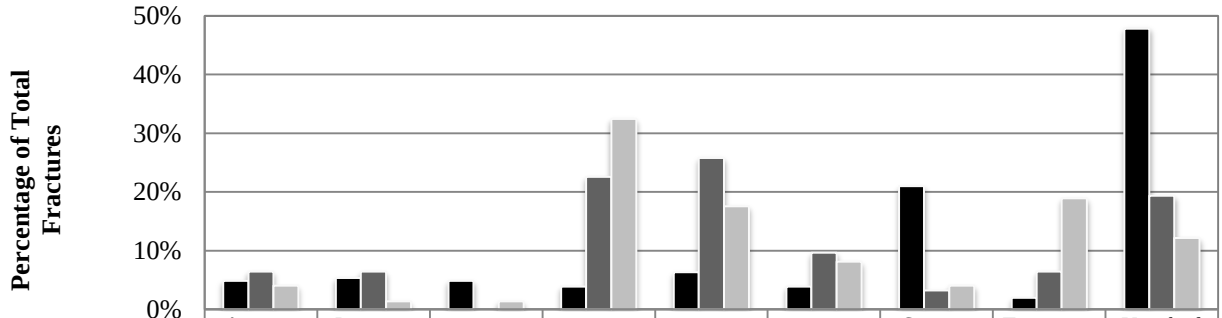

	Anterior Ring	Posterior Arch	Dens	Facet	Lamina	Pedicle	Spinous Process	Transverse Process	Vertebral Body
Loaded Mid-Sagittally (n=205)	4.9%	5.4%	4.9%	3.9%	6.3%	3.9%	21.0%	2.0%	47.8%
Loaded Non-Sagittally (n=31)	6.5%	6.5%	0.0%	22.6%	25.8%	9.7%	3.2%	6.5%	19.4%
CIREN Occupants (n=74)	4.1%	1.4%	1.4%	32.4%	17.6%	8.1%	4.1%	18.9%	12.2%

Figure 6: Fractures of cadavers and CIREN occupants by vertebral structure.

Twenty dislocations were identified in nine test-series by five different corresponding authors (Pintar et al. 1989, Myers et al. 1991, Yoganandan et al. 1986, 1990, Nightingale et al. 1996, 1997, Nusholtz and Kaiker 1986, Maiman et al. 1983, Sances et al. 1986). These included three atlanto-axial separations, ten instances of anterolisthesis exhibiting jumped facets, six instances of retrolisthesis and one instance of perched facets. There were no instances of unilateral facet dislocation.

There were a substantially greater number of symmetric than unilateral fractures produced in the cadaver tests where mid-sagittal loading was used (Figure 7). Cadaver tests employing laterally eccentric loading via angled plates (Toomey et al. 2009), lateral pre-positioning (Nusholtz et al. 1983), or axial rotation of the head (Nusholtz and Kaiker 1986) displayed a greater number of unilateral fractures than bilateral and mid-sagittal fractures.

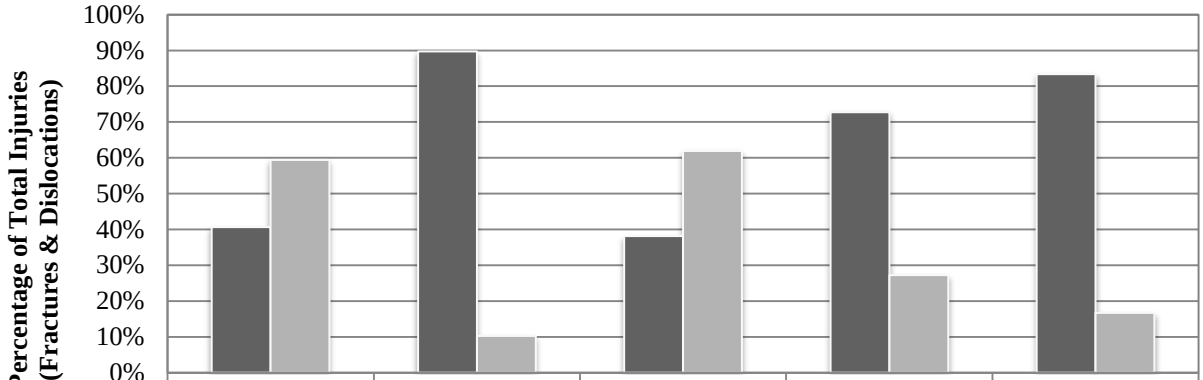

	Cadavers Loaded Non-Sagittally (n=31)	Cadavers Loaded Mid-Sagittally (n=205)	CIREN Occupants AIS 2+ (n=84)	CIREN Occupants AIS 3+ (n=11)	CIREN Occupants AIS 4+ (n=6)
Symmetric	40.6%	89.7%	38.1%	72.7%	83.3%
Unilateral	59.4%	10.3%	61.9%	27.3%	16.7%

Figure 7: Lateral nature of injuries by cadaver loading and CIREN injury severity.

In-Depth CIREN Analysis

The query of the CIREN database yielded 46 pure rollover cases. Twenty-three of the cases involved occupants with AIS 3+ or AIS 2 fracture to the cervical spine (Table 1). The 23 case occupants consisted of 14 males and nine females, spanning ages from 18-76 (mean= 41.2 years ±19.5 years), with average statures and weights of 172 cm (± 11 cm) and 81 kg (± 19 kg), respectively. All of the occupants were seated in the first row with 13 drivers and 10 right front passengers (RFPs), with 17 (73.9%) of the occupants positioned on the far side of the roll. Crashes occurred in seven sedans, two sports cars, 11 SUVs, two trucks and one van from model years between 1998 and 2008. Nine of the occupants sustained only one roof-to-ground contact, 13 sustained two roof contacts, and one occupant sustained three roof contacts (CIREN Case 857076778 was coded as a 6-quarter-turn rollover, but upon review from the research team was deemed a 10-quarter-turn event).

CIREN #	Height, [m]	Weight, [kg]	Age	Gender	Make	Model	Model Year	Occupant Position	Quarter Turns	Roll Direction
103304	1.8	82	76	Male	Chevrolet	Impala	2004	RFP	6	R
125299	1.75	66	53	Male	Chevrolet	Cavalier	2004	RFP	4	L
163690	1.78	77	42	Male	Chevrolet	Cavalier	2002	RFP	4	L
163694	1.6	91	21	Female	Chrysler	Sebring	2008	Driver	6	L
100074514	1.83	130	73	Male	Ford	F350 Crew Cab	2002	Driver	2	R
100084523	1.7	50	33	Female	Toyota	4-Runner	1999	Driver	8	R
100112055	1.57	68	34	Female	Ford	Taurus	2000	Driver	8	R
160110274	1.83	86	59	Male	Mazda	Miata	2000	Driver	2	R
160139536	1.52	52	20	Female	Suzuki	Reno	2006	Driver	8	L
537103134	1.55	86	43	Female	Jeep	Grand Cherokee	1998	RFP	6	L
551068562	1.83	79	21	Male	Chevrolet	Blazer	2000	RFP	4	L
558030923	1.8	88	72	Male	Ford	Escape	2006	RFP	4	R
590123589	1.65	54	25	Female	Ford	Mustang	2004	Driver	8	L
590144150	1.85	77	26	Male	Honda	Element	2004	Driver	8	R
781125527	1.6	102	50	Female	Kia	Sorrento	2006	Driver	6	R
852126192	1.91	95	50	Male	Chevrolet	Express Van	2006	Driver	4	R
852130600	1.57	86	78	Female	Buick	Regal	2000	Driver	2	R
852162058	1.73	76	32	Male	BMW	Z4 Roadster	2008	RFP	4	L
852172396	NA	NA	25	Female	Kia	Sportage	2006	RFP	8	R
852177768	1.8	77	28	Male	Ford	F150 SuperCrew	2008	Driver	8	R
857069807	1.7	102	44	Male	Ford	Explorer	2003	RFP	8	L
857076778	1.81	104	24	Male	Jeep	Cherokee	2001	RFP	10	L
965066489	1.73	61	18	Male	Jeep	Liberty	2002	Driver	6	R

Table 1: CIREN case vehicle and occupant information.

Among the 23 case occupants, 17 sustained cervical trauma as their most significant injury in terms of threat to life. Of these, 6 involved permanent cord injury (AIS 4+) or death (AIS6). Eighteen of the 23 occupants sustained at least one unilateral facet, lamina, pedicle or transverse process fracture. Of the 74 total cervical spine fractures sustained by the CIREN case occupants, 49 (66.2%) were unilateral with 27 occurring on the right-side and 22 on the left. For both drivers and RFPs, more unilateral fractures were sustained to their outboard lateral aspects (Figure 8). Fracture patterns based on rollover seating position (far-side or near-side occupant relative to the roll direction) showed that a greater number of outboard unilateral fractures were sustained by the far-side seated occupant and more symmetric fractures were sustained by the near-

side seated occupant (Figure 9).

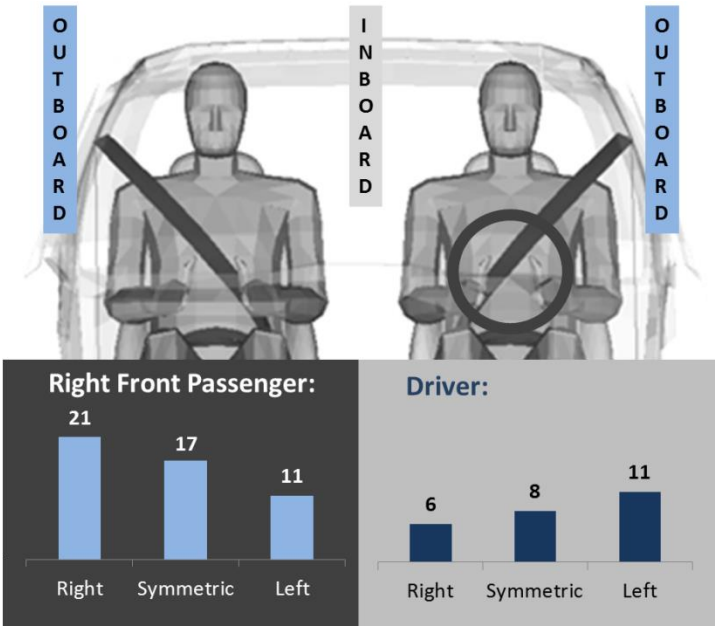

Figure 8: Lateral nature of CIREN front row occupant neck fractures, showing more outboard unilateral fractures for both the driver and right front passenger.

The AIS values for serious (AIS 3+) and catastrophic (AIS 4+) injuries were tabulated separately for the CIREN occupants, showing that as injuries increase in severity, more are oriented bilaterally or along the AP line (Figure 7). The lateral natures of serious (72.7% symmetric) and catastrophic (83.3% symmetric) injuries show better agreement with the mid-sagittally loaded cadaver population (89.7% symmetric), while the full collection of CIREN occupant injuries (61.9% unilateral) shows close agreement to the eccentrically loaded cadaver population (59.4% unilateral).

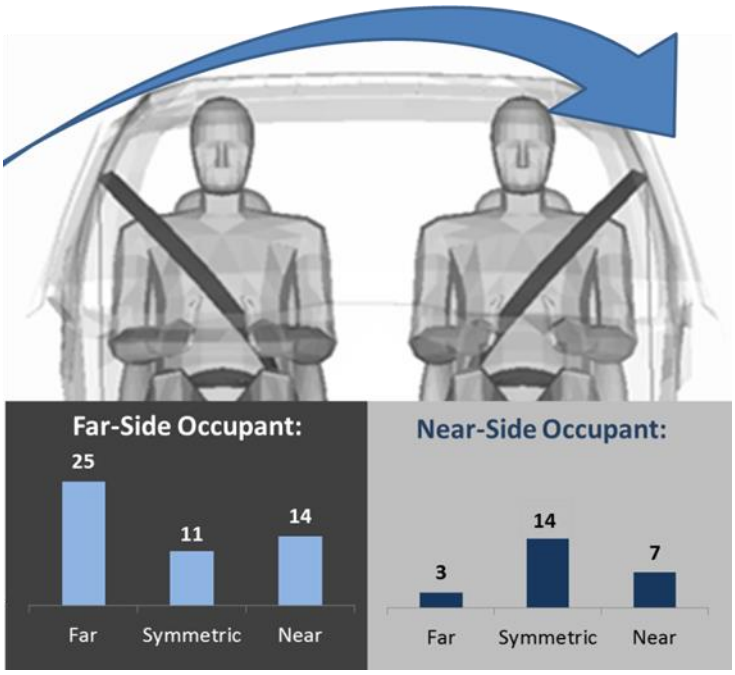

Figure 9: Lateral fracture location based on occupant seating position relative to roll direction, showing more far-side unilateral fractures. To the far-side seated occupant and fewer mid-sagittal fractures overall for the far-side seated occupant.

Cadaver spines loaded along the mid-sagittal plane exhibited lower (C5-C7) cervical spine fractures less frequently (35.6%) than specimens used in lateral loading investigations (71.0%). Nineteen of the 23 CIREN occupants sustained lower cervical spine trauma, comprising 64.9% of their total fractures (Figure 10).

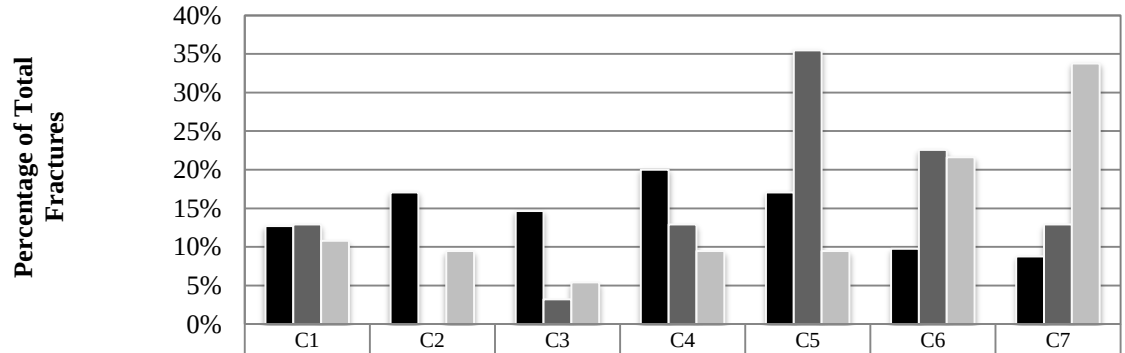

	C1	C2	C3	C4	C5	C6	C7
Loaded Mid-Sagittally (n=205)	12.7%	17.1%	14.6%	20.0%	17.1%	9.8%	8.8%
Loaded Non-Sagittally (n=31)	12.9%	0.0%	3.2%	12.9%	35.5%	22.6%	12.9%
CIREN Occupants (n=74)	10.8%	9.5%	5.4%	9.5%	9.5%	21.6%	33.8%

Figure 10: Fractures of cadavers and CIREN occupants by vertebral level.

Nine bilateral or unilateral facet dislocations or subluxations were observed in the case occupants. There were five instances of Grade I spondylolisthesis, including cases of perched facets. There were four instances of Grade II spondylolisthesis, accounting for locked facet dislocations of up to 50% antero-posterior slippage. There were three unilateral facet dislocations (UFDs). In eight of the nine cases of facet dislocation there were fractures to the adjoining articular surfaces, indicating shearing at the intervertebral space (Table 3).

Reference Source	No. Specimens Studied	Cadaveric Segment(s) Used	Padded/Rigid Impact	Lordosis Intact/Removed	Impact/Loading Velocity Range (cm/s)	Peak Contact Force Range (kN)	No. Passed Inclusion Criteria	Specimen IDs Not Included	Specimen IDs With Non-Sagittal Loading
Alem et al., 1984	19	Full cadaver	Padded	Intact	690-1090	3.0-17.0	19		
Culver et al., 1978	11	Full cadaver	Padded	Intact	676-1020	4.71-8.85	10	78H110 (swan neck)	
Maiman et al., 1983	13	Full cadaver, Isolated (C1-T3)	Actuator-attached	Intact	0.25-152	0.645-7.439	13		
McElhaney et al., 1983	14	Isolated (varied)	Actuator-attached	Pre-flexed	45-92	0.96-6.84	10	A80-289, 364, 368, 384 (retested)	
McElhaney et al., 1988	7	Isolated (C7-T1, BOS-T1)	Actuator-attached	Pre-flexed	Not provided	0.108-2.305	6	5C (load information missing)	
Myers et al., 1991	18	Isolated (BOS-T1)	Actuator-attached	Intact	Not provided	0.169-6.84	18		
Nightingale et al., 1996	11	Isolated (head-T1)	Rigid (x7) Padded (x4)	Intact	243-351	1.759-11.62	11		
Nightingale et al., 1997	Nightingale '96 data + 11 add.	Isolated (head-T1)	Rigid (x3) Padded (x8)	Intact	307-320	3.115-8.604	11		
Nusholtz et al., 1981	12	Full cadaver	Padded	Intact (x8) Pre-flexed (x4)	460-570	1.80-11.10	11	79L088 (lacks injury description)	
Nusholtz et al., 1983	8	Full cadaver	Padded	Pre-flexed	400-590	5.60-10.8	5	82L489, 82L494, 83L499 (retested)	82L501
Nusholtz and Kaiker, 1986	5	Full cadaver	Padded	Pre-flexed	550-570	4.89-13.35	5		84L514, 84L515, 84L516, 84L517, 84L518
Pintar et al., 1989	7	Isolated (Frankfurt plane -T1)	Actuator-attached	Pre-flexed	0.2	1.355-3.613	7		
Pintar et al., 1990	6	Isolated (head-T1)	Padded	Pre-flexed	295-813	5.856-19.205	6		
Pintar et al., 1995	Yoganandan '94 data + 11 add.	Isolated (head-T1)	Padded	Pre-flexed	250-800	Not provided	11		
Sances et al., 1986	15	Full cadaver	Rigid (x9) Padded (x6)	Pre-flexed	Not provided	3.00-14.66	15		
Toomey et al., 2009	5	Isolated (head-T1)	Rigid	Intact	291-326	6.064-17.48	4	2 (casting failure)	1, 3, 4, 5
Yoganandan et al., 1986	Sances '86 data	Full cadaver	Rigid (x9) Padded (x6)	Pre-flexed	Not provided	3.00-14.66	0	Sances et al., 1986 specimens	
Yoganandan et al., 1989	10	Full cadaver, Isolated (head-T2, C2-T2)	Actuator-attached	Intact (x5) Pre-flexed (x5)	0.254-142	0.50-2.936	10		
Yoganandan et al., 1990	Pintar '89 + Pintar '90 data	Isolated (head-T1, Frankfurt plane -T1)	Actuator-attached	Pre-flexed	0.2-570	1.08-3.04	0	Pintar et al., 1989,1990 specimens	
Yoganandan et al., 1994	Pintar '90 data + 3 add. tests	Isolated (head-T1)	Padded	Pre-flexed	540-782	Not provided	3		
						n=	*175*	*n=*	*10*

Table 2: List of studies used in the analyses of compression cervical spine injury assessment.

CIREN #	Loading evidence on Head	C-Spine Injury AIS Codes	C-Spine Injury Description	Notes	C-Spine Local Injury Mechanism	Other AIS 2 Fx and AIS3+ Injuries	Most Sig Injury
103304	Hematoma slightly anterior to vertex	6502262\6502242\ 6502302\6502322\ 6502202	C2, C4 pedicle fxs\ C3-4 lamina fxs\ C1 anterior ring 2-part fx\ C3-4 vertebral body fx\ C2-4 transverse process	Hangman's fracture with bilateral foramen transversaria fractures\ C4 R pedicle, C3-4 R lamina\ comminuted, displaced\\ bilateral at C2, C3-4 right foramen transversaria (S6,R5)	CE\LCE\CF\VC\LC	Multiple stable rib fxs, T2 transverse process fx	C-spine
125299	Abrasions to forehead	6502283\6502222\ 6502202\6502322	C2 (Type-III) odontoid fx\ C6-C7 right facet fxs\ C7 right transverse process fx\ C2 vertebral body fx	Anteriorly displaced dens fx extended into vert body\\\ (S1,R3)	CE\LC\LC\CE		C-spine
163690	Scalp abrasion at vertex	6402144\6502242\ 6502202	Cord contusion incomplete cord syndrome with fracture\ C6 laminae fx\ C7 trans process fx	BLF C5 on C6\with C6 right trans process fx, C5 left lamina fx and C5-C6 right facet fx\ C7 R trans proc (S2,L1,R4)	CF\LCE\LD		C-spine
163694	Scalp laceration left frontal to parietal region	6402766	Cervical Spine Cord laceration C-3 or above with fracture	Separated fracture of AO interface (S1)	D		C-spine
100074514	Scalp abrasion left side near vertex	6402184	Cervical Spine Cord contusion with fracture	C7 laminae fxs (S1)	CE	T1, T2 vertebral body fxs	C-spine
100084523	No head/facial injury	6502222	C7 left facet fx	Superior articular facet (L1)	LC		C-spine
100112055	Superior scalp lacerations	6502242\6502262\ 6502322	C1 lateral mass fx\ C1 right pedicle, trans process fx\ C7 vertebral body fx	Extends to right posterior arch\ including right foramen\ anterior aspect (S1,R3)	LC\LC\VC	T4-T10 fxs w/ complete cord laceration, multiple rib fxs w/ pneumothorax, clavicle fx, humerus fx	Thorax
160110274	Laceration to middle upper forehead	6402043\6502022	Cord contusion with transient neurological signs with fracture\ disc injury w/out nerve root damage	Left side fracture subluxation of C6-7 with perched facet, C6-7 left facet fxs\ displaced anterior wedge fx and small central disc herniation (S1,L3)	LCF\CF	Cerebral hematoma	TBI
160139536	Abrasion right side anterior to vertex	6502302\6502123\ 6502182\6502222	C1 anterior arch fracture\ C6-7 BFD\ C7 spinous process fx\ C7 facet fx	\perched facets\\bilateral superior articular facets (S4)	CF\CF\CE\VC	Cerebral hematoma, T1 facet fx, T3-4 vert body fxs	TBI
537103134	Bruising right posterior temporal region	6402285\6502222\ 6502242\6502322	Cord contusion complete cord syndrome C-4 or below with fracture and dislocation\ C5-C7 left facet fxs\ C6-C7 left lamina fx\C7 wedge fx	Grade I anterolisthesis C5-6, Grade II antero C6-7 resulting in quadriplegia\ inferior facet C5-6, superior facet C6-7\\ (S3,L5)	CF\LC\LC\CF		C-spine

CIREN #	Loading evidence on Head	C-Spine Injury AIS Codes	C-Spine Injury Description	Notes	C-Spine Local Injury Mechanism	Other AIS 2 Fx and AIS3+ Injuries	Most Sig Injury
551068562	Hematoma left parietal region	6402184\6502242\ 6502262	Cord contusion incomplete C4 or below with fracture and dislocation\ C5-C6 right lamina fxs\ C5-C6 right pedicle fxs	C6-7 Grade I anterolisthesis, Posterior ligamentous injury from C3-7, with cord contusion at C4-5\\ (S1,R4)	F\LC\LC		C-spine
558030923	Abrasion to forehead	6402285\6502242\ 6502322\6502182\ 6502202	Complete cord syndrome C4 or below \ C2,C6 laminae fx\ C7 wedge fx\ C2,C6 spinous process fx\ C7 left trans process fx	C6-7 Anterolisthesis, locked on left, perched on right\ bilateral, undisplaced\\ (S5,L2)	LCF\CE\CF\CE\LD		C-spine
590123589	No head/facial injury	6502022\6502222\ 6502202	C6-7 intravertebral disc injury\ C7 left facet fx\ C7 left transverse process fx	Without nerve root damage\ superior articulating facet\ (S1,L2)	CF\LC\LCE		C-spine
590144150	Abrasion to forehead	3210183\6502222	Vertebral artery thrombosis (occlusion) secondary to trauma\ C5 right facet fx	Right side caused by C5 facet fx\ into foramen transversarium (R2)	LC\LC	Right lung contusion	C-spine
781125527	Abrasion to left temporal region	6502302\6502302	C2 teardrop fx\ C1 anterior body fx	Mildly displaced inferior anterior aspect of vert body\ displaced left superior anterior aspect (S2)	CF\VC	Clavicle fx	C-spine
852126192	Right side scalp abrasion	6502102\6502242\ 6502222\6502202\ 6502202	C5-6 unilateral facet dislocation\ C5 laminae fx\ C6 left facet fx\ C4 left trans proc\ C6 left trans process fx	Left-sided, jumped facet\ bilateral\\ moderately comminuted, involves transverse foramen\ (S1,L4)	LCF\CE\LC\LD\LC		C-spine
852130600	Contusion above left eye	6402063	C6-7 BFD	Grade II Anterolisthesis with transient neurological signs (S1)	DF	Lumbar spine fxs, subarachnoid hemorrhage	C-spine
852162058	Right side facial lacerations	6502222\6502262	C3-4 right facet fx\ C4 right pedicle fx	C4 superior, C3-C4 inferior, involving lateral mass\ involving transverse foramen (R3)	LC\LC		C-spine
852172396	Contusion to right side temporal region	6502242\6502222	C6 left lamina fx\ C6 left facet fx	Minimally displaced\ left inferior articulating facet (L2)	LCE\LC		C-spine
852177768	No head/facial injury	6502222\6502202	C7 right facet fx\ C7 right transverse process fx	Superior articulating facet\ (R2)	LC\LC	Pulmonary contusion w/ rib fxs, right tibia fx, right fibula fx	Thorax

857069807	Laceration to posterior scalp	6502222\6502322	C6-7 right facet fx\ C7 vertebral body endplate fx	\with retropulsion into spinal canal (S1,R2)	LC\VC	Clavicle fx	C-spine
857076778	Facial skin contusion	6502242\ 6502202	C1 posterior ring fx\ C7 left transverse process fx	Jefferson fracture probable\ including superior facet (S2,L2)	VC\LC	Right tibia fx, T3-T4 vert body fx, right fibula fx, talus fx	Lower Extremity
965066489	Superficial avulsion to posterior scalp	6502202	C7 left transverse process fx	Extending into superior facet (L2)	LC	Bilateral pulmonary contusions	Thorax

Table 3: Cervical spine injury and mechanisms details for each CIREN case occupant. Number of symmetric (S), left-sided (L), and right-sided (R) injuries are displayed in parentheses. Local injury mechanisms (L – lateral, V – vertical, C – compression, D – distraction, F – flexion, E – extension) derived from cadaver-based studies (Nightingale et al. 1997, Myers and Winkelstein 1995, Allen et al. 1982, Winkelstein and Myers 1997, McElhaney et al. 2002).

Discussion

The compressive tolerance of the cervical spine has been well explored for applications including diving, contact sports, injuries due to falls, and automobile crashes. This study attempts to provide insight on the applicability of existing cervical spine compression literature to rollover crash injuries. Accurate pathology is targeted in any cadaveric biomechanical test; a goal of this study was to show whether or not consistencies exist between the clinical injuries sustained by rollover crash victims and the injuries produced in cadavera for the purpose of investigating injury mechanism in rollovers. A number of authors have documented that cervical spine traumas are some of the most frequent and debilitating injuries suffered by rollover-involved occupants (Ridella et al. 2009, Paver et al. 2008, Moffatt et al. 2005). It is important that accurate pathology and tolerance levels are ascertained from cadaver studies to make evident key loading patterns responsible for cervical spine trauma in rollover crashes. The need for dummy biofidelity with respect to rollover is paramount in light of recent advances in dynamic rollover testing (Kerrigan et al. 2011). Measuring injury risk through parametric sensitivity analysis is vital for assessing the biofidelity of current ATDs and computer models; these key factors can help researchers determine improvements and a path forward for dynamic test procedures aimed at evaluating vehicle crashworthiness using an assessment of occupant injury risk.

The inclusion criteria for the literature assessment were based on cadaver tests where the cervical column was subjected to axial compression, as compressive spine injuries have been routinely linked with rollovers. Papers containing the published results of biomechanical tests involving single or a few connecting functional spinal units were

not included in the database of cadaver specimens subjected to rollover-type loading because they cannot properly model the buckling kinematics of the cervical spine. In addition, tests on smaller segments cannot produce the concomitant and non-contiguous injuries that are common in both the field data and in full cervical spine experiments (Nightingale et al. 1996).

Other highly cited cervical spine papers did not include detailed injury description and were omitted (Bauze and Ardran 1978, Hodgson and Thomas 1980, Roaf 1960, Panjabi et al. 1998). A goal of this study was to compare clinical cervical spine injuries with those produced in cadaveric tests; this step could not be done for papers where injury description was not provided. Some experimental studies ascertained the believed mechanism for fracture, dislocation or ligamentous injury by using high-speed film to track the motions of reflective targets attached to the cadaver spinous processes and vertebral bodies during mechanical loading. Other studies use papers that specify fractures and injuries in separate injury classifications to indicate injury mechanisms. Studies by Allen et al. (1982) and White and Panjabi (1978) were used to retrospectively link an injury outcome with its surmised mechanism. One limit to this method exists in that Allen's classifications were initially performed for lower cervical spine injury, but have been used by researchers to classify injuries throughout the entire cervical column (Nightingale et al. 1996, 1997). Still, a similar analytical approach was used for the CIREN occupants in this study to classify injury mechanism.

The current body of cervical spine compression literature seems to capture the distribution and mechanism of catastrophic cervical spine injuries in rollover. This is evidenced in Figure 7, where it can be seen that the incidence of unilateral AIS 3 and 4+

CIREN injuries is closer to the distribution of mid-sagittally loaded cadaver fractures. However, the cadaveric representation of the full spectrum of CIREN field injuries seems to be significantly different. One suggested reason for this difference is that cadaveric specimens lack musculature. This infers that the clinical presentation of injury to a live subject could be altered or aggravated by the contraction of active neck musculature, even though muscle contraction occurs after bony fracture to the spine, thus too late in the loading time-history for active musculature to have effect (Nightingale et al. 1996, 1997, Pintar et al. 1998, Crawford et al. 2002, Cusick et al. 2002, Foust et al. 1973).

Passive musculature, which preloads the cervical column, could have an effect on injury outcome and could be a possible reason for injury differences in CIREN occupants and cadaver specimens. In the crash cases, eight of the 23 case occupants exhibited bilateral or unilateral facet dislocations or subluxations, almost always (7 out of 8) with evidence of shearing at the intervertebral space (i.e., facet fracture). Evidence of shearing involves articular facet, or lateral aspect fractures at the subluxed zygapophyseal joint (Figure 11). These "impaction fractures" have been closely associated with facet dislocations (Harris et al. 1986). Although they typically do not have significance to the patient's outcome, fractures to the articular masses during facet dislocation evidence a shearing translation without distraction of the upper motion segment with respect to inferior vertebra. Facet dislocations have previously been associated with a distractive-flexion mechanism at the local level (Nightingale et al. 1997, Allen et al. 1982). The high incidence of facet dislocation impaction fractures *in vivo* indicates an injury mechanism where the inferior articular facets are shearing through the superior facets of the inferior vertebra and not "jumping" the facets as its colloquial name implies. Such adjoining

articular mass fractures are absent in the 19 facet dislocations found in the existing literature. One specimen, 202 from Pintar et al. (1989), had contiguous facet fractures, or evidence of possible shearing. However, this specimen displayed retrolisthesis, or posterior dislocation, which is not clinically seen in compressive neck trauma. Passive musculature or pre-loading due to bracing before impact could explain why shearing fractures are present in the field and not in cadaveric specimens.

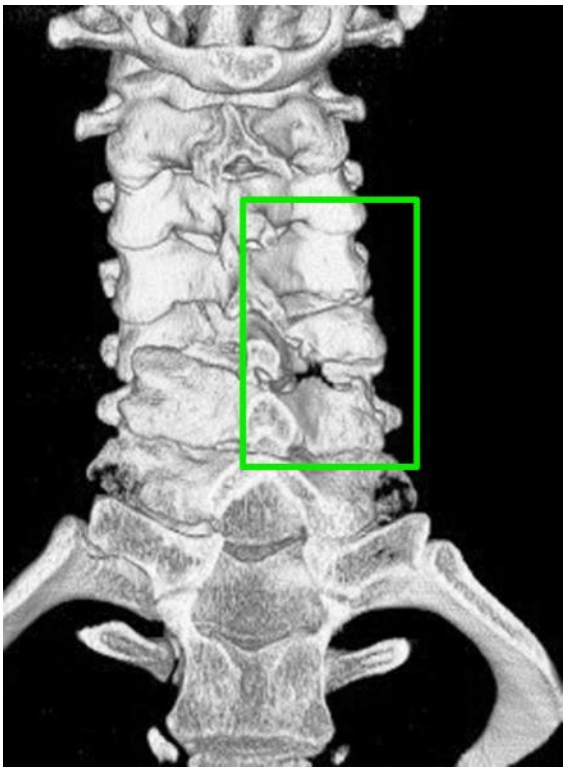

Figure 11: Posterior view of the cervical spine of CIREN occupant 163690, showing shearing during anterior dislocation evidenced by pedicle and facet fractures at the C6-7 zygapophyseal joint. Impaction fracture patterns were present in 8 of 9 CIREN occupant facet dislocations.

None of the case occupants sustained a collection of injuries that have been fully replicated by a single specimen *in vitro*. In other words, in no case did one experimental specimen fully encapsulate an entire case occupant's injuries. It should also be noted that

injury patterns within each set of experiments were not internally consistent either, despite the best efforts of the researchers to control the impact orientations and energies.

Major differences between the current body of literature and the epidemiological findings lie in the distributions of clinically-relevant rollover injury types, location of fracture and symmetry of fracture (Figures 6, 7, 10). It is understood that the distribution of injuries in the CIREN cases need not match the distribution of injuries in the biomechanics literature; the percentages have been compared as a way of describing the discrepancies in injury distributions between field data and laboratory tests. Exact distributions are not necessary, but it should be expected that the relative rankings of the type of injury and fracture location be fairly similar and that a general match among injuries with the same biomechanical mechanism (e.g., vertebral body or spinous process fractures) exists. Ryan and Henderson (1992), in an epidemiology study of 657 patients with cervical spine injury, found that older age groups were more likely to sustain upper cervical spine trauma, while a greater percentage of younger age groups sustained lower cervical spine trauma. Age could account for the higher number of C6-C7 fractures seen in the case occupants versus the mid-sagittally loaded cadaver specimens (Table 4). The average age of cadavers included in this study was 63.8 years (±12.4 years), which is 22.6 years older than the average age of the CIREN occupants.

CIREN case occupant 163690, a 42 year-old male seated as the front right passenger, was involved in a 4-quarter turn rollover. He was positioned on the far side of the roll. The vehicle traveled down an embankment and underwent significant intrusion over the passenger seat from the A-pillar and B-pillar. He sustained a bilateral facet dislocation at the C5-6 level, with fractures to the C5 laminae, the right C5 superior facet,

C6 right facet and transverse process, and right C7 transverse process (Table 3). The occupant suffered a scalp abrasion and contact evidence (hair) indicated contact with the roof near the roof side rail. It is likely that the C5-6 BFD was the result of global compressive buckling and subsequent compression-flexion at that level (Nightingale et al., 1997). The adjoining (C5, C6) facet, lamina, and transverse process fractures are a result of compression favored to the right side. The C7 transverse process fracture was likely due to an avulsion, as there was no facet fracture that extended into the posterior tubercle of the transverse process at C7. Transverse process fractures are underrepresented in the experimental studies as their mechanism is likely due to tractions from the active levator, longissimus, and intertransversarii muscles, which all insert or originate on the tubercles of the transverse processes. This is an inherent limitation of cadaveric tissue. This example demonstrates that global axial compression was the key loading component, but deducing injury mechanism at the local level can be more complicated due to lack of representation *in vitro*.

Axial loading in the cephalocaudal direction was found to be the predominant global loading component responsible for injury in all of the CIREN occupants. Previously, authors have surmised that axial loading takes place during the rollover event based on dummy loading in dynamic rollover tests (Viano and Parenteau 2008, Bahling et al. 1990, James et al. 2007). The current study tested this hypothesis by analyzing clinical rollover injuries. Through assessing this finding, laterally eccentric load vectors were found to be associated with injury in the field data at a high level of incidence. This is the case in only three existing cadaver studies. Fracture of the articular facets was the most common injury sustained by the rollover-involved CIREN occupants at 32.4% of

their total fractures, while this fracture was only seen 8 times in the 165 cadaver specimens loaded axially. Vertebral body fractures, including burst, teardrop, and wedge fractures, were the most prevalent injuries produced in these cadaver tests; 98 of these injuries were produced. In contrast, vertebral body fractures were the third most common injury in the CIREN occupants. The second most prevalent injuries in cadaver studies were spinous process fracture, which occurred 43 times (21.0%) in the axially-loaded cadaver but only three times (4.1%) in the CIREN occupants. Injuries to the vertebral body and spinous process usually do not require any lateral, asymmetric loading to occur. In a similar finding, epidemiological evidence of laterally directed compression during rollover has been shown by Bambach et al. (2013), proving the importance for lateral bending moment as an injury risk parameter for the assessment of ATDs and the development of neck injury criteria with some level of clinical relevance.

Nusholtz et al. (1983) conducted a test series attempting to study the effects of loading upon non-mid-sagittal initial postures. Eight cadaver specimens were dropped on their heads in seated positions with their head, neck, and mid-spine positioned in various orientations. Multiple specimens were given lateral eccentricities of the head and neck, as well as initial torsion or twist about the neck's longitudinal axis before impact. However, all but one of these specimens (Specimen 8) were retested several times. Nusholtz and Kaiker (1986) loaded the axially-rotated heads of five full cadavers, producing unilateral and lower cervical spine fractures in three specimens. One BFD was created with the absence of adjoining impaction fractures. Toomey et al. (2009) loaded head-cervical spine specimens obliquely or with initial lateral eccentricity, citing rollover as an experimental motivation. As a result, the authors produced injuries similar in fracture

type and location to those seen in the CIREN occupants. As they loaded the skull with an oblique vector, they produced 12 fractures, eight of which were purely unilateral in nature, including facet, pedicle and lamina fractures. The data from these studies associate the authors' methods to a spectrum of injuries that is more similar to the CIREN field data. As these studies have involved only nine cadaver tests that displayed injury, future investigations are needed and should involve a similar asymmetric load vector.

The unilateral articular facet fracture that extends into the ipsilateral pedicle or transverse process is one of the most common cervical spine injuries sustained in rollover crashes, present in eleven different CIREN case occupants, and likely the result of lateral compression. Allen et al. (1982) attributes a compression-extension mechanism to this injury, 27 years before the first of its type was produced experimentally in a cadaver (2009). While this fracture pattern may be associated with extension and compression, it is typically seen on one side rather than bilaterally in rollover-involved occupants. Further, three of the CIREN case occupants sustained unilateral facet dislocations. The mechanism associated with this injury is believed to be flexion with simultaneous rotation about the longitudinal axis (Braakman and Vinken 1967). There were no UFDs represented by either subset of cadaver loading. It is the understanding of the authors of this study that tested cadaver specimens have displayed facet dislocations visible in high speed video that were not detected in post-test necropsy due to the lack of musculature that would hold the locked facet configuration in place. Therefore, the number of UFDs and BFDs may be underrepresented in the cadaver population.

Reasons for the infrequent employment of lateral loading bias in the literature may be related to the lower severity nature of unilateral injuries compared to bilateral or

AP injuries. Of the CIREN occupants' 52 unilateral fractures and dislocations, 49 (94.2%) were AIS 2 fractures; the remaining were two AIS 3 unilateral facet dislocations and an AIS 5 unilateral locked facet resulting in a cord contusion. Of the occupants' AIS 3 or higher injuries, 72.7% were symmetric injuries, reinforcing the conventional wisdom that AP and bilateral injuries are more catastrophic and a reason why they have been more extensively investigated.

Conclusions

Existing research adequately characterizes serious injuries, which appear due primarily to mid-sagittal axial loading, while more common, less severe injuries due to asymmetric axial loading are not well covered in the literature. The current study examined this by analyzing the pathologies and specific spinal injury mechanisms from 23 CIREN rollover crash cases and comparing the cervical spine injuries suffered by the case occupants to those produced in 165 axially-loaded and 10 eccentrically-loaded cadaver tests. This methodology for determining injury mechanism was applied to each CIREN case, where single cadaveric specimens could not be used to fully explain a CIREN occupant's collection of injuries. In most CIREN cases, occupants suffered at least one unilateral fracture, indicating an asymmetric loading scenario, one that has been infrequently recreated *in vitro*. Possible reasons for this may be due to the less severe nature of lateral injuries compared to AP or bilateral injuries, such as BFD. Facet dislocations were produced experimentally, but often lacking the associated fractures evidenced in most of the case occupants with facet dislocations. Passive musculature and muscle tensing may be responsible for the associated fractures in the living population and muscle spasms may also explain the deficit in UFDs in the cadaveric population. The

overarching conclusion of the study is that all rollover-involved CIREN occupants appeared to experience an axial load as the primary loading mechanism with a laterally eccentric compressive component present in about two-thirds of occupants with neck injury. However, more compressive neck injury tolerance studies are needed to highlight differences in injury patterns in rollovers versus the current experimental body of literature before they can be used to develop injury criteria for the human neck. The presence of non-sagittal loading can alter the injury pattern and is a likely cause of this difference. These findings further emphasize the need to examine the effects of asymmetric loading and active musculature on cervical spine injury patterns.

Acknowledgments

This study was supported by the National Highway Traffic Safety Administration (NHTSA) under Cooperative Agreement No. DTNH22-09-H-00247. Views or opinions expressed or implied are those of the authors and are not necessarily representative of the views or opinions of the NHTSA.

Chapter Two

Motivation, Methods, and Analysis of UVA Cervical Spine Testing with Post Mortem Human Surrogates

INTRODUCTION

Quadriplegia is the signature consequence of injury in rollover crashes. Due to the catastrophic nature and frequency of cervical spine injury in rollover, it has rightly received special attention in the scientific literature (Ridella et al., 2009; Toomey et al., 2009; Viano et al., 2008; Bambach et al., 2013). Any attempt to address rollover crash injuries comprehensively should address the cause and potential prevention of serious neck injuries.

The roof and seatbelt work together to limit the vertical excursion of an occupant in a rollover crash. A role of a strong roof is to hold the seatbelt anchors as far above the ground as possible when the vehicle is inverted. When the roof crushes, the seatbelt anchors lower which effectively increases the vertical excursion of the occupant. Other contributors to vertical excursion are changes in seatbelt geometry and the compliance of the human body. In a significant roof-to-ground impact, the vertical excursion of the occupant can exceed the available headroom, often rendering a head impact into the roof. The head interfacing with a deforming roof can act as a pocketing end condition for the head, restricting the head's planar motion to the roof as the torso augments cephalically and compresses the neck (Burke et al., 2009). The mass of the occupant's torso is decelerated primarily by axial loading through the neck, which can lead to injurious levels of neck compression.

A key parameter that must be determined in order to understand how torso augmentation causes neck injury is the effective mass of the torso. A simple rigid body lumped-parameter model of the upper body can be used to illustrate the concept of effective mass. If the head, neck, and upper torso are assumed to be rigidly coupled

together, then a drop onto the top of the head can be modeled by lumping the upper torso into a single effective mass. The expected force response in the neck is a sinusoid whose amplitude and duration are determined primarily by the effective mass of the torso and the stiffness of the contact between the head and roof of the vehicle (Figure 1).

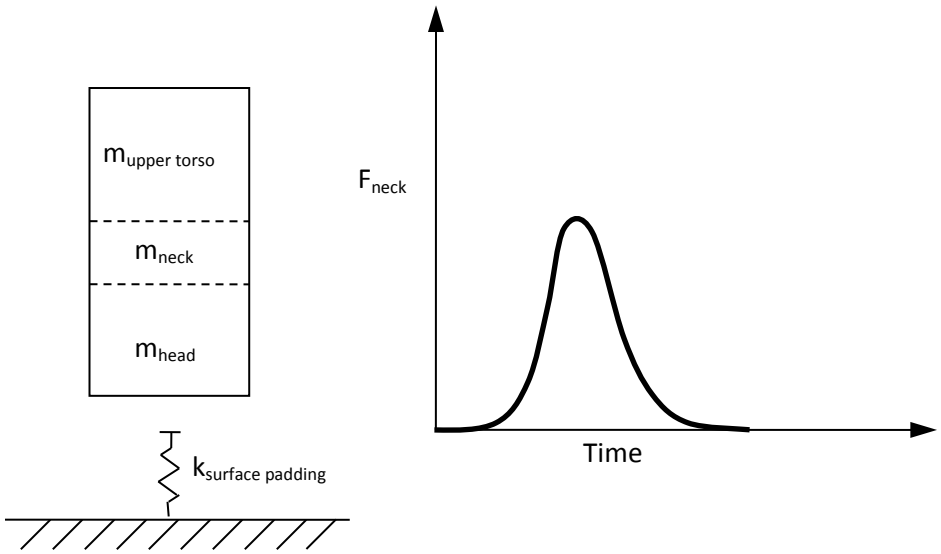

Figure 1: Lumped-parameter model of the upper body in which the torso is modeled as a single effective mass.

Obviously, this type of model is an oversimplification; the human body is deformable and the head, neck, and torso are not rigidly coupled together. It is more realistic, perhaps, that a lumped-parameter model be used in which the torso is modeled as a progressively falling mass. A biphasic response, like those produced in cervical spine studies by Nightingale et al. would therefore be experienced (Figure 2). In this model, the first peak in neck force is due to the suddenly stopped head being loaded by the portion of the upper torso that is well-coupled to the neck. The second peak is likely to occur when the entire neck and torso has reached maximum compression, which would correspond to peak compression of the torso spring in the lumped-parameter model. Biphasic response has been published in the findings by several authors studying neck

compression (Nusholtz et al., 1981, 1983; Nightingale et al., 1997; Pintar et al., 1990).

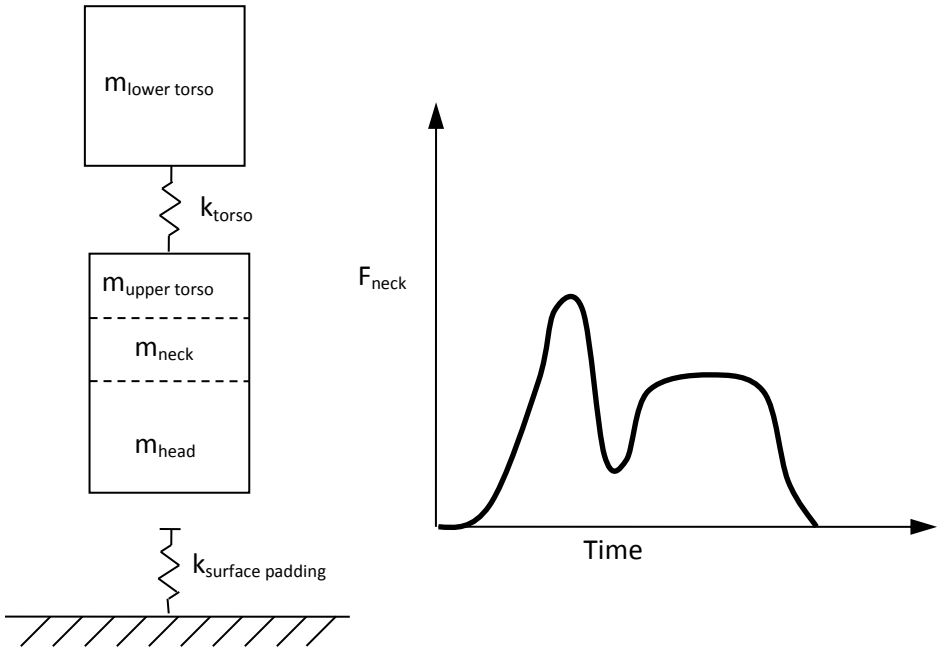

Figure 2: Lumped-parameter model of the upper body in which the torso is modeled as a progressively applied mass.

In testing by Nightingale et al. (1997), cadaveric head-neck complexes were rigidly mounted to a block weighing 16kg (35lbs), which was chosen (somewhat arbitrarily) to represent the effective mass of the torso, estimated through a total human body computer model called the Generator of Body Data (GEBOD). All of the specimens in these tests were subjected to impact velocities greater than 3 m/s sustained neck injuries. The neck injury rate in full-body cadaveric testing is considerably lower than this (Viano et al., 2008), which suggests that the actual effective mass of the upper torso may be less than 16 kg. As a long-term goal of this study, head force and upper neck force measured on a full cadaver could be used in a finite element (FE) simulation to extrapolate a transient effective mass of the torso, an improvement from the single mass model of Nightingale et al. (1997).

A second goal of this study pertains to evaluating the effect that a fixed lower neck end condition has on injury outcome. Nightingale's test fixture uses a fixation method that allows one DOF on a vertical track. A previous study by Myers et al. (1991) explored the influence of end condition on injury to the cervical vertebrae. The authors received very different cadaver pathologies in spines subjected to three different end conditions: lower cervical spine bilateral facet dislocations in the rotationally constrained group, bony compression fractures in the fully constrained group, and no injuries in the unconstrained group (Figure 3). The end condition that most accurately represents a full cadaver's lower neck-to-thorax interface has yet to be determined and is explored in this study.

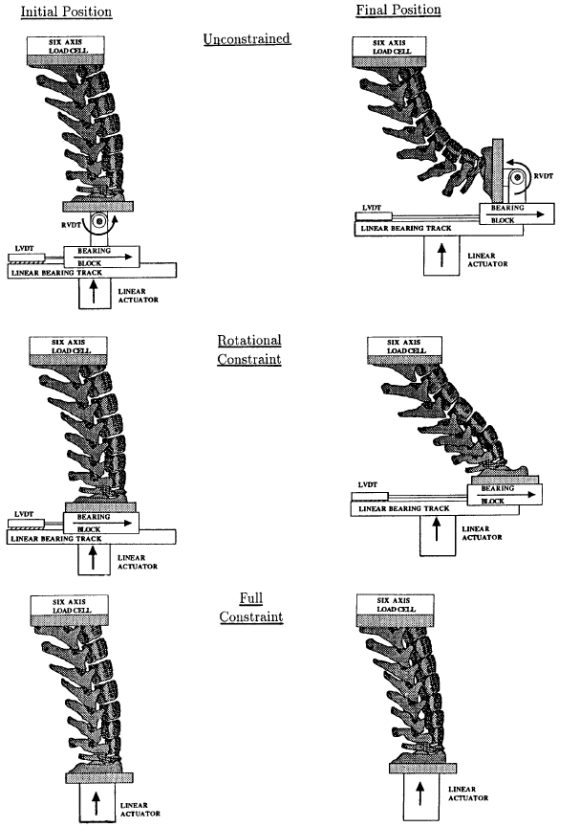

Figure 3: Schematics of Myers et al. (1991) three boundary conditions for spines subjected to a quasi-static compressive load, achieving strikingly different cervical spine injuries for each constraint.

Finally, this study intends to explore the effects of torso augmentation on dynamic

cervical spine buckling, a phenomenon witnessed by several authors in *in vitro* spine tests (Nightingale et al., 1996, 1997; Toomey et al., 2009; Yoganandan et al., 1986; Bauze and Ardran, 1978). Buckling, according to Duke Researchers (Nightingale et al.), is characterized by a "snap-through," visible, and rapidly occurring transition from one equilibrium configuration to another. Typically, buckling of the cervical spine is associated with extension to the mid and upper cervical spine (C1-C5) and flexion to the lower (C5-C7) cervical spine. This two-wave or 2^{nd} order buckling mode that the cervical spine has been shown to take on at a critical axial load should be highly dependent on end condition, as other columns and slender beams show buckling deformation to be contingent upon end condition (Hibbeler, 2004). The type of 2^{nd} order buckling seen in previous cervical spine biomechanical studies should be investigated for an unconstrained lower neck end condition, in which a veritable human torso is connected.

From Nightingale et al.: "Buckling does not necessarily result in fracture or dislocation, but plays a central role in the pre-injury kinematics." To aid the authors of this current study and of future investigations in determining injury mechanism on the local vertebral level, it is paramount to ascertain pre-injury kinematics through the timing and geometric configurations associated with cervical spine buckling. Previously, high-speed film and retroreflective targets have been used to observe dynamic buckling modes which have been observed in both entire neck tests and in ligamentous cervical spines (Yoganandan et al., 1990; Nightingale et al., 1997). Radiological viewing of the column during dynamic loading will not be subject to obstruction from skin and soft-tissue, and could be a useful tool in establishing the point during the loading sequence in which

higher-order buckling occurs.

Buckling also helps to explain why minimal head-to-torso (cephalocaudal) motion is required to create neck trauma, occurring very shortly after loading to the head. In one of their specimens, Duke saw the spine take on a new equilibrium position 2.0msec after the peak axial force was registered. After the new equilibrium position was established, the axial load continued and reached a second peak load (Nightingale et al., 1997). Other authors, such as Pintar et al. (1995), did not report neck compressive buckling but still reached neck fracture at relatively low head-to-neck displacements (17.95±3.00mm). The same authors report short time windows (5-6msec) between impact and compression fracture (Yoganandan et al., 1990). Still, studies of this kind have never been performed on full cadavera. Similarly, vertebral buckling kinematics are difficult to characterize using external video due to obstruction from skin and soft tissue. Ultimately, this study aims to relate head-neck kinetics to buckling kinematics for better understanding of the head-neck-torso complex during axial compression.

Materials and Methods

Full cadaver drop tests were performed at the Center for Applied Biomechanics (Charlottesville, VA, USA). Four unembalmed full male cadavers were used for this initial, self-funded test series. 50^{th} percentile male cadavers were targeted; specimens with the following heights and weights were used.

UVA Specimens	Age	Weight (kg)	Stature (cm)
516	89	54.4	155
552	82	77.6	170
631	71	68.9	178
553	60	57.2	170

For all tests, subjects were positioned upside down with a load platform centered beneath the crown of the head. A tactical harness (Yates Gear Inc, Redding, CA, USA) was firmly fitted to the subject's torso and pelvis. Tethers were attached to several locations on the harness and the body; the rope lengths adjusted using Nylon rope tenting attachments (Taut-Tie, Turin, NY, USA) to fix the orientation of the body into a nominal driver's seated position (Figure 2). A Solenoid release mechanism was used to release the system of Nylon rope tethers attached to the cadaver in unison.

A standard seating position established by University of Michigan Transportation Research Institute was implemented, using a torso angle of 20-27 degrees from the vertical (Manary et al., 1998), similar to nominal seatback angles. The positioning of the head and neck complex was performed to identically match the cadaver tests series ran at Duke University by Nightingale et al. (1996). A 25-degree C7-T1 disc orientation was chosen by Nightingale et al. (1996) to preserve the resting lordosis present in drivers as per a study by Matsushita et al. (1994).

Cadaver drop heights, measured from cadaver apex to the top of the foam, were targeted around 0.53m, the same height used by Duke University. This drop level was chosen as the height that is less than what is required to cause skull fracture, but still able

to produce fracture to the cervical spine (Nightingale et al., 1996). An impact velocity of around 3.14 m/s was anticipated.

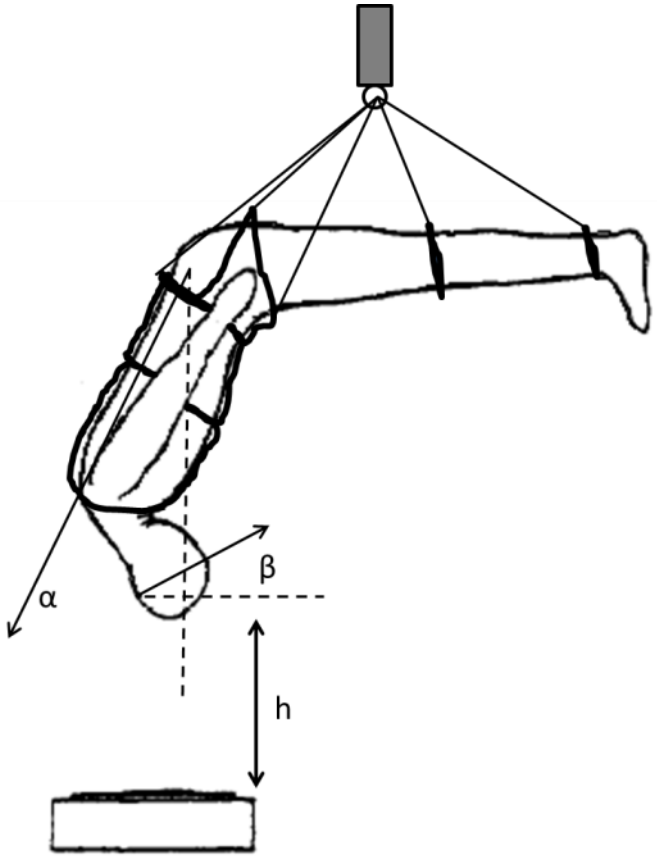

Figure 4: Schematic of the inverted cadaver drop test. Nylon rope was used to suspend the subject and a Solinoid release mechanisms released the tethers. The tethers are used to adjust the torso angle, α, to 25-degrees from the vertical, and the Frankfurt plane angle, β, to 0-degrees from the horizontal. The height, h, is set to achieve an impact speed of at least 3.1m/s.

A 25-degree lordosis angle was implemented at the first thoracic vertebrae. Full cadaver drop tests do not have transected necks, making this angle more difficult to achieve. The angle was achieved by inserting metal screws into the pedicles of the cadaver's first thoracic vertebrae, using CT radiology to ascertain the angle of the screws relative to the T1 endplate, and adjusting the inverted cadaver's screw angles to achieve the desired (25-degree) lordotic orientation (Figure 5).

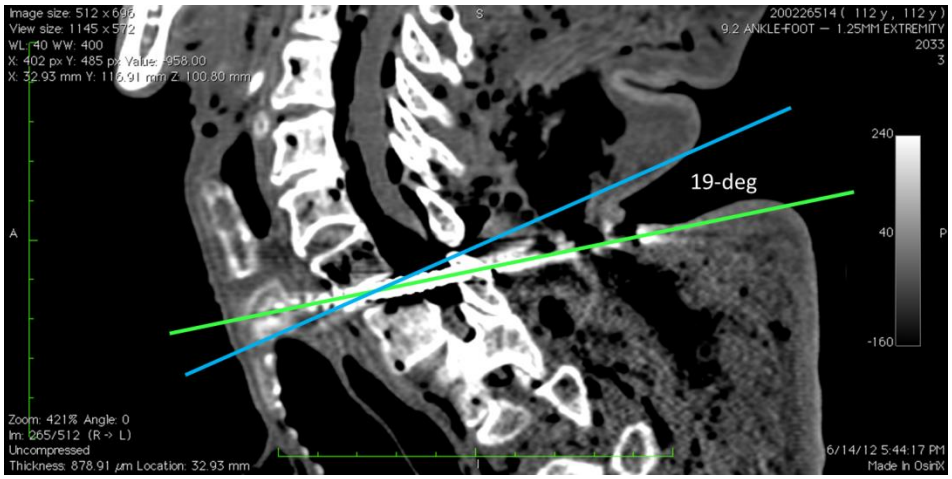

Figure 5: Angle between C7-T1 endplate and right pedicle screw: 19-degrees. For this example, a 6-degree screw angle from the horizontal will result in a 25-degree endplate angle, matching the nominal driving head orientation published by Matsushita et al. (1994). Others shown in Appendix B.

Instrumentation

The pedicle screw orientation was used to gain a reading of the endplate angle at T1 and also served as a mounting location for a 6-channel sensor cube. Each cube contained a Tri-axial accelerometer array (Endevco 7264 Piezoresistive accelerometer, San Juan Capistrano, CA, USA) and three angular rate sensors (ARS) (Diversified Technical Systems, Seal Beach, CA, USA). Another cube was placed just superior to the lateral Frankfurt Plane on the right side of the head to measure head center of gravity (CG) acceleration (Figure 6). The head cube location relative to the Frankfurt Plane and head CG was determined using a coordinate measurement machine (CMM), a 3D measuring arm (FARO Technologies, Lake Mary, FL, USA). The CMM also defines the exact position and orientation of the subject and 6-degree-of-freedom (6DOF) cubes once the final position of the surrogate has been set. A cube at T8, the vertebrae closes to the CG of the torso, was inserted to measure the torso CG accelerations for two of the four tests.

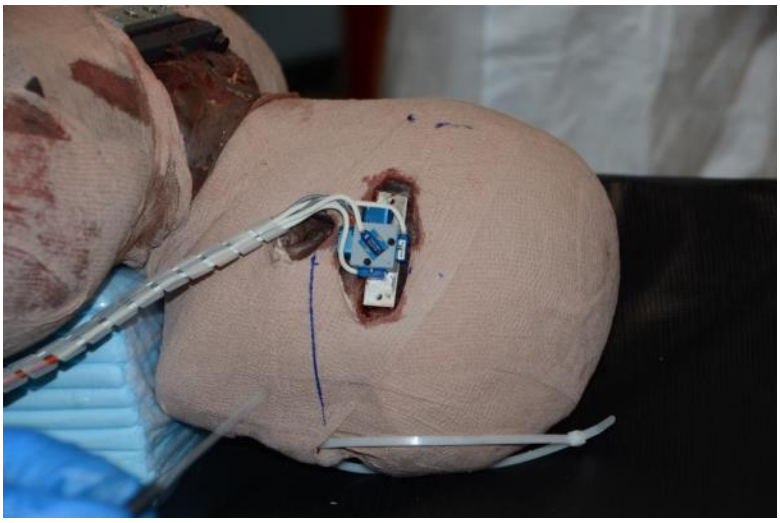

Figure 6: A mounted 6 degree-of-freedom cube adjacent to the blue Frankfurt plane line. CMM data allows the research team to develop transformation matrices needed to transform cube data to the CG of the head.

A five-axis load cell (Denton B-3868-D, Humanetics, Plymouth, MI, USA) was placed beneath the crown of head and the targeted impact location. The load cell was rigidly mounted to an impact plate. A padded surface, used to prevent planar movement of the skull during neck compression, was firmly adhered to the impact plate. One-inch padding, a light-density polyvinyl chloride foam (V700 Series 1.00", Gaska Tape Inc., Elkhart, IN, USA), matches the padding used in Nightingale et al. (1996, 1997) and Frechede et al., who mimicked Nightingale's study for ATDs (2009). The specifications of the padding are provided in Appendix B.

Two DTS Slice data acquisition systems (Diversified Technical Systems, Seal Beach, CA, USA) were used as well as two high-speed video cameras (NAC GX1, NAC Image Technology, Simi Valley, CA, USA). Two of the four tests were radiographed using a Dynamic X-ray System to capture the compressive kinematics of cervical spine upon loading. The X-ray tube and generator were placed laterally, viewing the full cervical spine upon impact at a sagittal angle. The subject's hands were tied behind their

backs, lifting the shoulder slightly as to not obstruct the radiology of the cervical spine.

Radiology will aid the research team in discerning the point of cervical spine buckling post-impact, typically occurring within the first 15ms of axial loading (Yoganandan et al., 1990; Nightingale et al., 1997). For these studies, injury to the specimen was determined via post-test necropsy and diagnostic CT, linking a given cervical spine fracture, dislocation, or soft-tissue damage with its surmised injury mechanism. This retrospective linking of an injury outcome with a previously accepted injury mechanism has been widely used and subject to criticism in cervical spine biomechanical literature (Myers and Winkelstein, 1995; Allen et al., 1982; Foster et al., 2012). Dynamic x-ray in this test series allows the research team radiological viewing capabilities yet to be achieved in cervical spine injury testing. Following the test series, post-test necropsies were performed on each subject to determine location and type of skeletal fracture. Specifications on the x-ray equipment used are included in Appendix B.

Pre-test cadaver orientation and anthropometric measurements were taken prior to drop initiation (Appendix B). It was the intent of the research team to match each position closely between cadaver tests, as slight changes in neck eccentricity and alignment can influence injury outcome (Pintar et al., 1995; Nusholtz et al., 1983; Nusholtz and Kaiker, 1986).

Data Processing

Data from the impact load plate and Head accelerometer cubes were transformed to consistent global coordinates. Prior to positioning the specimen, with the surrogate supine, the lateral projections of the head CG were marked bilaterally. Using data

presented by Robbins (1983), the lateral projection of the head CG, as determined from exterior anatomical landmarks, will most accurately be at a location superior to the Frankfurt Plane by a distance equal to 25 % of the distance from the Frankfurt plane to the top of the head, and 8.5 mm anterior to the tragion. The posterior projection of the head CG will be marked at a distance half way between the lateral projections, measured by traversing the exterior of the head posteriorly along a line parallel to the Frankfurt Plane. The head CG is located at the center of the line connecting the lateral projections. The lateral projections determined the local Y-axis of the head, with positive oriented to the right. The local Z-axis is determined to be perpendicular to the plane containing the lateral and posterior projections of the head CG, with positive oriented toward the torso. The X-axis of the local system is the cross-product (perpendicular) to the Y and Z-axes, with positive pointing anteriorly (Figure 7). This coincides with the head coordinate system methodology used by Kerrigan et al. (2008).

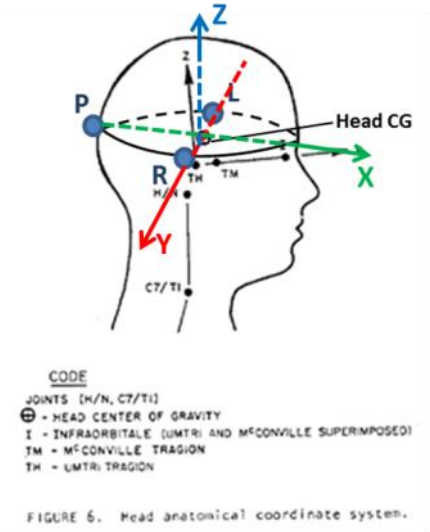

Figure 7: Three FARO points at the three (left, right, and posterior) landmarks shown here will be used to determine the head CG location and coordinate system.

Using the CMM data, the location and orientation of the head local reference

frame was defined from the three projections of the CG in the CMM reference frame. The least squares pose estimator was used with locations of the cube digitizing points in the cube's reference frame (from the cube drawing) and the locations of the cube digitizing points in the CMM reference frame (from the CMM data) to determine the location and orientation of the cube in the CMM reference frame. Then, using the location and orientation of the head's reference frame and the location and orientation of the cube's reference frame (both defined in the CMM reference frame) the vector transformation relating the cube's local reference frame to the head's local reference frame and the vector between the cube center and the head CG (segment origin) was determined (Cappozzo et al., 1997).

Transformation of locally measured kinematics data to the global reference frame relies on the calculation of the time history of the transformation matrix. Kerrigan et al. (2008) shows the time history of the local-to-global transformation can be determined by simultaneously solving nine coupled ordinary differential equations or by simultaneously solving three ordinary differential equations and applying the geometry-based transformation matrix equation discussed by Bortz (1971). This allowed for the head acceleration, velocity, and position data to all stay oriented to the original global coordinate system.

The linear accelerations measured by the head cube sensors were transformed from the locations of the accelerometers to the center of the 6DOF cubes by applying the rigid body kinematics equation (Shames, 1999):

$$\mathbf{a}_p = \mathbf{a}_o + \boldsymbol{\omega} \times \left(\boldsymbol{\omega} \times \boldsymbol{\rho}_{op}\right) + \boldsymbol{\alpha} \times \boldsymbol{\rho}_{op} \qquad (1)$$

where, in this case, $\boldsymbol{a}_o$ is the acceleration of the CG of the head, $\boldsymbol{a}_p$ is the acceleration

measured by the accelerometers at the cube, $\boldsymbol{\rho}_{op}$ is the vector from the head CG to the seismic mass of each accelerometer, and $\boldsymbol{\omega}$ and $\boldsymbol{\alpha}$ are the angular velocity and the angular acceleration of the cube, respectively. The cube's angular acceleration vector $\boldsymbol{\alpha}$ was determined using the cube's angular velocity data and a custom forward and backward filtering technique with a second-order Butterworth algorithm with zero phase shift and -3dB.

Load cell, accelerometer, and ARS data was filtered using Channel Frequency Class (CFC) filters built into the DIAdem Software (National Instruments, Austin, TX, USA). Acceleration and force channels were filtered with CFC 180 filters while angular rate channels filtered with CFC 60. Initial offset was debiased for all channels.

Using the global head CG acceleration, a free-body diagram was used to calculate the force at the upper neck, or the force applied to the occipital condyles by the atlas (C1):

$$\mathbf{F_{LC}} = \mathbf{F_{UN}} + \mathbf{a_{CG}}\mathbf{m_H} \tag{2}$$

where $\mathbf{a_{CG}}$ is the acceleration at the Head CG and $\mathbf{m_H}$ is the mass of the head, measured during post-test necropsy. Because the connection between the Head CG and occipital condyles is rigid (given the absence of skull fracture), then the acceleration at the upper neck, $\boldsymbol{a_{UN} \approx a_{CG}}$.

So, the force at the upper neck (Figure 8),

$$\mathbf{F_{UN}} = \mathbf{a_{CG}}\mathbf{m_{N+T}} \tag{3}$$

where $\mathbf{m_{N+T}}$ is the effective mass of the neck and torso.

Therefore, the effective mass of the neck plus torso can be solved with the measurable data,

$$\frac{\mathbf{F_{LC}}}{\mathbf{a_{CG}}} - \mathbf{m_H} = \mathbf{m_{N+T}} \tag{4}$$

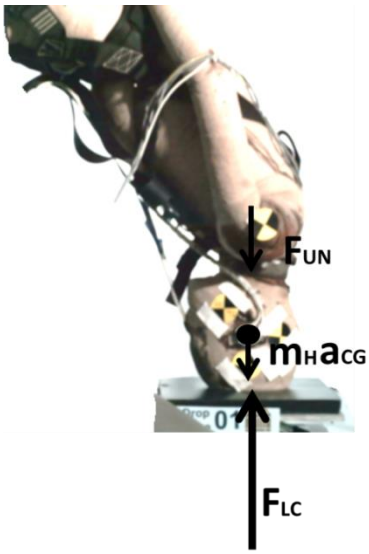

Figure 8: Visualization of the free-body diagram used to derive the upper neck force.

All force, acceleration, and time data were scaled to the 50th percentile male based on a dimensional analysis approach, assuming that the four male subjects were geometrically similar with equivalent mass density. The transverse cross-sectional area (CSA) of the sixth cervical vertebrae's inferior endplate was arbitrarily chosen as an area scaling factor for the four cadavers, which were scaled to a reference cross-sectional area of the C6 inferior endplate in the Global Human Body Models Consortium (GHBMC) 50th percentile male. These CSA values were taken via transverse slices of the pre-test CT scans and measured at the point of interest using imaging software (OsiriX Viewer). Screenshots of the endplate traces are shown in Appendix B. Endplate CSA ranged from 3.124 – 4.686 cm^2, with Cadaver 552 having much larger endplate area than the other three cadavers. This cadaver was also the heaviest and bulkiest specimen with the

highest bone mineral density.

RESULTS

Appendix B presents raw and scaled data measured from the four cadaver drop tests. A summary of the biomechanical data scaled to the 50th percentile male is shown in Table 1.

UVA Specimen Number	Impact Velocity (m/s)	Maximum Axial Head Force [N] (time in ms)	Maximum Axial Upper Neck Force [N] (time in ms)	Peak Resultant Head Acceleration [g] (time in ms)	HIC	Peak Resultant T1 Acceleration [g] (time in ms)
516	3.08	3589 (9.1)	2472 (9.6)	50.74 (8.4)	38.53	63.87 (16.1)
552	3.01	3355 (7.9)	2217 (19.5)	43.45 (7.1)	29.81	50.35 (10.5)
631	3.63	3982 (8.4)	2709 (10.4)	63.83 (8.0)	69.71	105.2 (16.7)
553	3.54	3778 (9.8)	2416 (11.7)	73.44 (8.6)	119.96	42.03 (18.3)

Table 1: Maximum forces and peak loads with respective time points for head impact tests of the four cadaveric specimens. Scaled data is shown. Time data is in milliseconds following head impacting the foam surface. Resultant head acceleration given for applicability to Head Injury Criteria (HIC) formula.

The vertical drop heights and associated impact velocities were lower for 516 and 552 and higher for 552 and 631. Specimens were subjected to compressive forces ranging from 3355 to 3982 N when scaled to the 50th percentile male. Figure 9 shows the scaled force history data, illustrating the hypothesized biphasic load response for all four specimens.

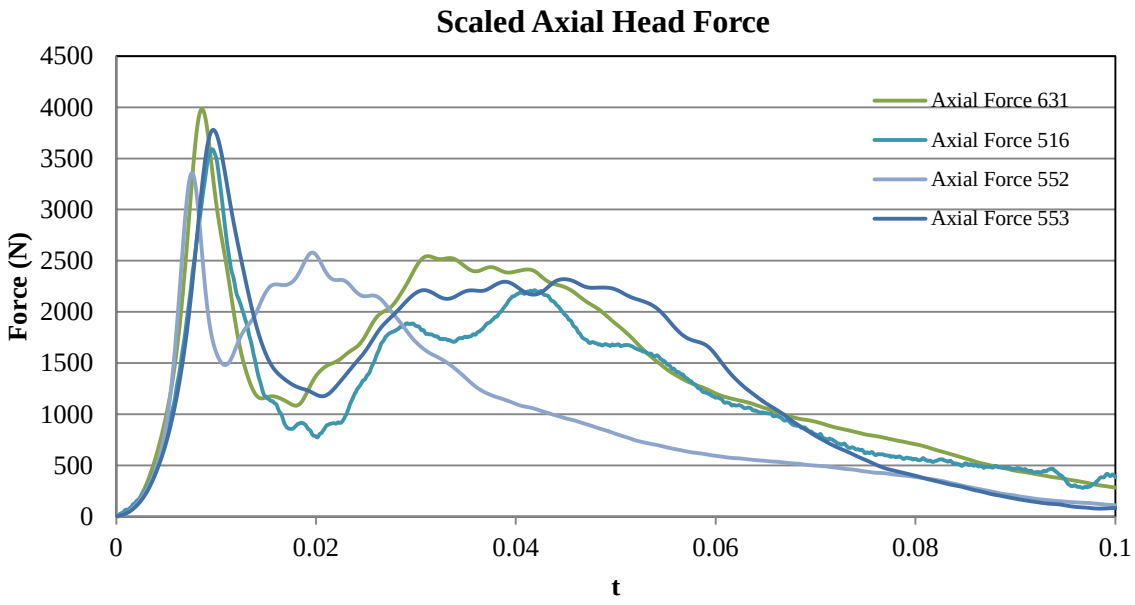

Figure 9: Axial (z-direction) head force traces for the first 100msec of head loading from the padded impact plate. Raw data shown in Appendix B.

Force reached critical loads (maximum axial load) between 7.9 and 9.8msec following head loading. These bifurcation points then saw sharp drops in compressive load. The first peak is associated with the stiffness of the head, neck in original lordotic configuration, and some mass of the upper torso. Here, the head force reaches a maximum before T1 maximum acceleration. While the first peak is associated with head-neck-upper torso inertia, a second peak is associated with the inertia of the lower torso mass. The first local maximum in each second loading phase was reached within 12 to 23msec for the four tests. The torso inertia is also reflected in the upper neck force plots, loading the cervical spine axially as it augments toward the head and then again upon reconfiguration of the column after buckling. Upper neck force peaks were reached within 0.5 and 2.0msec following axial head force peak and reflected values within 63.9-68.9% of the peak axial head force, equaling 2217-2709N, respectively (Figure 10). T1 accelerations were greater than head CG accelerations in three of the four specimens, due

to the considerably smaller relative mass of the T1 vertebra to the head.

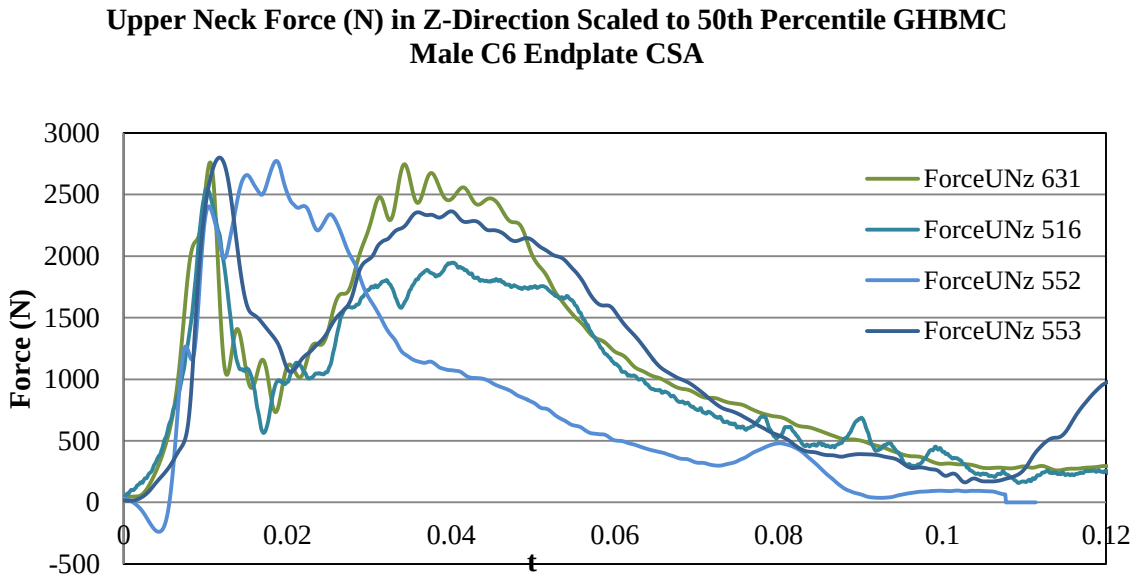

Figure 10: Scaled upper neck force calculated for each specimen.

Injuries

The compression tests produced the injuries shown in Table 2. Also shown are the injuries produced in Nightingale et al. (1997) from the same head end conditions: padding on a flat impact surface. Three of the four cadavers sustained bony fracture while Cadaver 516 sustained no bony fracture. Joint laxity or attenuation was felt by autopsy surgeons; however, spondylolisthesis or facet dislocation was not definitely determined for any specimen. All three sustained symmetric fractures, either to structures along the antero-posterior line (odontoid, vertebral body) or bilaterally (pedicles). No asymmetric fracture or attenuation was noted.

UVA Specimens	Injuries	Duke Specimens	Injuries
516 (89, M)	**None**	N03 (75, M)	**C5-6 disc, C6-7 BFD**
552 (82, M)	**C7 bilateral pedicle fractures**	N02 (75, F)	**C1 anterior ring, C2 Hangman's, Type-III odontoid, C7 burst, C6 lamina and pedicle**
631 (71, M)	**C4 horizontal vertebral body fracture into superior teardrop**	D40 (53, F)	**C1 partial Jefferson, C5 burst, C6 lamina and pedicle**
553 (60, M)	**Type-III odontoid**		

Table 2: Cadaver pathologies discovered by UVA via post-test necropsy. Injuries produced in same head end condition tests by Nightingale et al. at Duke University shown on the right (1997).

Photographs of the three fractures are shown in Figure 3. All three fracture types have been associated with a compression-extension injury mechanism according to prior literature (Althoff et al., 1979; Nightingale et al., 1997; Winkelstein et al., 1997; Pintar et al., 1989; Maiman et al., 1983). The injuries are consistent with external high speed video as well as radiological video capturing the top four vertebrae for Cadavers 631 and 553. Kinematic analysis determined that the upper cervical spine shifts anterior to the original orientation of the column, bending backward into extension. The lower cervical spine appears to bend in flexion concomitantly.

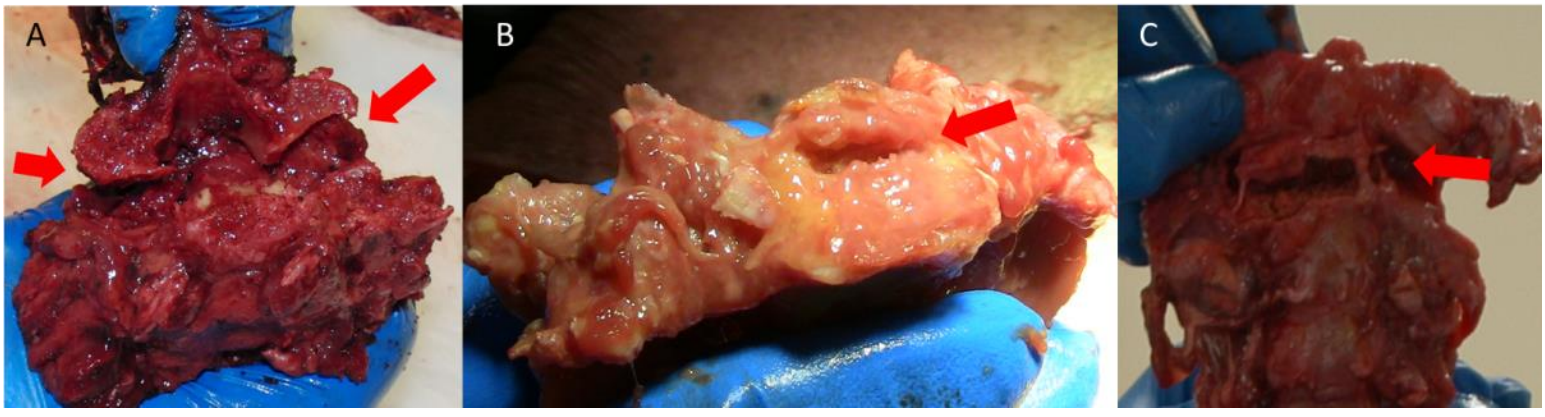

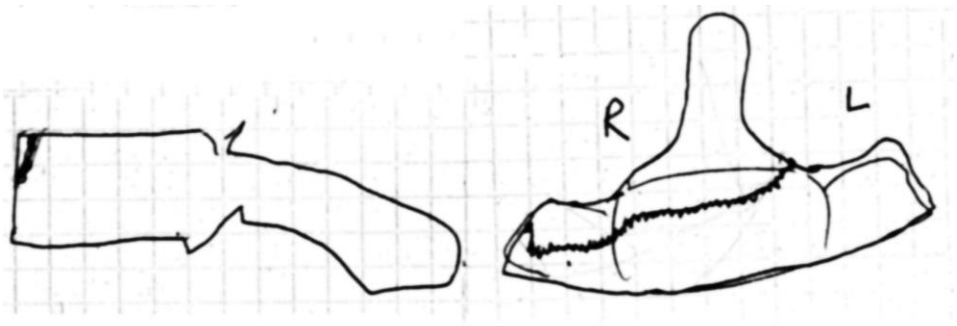

Figure 3: Photographs and sketches of cadaver pathologies of 552 (A), 631 (B), and 553 (C) taken during post-test necropsy. Left sketch is side view of superior teardrop fracture to 631 and right sketch is coronal view of Type-III odontoid fracture.

Buckling Behavior

Instantaneous buckling of the cervical spine was observed in all four cadaveric specimens. There are two observable events occurring quickly after head contact that evidence buckling phenomena: the first is a steep decrease in the axial load to the top of the head occurring at a bifurcation point. An orientation change occurs at the onset of buckling where *l*, the longitudinal length of the membered column, rapidly decreases. The critical load, P_{CR}, represents the load for which the spine is on the verge of buckling. The time of peak critical load is shown in Table 4. For specimens 631 and 553, the next event evidencing dynamic buckling was seen in the X-ray footage, characterized by gross anterior motion of the upper cervical spine segments. The rapidity of this occurrence was evidenced via motion artifact, despite videography taken at 1000Hz. Therefore, Cadavers 631 and 553 have two time points associated with buckling: buckling measured (time where $P = P_{CR}$) and buckling seen (time at video where orientation change seen). The corresponding external motion for each of these relevant time points is shown in Figure 11 for Cadaver 631.

UVA Specimen Number	Critical Load/Bifurcation Time P = P_{CR} (ms after contact)	Time of Head Arrest (v=0) (ms after contact)	Video frame buckling first seen (ms after contact)	Time of torso inertial loading onset (2nd load phase)
516	9.7	18.6	-	20.9
552	10.3	24.7	-	14.8
631	9.4	27.4	10	20.1
553	10.1	15.8	11	21.3

Table 4: Times in raw time scale. T=0 is at point of initial head contact with foam.

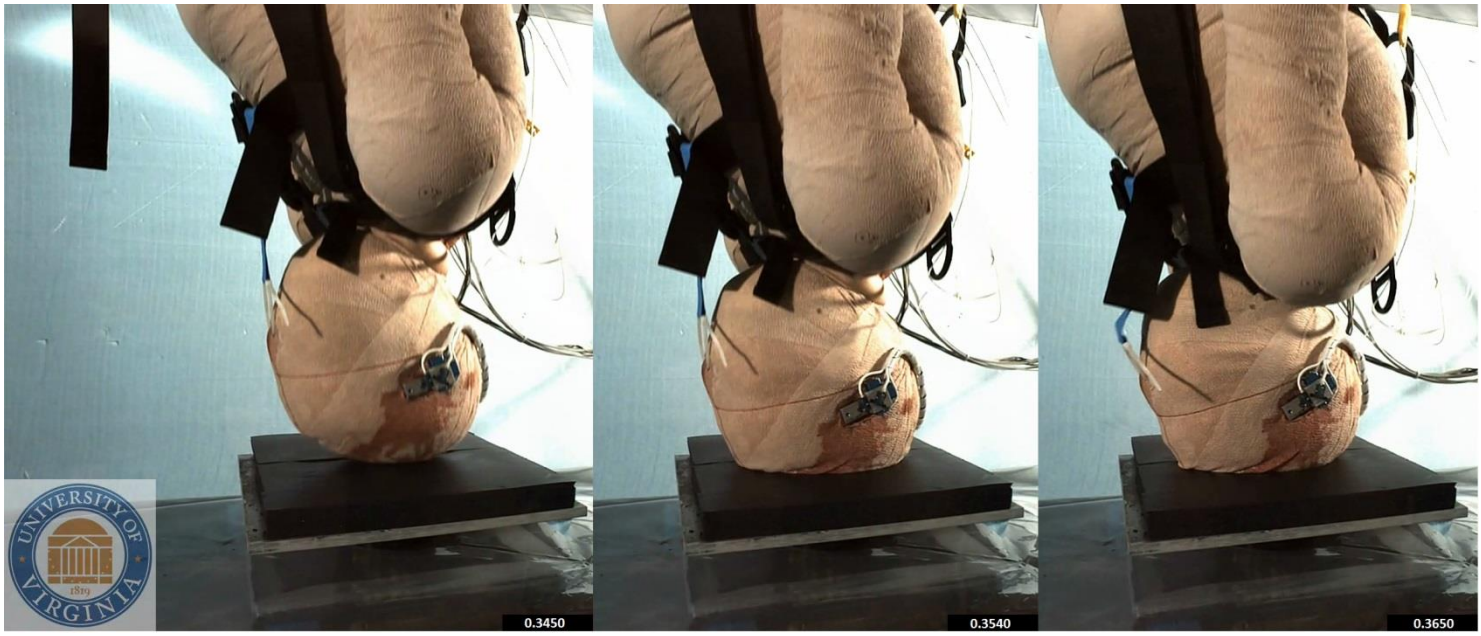

Figure 11: Frames of point of initial head contact (left), point of critical peak load (center), and point of onset of inertial torso load (right) for Cadaver 631. For this specimen, the time between head contact and the point of torso inertial load was 20.1msec, separated by 20 frames of video taken at 1000Hz. The amount of torso augmentation is noticeable by the point drawn on the acromion on the right shoulder. Also, the head is noticeably in extension by frame 0.3650, indicating upper cervical spine extension buckling, seen in the radiology at 0.3550s.

The relative time points in which buckling is evidenced by the drop in axial force and the vertical velocity of the head goes to zero can be seen in Figure 12 for Cadaver 631, showing that the head does not arrest fully (V_Z=0) until after the torso begins augmenting load to the base of the cervical column. Cadaver 631 experienced a

momentary increase in downward velocity between 0.3563 and 0.3654s, attributed to the point when the torso inertia begins to compressively load the buckled column. This sudden increase in the downward velocity of the head is also observed in Cadavers 516 and 552. Head arrest does not occur for specimen 631 until 0.372s after drop (raw time scale in Figure 12), which is 18msec after peak head load occurs and 17msec after buckling kinematics are first seen in radiological footage.

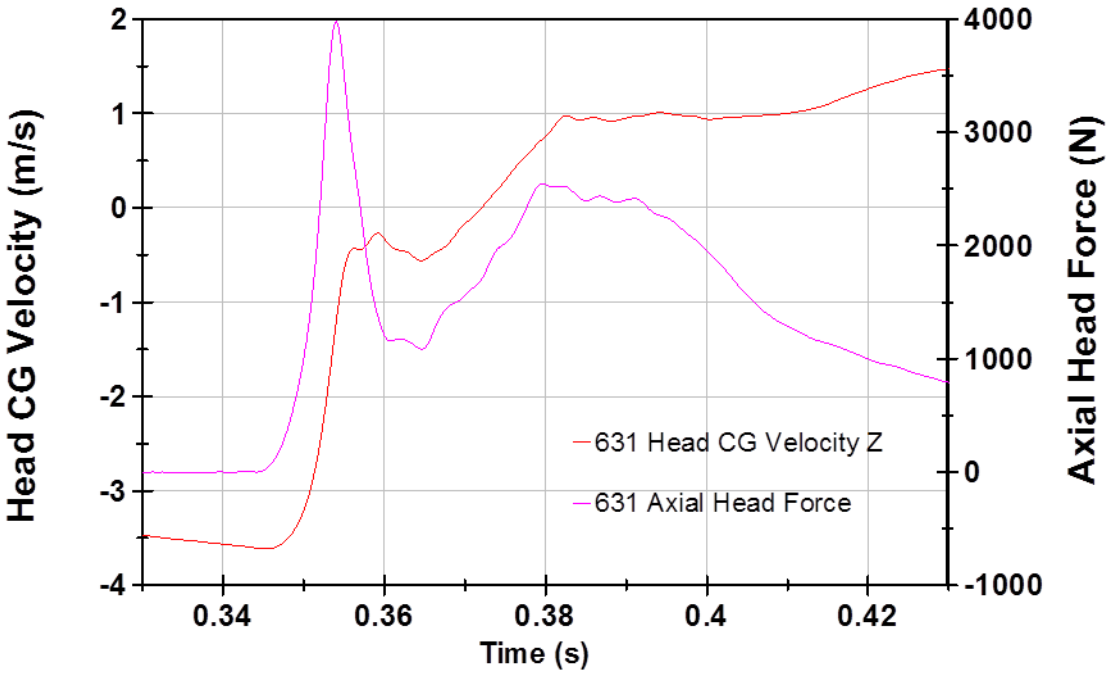

Figure 12: Head CG vertical velocity and axial head force histories, showing head kinematics versus cervical spine kinetic peaks.

Visual interpretation of the onset of buckling is shown in Figure 13. Compression is seen occurring in the intervertebral discs as the original lordotic configuration undergoes compression while the head travels through the foam. The angle between C2 and C3 becomes less parallel and opens slightly into extension in frame 0.3550.

For each time point in Table 4, the displacement change between the Head CG and the T1 accelerometer cube is shown in Table 5. The initial displacement at the point

of head contact was offset to zero and the difference between Head CG to T1 positions was taken for each of the time points related to buckling. The displacement time history between these two landmarks is shown for Cadaver 516 in Figure 14. This plot shows the augmentation of T1 occurring from the point of head contact with the foam. For 516, the axial load peaked and the cervical spine buckled after only 5.38mm of torso-to-head augmentation. Cadaver 552 showed the least torso augmentation due to a considerably shorter neck than other specimens.

UVA Specimen Number	Torso Augmentation at Critical Load (cm)	Torso Augmentation at time of Head Arrest (v=0) (cm)	Torso Augmentation at Video Frame Buckling First Seen (cm)	Torso augmentation at time of torso inertial loading onset (2nd load phase) (cm)
516	0.54	3.05	-	3.35
552	0.19	1.62	-	1.08
631	0.75	5.29	1.02	3.52
553	1.04	3.45	1.28	5.66

Table 5: Displacement between T1 and Head CG measured at each buckling time point by second derivative of acceleration curves (Appendix B). Little augmentation (1cm or less) is required to reach peak axial load, but possibly more (3 cm) until injury occurs.

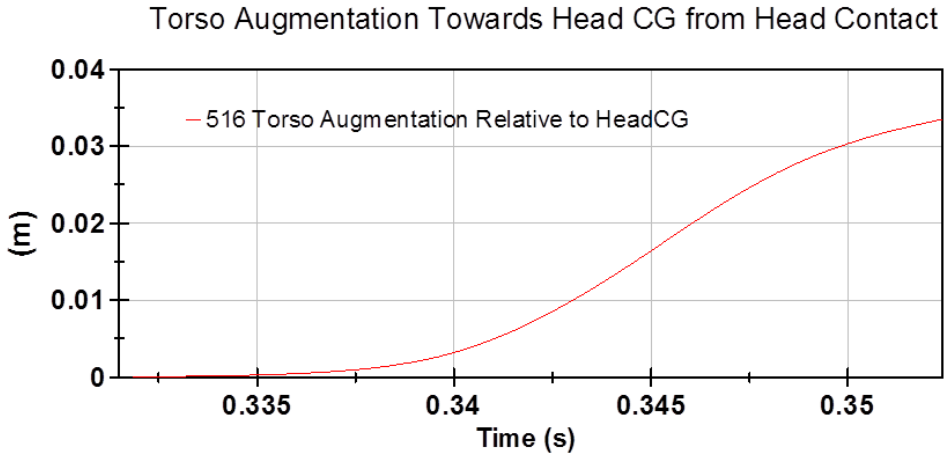

Figure 14: Plot of the relative augmentation of T1 toward the head over the critical window from 0.3315s (head contact) and 0.3524s (inertial torso load onset). The point of buckling (0.3412s) was reached with only 5.38mm of T1 to head displacement.

DISCUSSION

Injury

While radiological viewing capabilities allowed the researchers of this study to view buckling dynamically, the point of injury could not be ascertained in the window of usable video. For Cadaver 553, C2 appears to remain intact until the test is complete, and then fracturing as the remaining cadaver body forced the neck into hyperflexion when the test was terminated (X-ray video frame 0.558). It appears an avulsion fracture due to the transverse ligament occurs, an injury mechanisms cited by several authors (Yoganandan et al., 2004; Mouradian et al., 1978). Thus, the Type-III odontoid fracture of Cadaver 553 was unrelated to the axial loading event.

There are caveats for the injuries observed in specimens 552 and 631 as well. While it is likely the C4 fracture of 631 occurs as a result of compression-extension (after or during buckling which places C1-C4 into extension) and caused by the anterior longitudinal ligament avulsing a superior chip from the vertebral body, it is possible that 631's C4 injury occurred after the compression event was over. The head of 631 left the impact plate, whipping backward into extension. C4 horizontal fractures are seen in whiplash cases and can also be the result of a tension-extension injury mechanism (Winkelstein et al., 1997). The injuries to the bilateral pedicles of C7 of Cadaver 552 were potentially influenced by the presence of the adjacent T1 pedicle screws. Therefore, it is possible that no UVA specimens sustained fracture during the pure loading event, furthering the finding that Duke experimental set-up exacerbated compressive fracture.

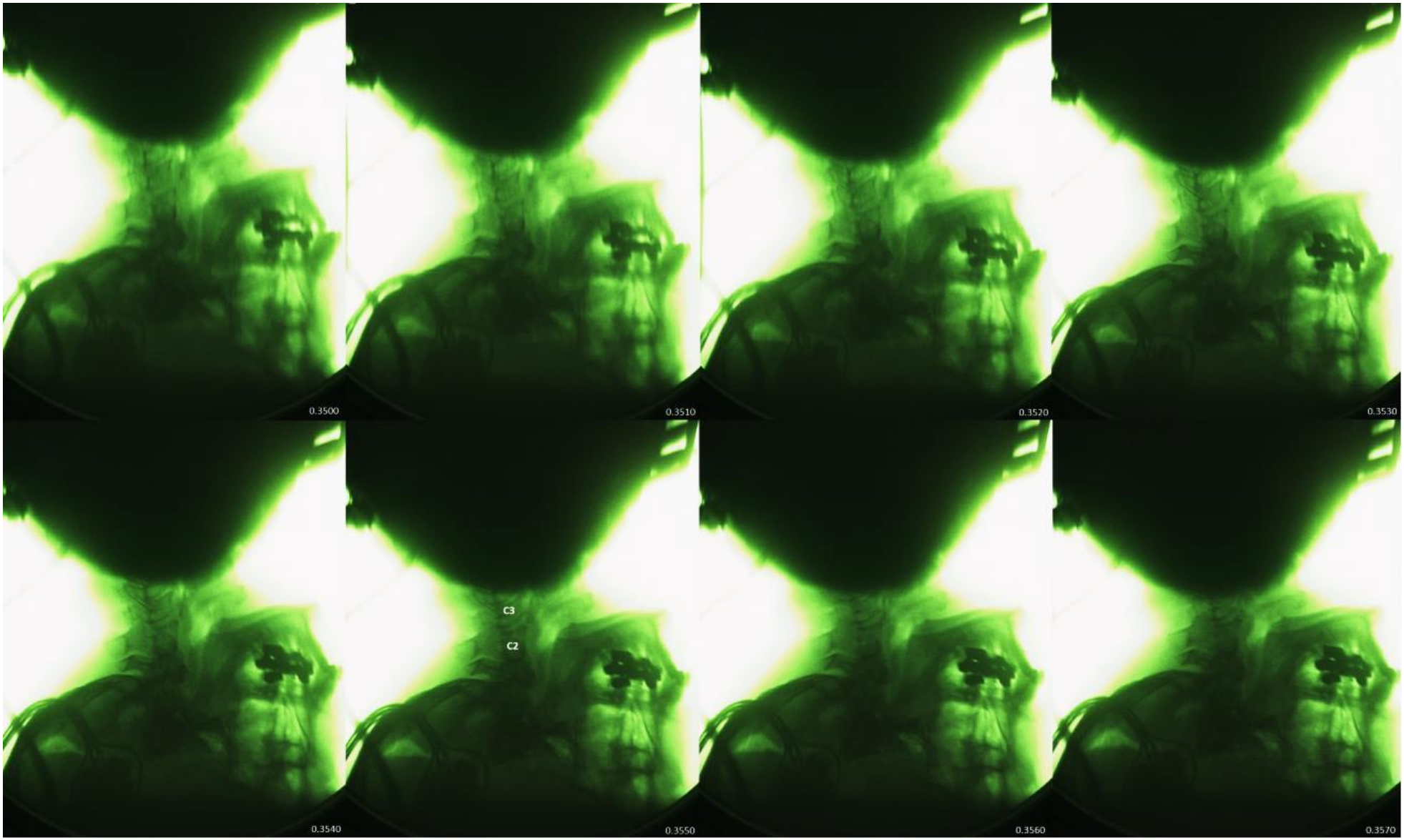

Figure 13: Eight milliseconds of radiology still shots, showing anterior motion of the C1-C3 vertebrae and disc space extension widening during buckling onset at 0.3550. The peak axial load was registered at 0.3540. These time values are in the raw time scale where drop occurs at t=0.

Still, the fractures sustained by 552 and 631 in this test series, if associated with the compression sequence, are not severe in nature (AIS 2). If 553 is ruled out, then UVA specimens on the whole sustained less severe cadaver pathologies than Duke's cases (Table 2). In their cadavers dropped onto a padded, flat plate, the three specimens each sustained at least one AIS 3+ injury, a total of 4 created (BFD, burst fractures, Type-III odontoid).

This injury discrepancy finding suggests that Duke's end conditions may be over-constraining, as in the Myers et al. (1991) full constraint condition, resulting in catastrophic hard tissue fracture and loss of vertebral body height. The over-constraint may be unrealistic considering UVA registered planar accelerations (x and y) accelerations as well as moments about x and y axes at T1. This indicates the vertebrae caudal to the cervical spine were moving horizontally and rotating in response to compression in the membered column. The full torso allows for more rotation and planar motion than the potted, 1-DOF track used at Duke. As Myers et al. show, end conditions have direct relationships with injury outcomes; the lower severity of UVA's specimens shows that Nightingale et al. may have been over-constraining the inferior end condition.

Component level research similar to Nightingale et al. (1997) and Pintar et al. (1995) still has vital importance in studying injury thresholds of the neck. One major reason is a significant experimentation cost reduction; some quotes cite a four-fold decrease in cost when using a cadaveric head-neck complex versus a full cadaver donor (Heltzel, personal communication, 2013). Therefore, these findings aid in the development of an appropriately constrained and configured component level test that most accurately mimics the boundary conditions of a full human subjected to axial load.

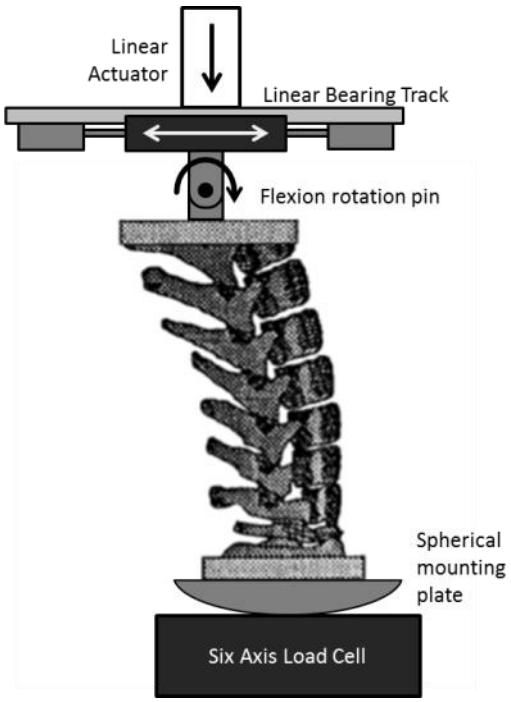

Figure 15: Proposed test fixture for component level cervical spine compression study incorporating motion and rotation evidenced in full cadaver drop tests.

Here, a hypothetical test fixture is proposed (Figure 15). The head end condition allows for slight flexion or extension at the atlas (C1). Radiological findings of UVA tests found slight sagittal rotation of the occipital condyles. The T1 end condition should allow for antero-posterior translation as well as rotation in flexion to permit 2nd order buckling and associated lower cervical spine flexion to occur.

Buckling Behavior

In every case, the Head CG vertical velocity reached zero after the bifurcation point, $P = P_{CR}$ (Appendix B). In other words, the head was still travelling downward through the foam as the force transmitted through the head and neck decreased. The only explanation for this is that the stiffness in the column instantaneously dropped, the result of 2nd order buckling of the column, shortening its effective longitudinal length. This phenomenon has been witnessed by several authors of neck compression studies

(Nusholtz et al., 1981, 1983; Nightingale et al., 1996, 1997; Pintar et al., 1990). Head rebound, an occurrence described by Nightingale et al. in many of the 22 specimens tested in their study, would be able to explain the first peak drop before the 2nd peak indicating torso inertia. However, this would only be possible if the head vertical velocities reached zero before or at the bifurcation point in UVA's testing. The time between critical bifurcation point and head is the period in which 2nd order buckled configuration is taking form. In both 631 and 553, the head slows considerably during head/neck inertial loading (first peak), down to within 0.5m/s.

The peak head force in Cadaver 631 occurs at 0.354 seconds in raw time after the drop is initiated. The coinciding X-ray frame (Figure 13) shows this to be the last frame in the initial lordotic configuration. The frame 1msec later (0.3550s) shows anterior motion of the upper (C1-C3) segments. The subsequent frames (0.3560-0.3580) all show continuation of extension of the upper contiguous segments as buckling configuration is taking form, all coinciding with the steep decrease in the peak load. Nightingale et al. associates this period (during steep decrease in the first inertial peak) with the time point of injury for padded tests. For specimen I08-P+15, buckling occurred after peak head force, and injury (C2 Hangman's fracture and burst fracture) during the descending head force data and before the torso mass loads (Figure 16).

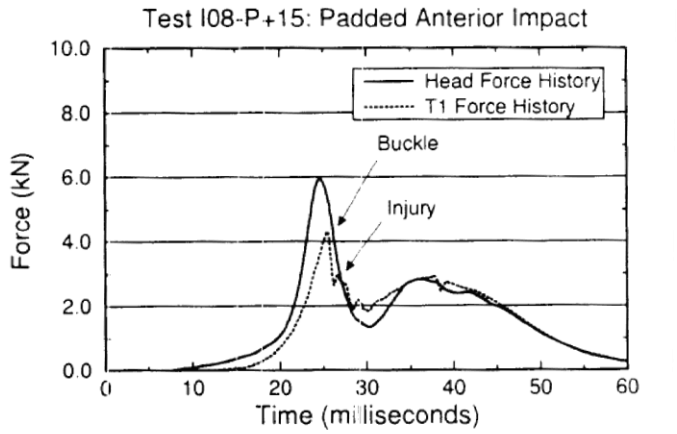

Figure 16: Plot showing head and neck force time histories for the padded impact of test number I08-P+15 from Nightingale et al. (1997). Here injury occurs (deemed through retroreflective markers and high speed video as well as via a local maximum in the T1 force data) during the axial head force decline.

Yoganandan et al. (1990) and Pintar et al. (1995) each published head displacement to failure which ranged from 1.7-3.2cm and 1.3-2.5cm, respectively for the cadavers of each study. Both studies used straightened necks which increases the stiffness and "minimizes the effects of stresses due to bending" (Nightingale et al., 1997). Nightingale reports injury to occur an average of 18.0±4.5 msec after impact for cadavers impacting padded surfaces. This most closely associates with the point of inertial torso loading initiation in this current study, occurring 19.3±3.0 msec after impact with the foam. If this is the case, UVA specimens underwent 3.40±1.87cm of T1 to head CG displacement until injury occurred in the buckled spine of specimen 631.

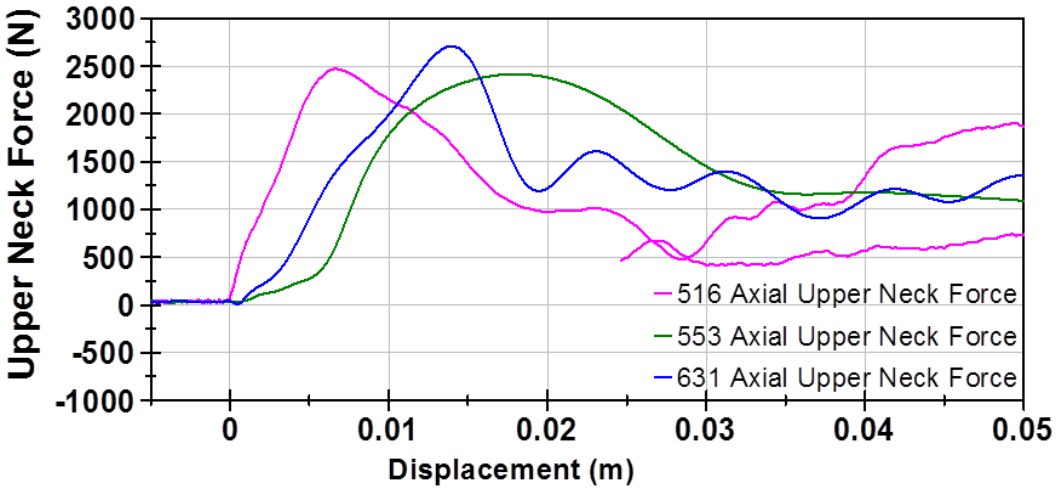

Figure 17: The Upper Neck Force versus Displacement of T1 to Head CG for 516, 553, and 631. Cadaver 552 left out of calculation due to specimen neck deficiencies.

Dynamic upper neck force-deformation response curves for Cadavers 516, 553, and 631 were generated (Figure 17), showing 553 and 631 peak upper neck loads occurring at deformations that fall within Pintar et al. (1995) derived dynamic force-deformation corridor (Figure 4, Chapter 1). The force at failure for UVA tests however still needs to be discerned from future data, as compression fracture was not achieved in these tests.

Kinetics Data and Effective Mass

A long-term research goal of this study is to evaluate the effective mass of the human torso during loading of a 3m/s head impact. It is hypothesized that Duke's 16kg value is too high, attributing to the higher severity of cadaver injuries produced. Kinetic data measured in this test series, namely axial head force and upper neck force, intend to be used by a third party for FE extrapolation.

Upper neck forces when scaled to the 50th percentile male (mean = 2.45±0.20 kN) fail to reach:

1) The 4.50kN injury assessment reference value used in NHTSA-developed Nij (Eppinger et al., 1999),
2) Pintar et al. (1995) mean failure load for the 11 male cadavers (mean age = 62) of 3.81±0.97 kN, or
3) The averaged failure load for Nightingale et al. (1997) and Pintar et al. (1995) male cadaver neck loads for injured specimens of 3.03kN.

Still, these values generated in the current study reflect the full male 50^{th} human sustaining a 3m/s head impact, the value now ubiquitously used among injury litigation experts as a velocity-based criterion for injury. With FE extrapolation, the lower cervical spine (T1) neck forces and the effective mass properties of the contiguous human torso can be gleaned, showing improved efficacy for neck injury criteria over the less than ideal phantom torso conditions.

Limitations

The test methodology carried out in the current study was unable to evaluate the effective torso mass, the portion of the torso's inertia augmented during compressive loading, due to the fact that minimal invasive instrumentation was desired by the research team. Mounting a load cell inferior to T1 is not feasible; likewise, mounting an accelerometer array would be needed to measure the acceleration of the CG of the neck in the same manner the head CG acceleration was used to find $\boldsymbol{F_{UN}}$. Finding the force at the lower neck was therefore troublesome, hindering an effective mass calculation if accurate injury pathology to the neck would remain uncompromised by the presence of screws drilled into the pedicles of C4 (the rough CG location of the neck).

Forces due to passive and active muscle tone or contraction are absent in the

current tests. Musculature likely plays a role in the preloading of the column, evidenced by the epidemiological findings in Chapter One pertaining to impaction fractures (lateral aspect fractures to adjoining vertebrae of a spondylolisthesis or facet dislocation). Active musculature likely does not play a role, occurring too late in the loading sequence to have an effect on injury using the axial loading rates implemented in this study (Pintar et al., 1998; Cusick et al., 2002; Foust et al., 1973). Passive musculature, however, may play a role in exacerbating injury in the living population, its absence serving as a limitation to this study.

A single sagittal view from the dynamic x-ray technology was useful in only the first 20msec of head contact before the images are obstructed by the specimen's shoulders. The voltage and amperage of the system were adjusted and tailored to the density of the desired tissue and the thickness of the material the x-ray is passing through. As this thickness drastically changes as the shoulders pass over the neck, the x-ray settings used to view the neck during onset of loading and buckling are not powerful enough to pass through the lateral girth of the thorax. Therefore, the point of injury (if it occurred during or after buckling) could not be seen for Cadaver 631. Future tests should study the effects of the removal of cadavers' upper limbs by comparing full body head force magnitudes and durations with those from bodies lacking upper extremities. If similar, the removal of the upper limbs could aid in the viewing capabilities and determination of more exact times and displacements when bony compression injury occurs for loading of this nature.

Ideally, it is a long-term effort of this research to improve upon current neck injury criteria for compressive loading. However, improved dummy kinematics would be

pivotal to the applicability of a better injury criteria based on axial loading and bending. While a dummy that responds with kinematic biofidelity would be desired for a dynamic rollover test for vehicle crashworthiness, in order to really understand the force measurements required to generate neck fracture, specific loads should be generated on a highly localized level. Buckling, initial orientation, and end conditions affect vertebral compression response on the local, vertebral level, so a dummy with individual functional spinal units may be vital to truly assess when and where the critical loads associated with injury are occurring. It is with these data that *in vivo* occupant injury risk could be assessed.

REFERENCES

Adamec J, Praxl N, Miehling T, Muggenthaler H, Schonpflug M. The occupant kinematics in the first phase of a rollover accident- experiment and simulation. *Proceedings of the International Research Council on Biomechanics of Injury*, Prague, Czech Republic. 2005; 145-56.

Alem NM, Nusholtz GS, Melvin JW, Head and Neck Response to Axial Impacts. *Proc of the 28th Stapp Car Crash Conf*. 1984; 275-88.

Allen BL, Ferguson RL, Lehmann TR, O'Brien RP. A mechanistic classification of closed, indirect fractures and dislocations of the lower cervical spine. *Spine.*1982;7(1):1-27.

Althoff B. Fracture of the Odontoid process: an experimental and clinical study. *Acta Orthopaedica Scandinavica*. 1979; 1-48.

Braakman R, Vinken PJ. Unilateral facet interlocking in the lower cervical spine. *J Bone Joint Surgery*. 1967;49B(2):249-257.

Bahling GS, Bundorf RT, Kaspzyk GS, Moffatt EA, Orlowski KF, Stocke JE. Rollovers and drop tests: the influence of roof strength on injury mechanics using belted dummies. *Proc of the 34th Stapp Car Crash Conf.* 1990;101-12.

Bambach MR, Grzebiata RH, McIntosh AS, Mattos GA. Cervical and thoracic spine injury from interactions with vehicle roofs in pure rollover crashes. *Acc Anal and Prev*. 2013;50:34-43.

Bauze RJ, Ardran GM. Experimental production of forward dislocation in the human cervical spine. *J Bone Joint Surgery*. 1978;60: 239-45.

Bortz J. A new mathematical formulation for strapdown inertial navigation. IEEE Transactions on Aerospace and Electronic Systems. Vol. AES-7, No. 1. January, 1971.

Burke DS, Bidez MW, Mergl K. Cervical spine tolerance to catastrophic injury in rollover crash environments. Proceedings from ASME. 591-2. 2009.

Cappozzo A, Cappello A, Della Croce U, Pensalfini F. (1997) Surface-marker cluster design criteria for 3-D bone movement reconstruction. IEEE Transactions on Biomedical Engineering. December 1997; 44(12): 1165-1174.

Cooper ER, Moffatt EA, Curzon AM, Smyth BJ, Orlowski KF. Repeatable dynamic rollover test procedure with controlled roof impact. Society of Automotive Engineers, Warrendale, PA. 2001.

Crash Injury Research Engineering Network Coding Manual Version 2.0.July, 2010.

Crawford NR, Duggal N, Chamberlain RH, Park SC, Sonntag VK, Dickman CA. Unilateral cervical facet dislocation: injury mechanism and biomechanical consequences. *Spine.* 2002; 27(17): 1858-64.

Culver RH, Bender M, Melvin JS. Mechanisms, Tolerances, and Responses obtained under dynamic superior-inferior head impact. Final Report: UM-HSRI-78-21, 1978.

Cusick FJ, Yoganandan N. Biomechanics of the cervical spine 4: major injuries. *Clinical Biomechanics*. 2002;17: 1-20.

Eppinger R, Sun E, Nadak F, Haffner M, Khaepong N, Maltese M, Kuppa S, Nguyen T, Takhounts E, Tannous R, Zhang A. Development of Improved Injury Criteria for the Assessment of Advanced Automotive Restraint Systems – II. NHTSA Technical Report, 1999.

Foster J, Kerrigan J, Nightingale R, Funk J, Cormier J, Bose D, Sochor M, Ridella S, Ash J, Crandall J. Analysis of Cervical Spine Injuries and Mechanisms for CIREN Rollover Crashes. *Proceedings of the International Research Council on Biomechanics of Injury*, Dublin, Ireland, 2012.

Foust DR, Chaffin DB, Snyder RG, Baum JK. Cervical range of motion and dynamic response and strength of cervical muscles. *Proc of the 17th Stapp Car Crash Conf.* 1973; 285-308.

Frechede B; McIntosh A; Grzebieta R; Bambach M. (2009) Hybrid III ATD in inverted impacts: influence of impact angle on neck injury risk assessment. Annals of Biomedical Engineering, 37(7): 1403-1414.

Friedman D, Nash CE. Measuring rollover roof strength for occupant protection. *IJCrash*. 8, 97–105. 2003.

Friedman D, Caplinger J, Bish J. Human/Dummy Rollover Falling (Excursion) Speeds. *International Technical Conference on the Enhanced Safety of Vehicles* (ESV), 20. 2007.

Harris JH Jr, Edeiken-Monroe B, Kopaniky DR. A practical classification of acute cervical spine injuries. *Orthopedic Clinics of North America*. 1986;17(1): 15-30.

Hibbeler RC. Statics and Mechanics of Materials. 2nd Edition. 2004.

Hodgson VR, Thomas LM. Mechanisms of cervical spine injury during impact to the protected head. *Society of Automotive Engineers.*1980; 17-42.

James MB, Nordhagen RP, Schneider DC, Kosh SW. Occupant injury in rollover crashes: a reexamination of Malibu II. *SAE World Congress Technical Paper.* 2007.

Kerrigan JR, Crandall JR. A Comparative Analysis of the Pedestrian Injury Risk Predicted by Mechanical Impactors and Post Mortem Human Surrogates. *Stapp Car Crash Journal*, 52, 2008.

Kerrigan JR, Dennis NJ, Parent DP, Purtsezov S, Ash JH, Crandall JR, Stein D. Test system, vehicle and occupant response repeatability evaluation in rollover crash tests: the deceleration rollover sled test. *International Journal of Crashworthiness*. 16:6, 583-605. 2011.

Kerrigan JR, Jordan A, Parent DP, Zhang Q, Funk J, Dennis NJ, Overby B, Bolton JR, Crandall JR. Design of a dynamic rollover test system. *Society of Automotive Engineers*. 2011.

Kleinberger, M, Sun, E, Eppinger, R, Kuppa, S, Roger Saul. Development of Improved Injury Criteria for the Assessment of Advanced Automotive Restraint Systems. NHTSA Technical Report. 1998.

Maiman DJ, Sances A, Myklebust JB. Compression injuries of the cervical spine; a biomechanical analysis. *Neurosurgery*. 1983;13(3): 254-60.

Manary MA, Reed MP, Flannagan CA, Schneider LW. ATD Positioning Based on Driver Posture and Position. *42nd Stapp Car Crash Conference*. 1-13, 1998.

Matsushita T, Sato TB, Hirabayashi K, Fujimura S, Asazuma T, Takatori T. X-ray study of the human neck motion due to head inertia loading. *Proceedings of the 38th Stapp Car Crash Conference*, 55-64, 1994.

McElhaney J, Snyder RG, States JD, Gabrielsen MA. Biomechanical analysis of swimming pool neck injuries. *Society of Automotive Engineers.* 1979; 47-53.

McElhaney JH, Paver JG, McCrackin HJ, Maxwell GM. Cervical spine compression responses. *Proc of the 27th Stapp Car Crash Conf.* 1983; 163-77.

McElhaney JH, Doherty BJ, Paver JG, Myers BS, Gray L. Combined bending and axial loading responses of the human cervical spine. *Proc of the 32nd Stapp Car Crash Conf.* 1988; 21-28.

McElhaney JH, Nightingale RW, Winkelstein BA, Chancey VC, and Myers BS. Biomechanical aspects of cervical trauma. *Accidental Injury: Biomechanics and Prevention, 2nd ed.,* Springer-Berlag, New York, New York, 2002.

Moffat EA, Cooper ER, Croteau JJ. Matched-pair rollover impacts of rollcaged and production roof cars using the controlled rollover impact system (CRIS). Society of Automotive Engineers World Congress. 2003.

Moffatt EA, James MB. Headroom, roof crush, and belted excursion in rollovers. *SAE World Congress Technical Paper*. 2005.

Mouradian W, Fietti VJ, Cochran G, Fielding J, Young J. Fractures of the odontoid: a laboratory and clinical study of mechanisms. Orthop Clin North Am. 1978;9(4):985–1001.

Myers BS, Nightingale RW, McElhaney JH, Doherty DJ, Richardson WJ. The Influence of end condition on human cervical spine injury mechanisms. *Society of Automotive Engineers.* 1991; 391-99.

Myers BS, Winkelstein BA. Epidemiology, classification, mechanism, and tolerance of human cervical spine injuries. *Critical Reviews in Biomedical Engineering*. 1995; 23(5): 307-409.

Nightingale RW, McElhaney JH, Richardson WJ, Myers BS. Dynamic responses of the head and cervical spine to axial impact loading. *J Biomechanics*. 1996; 29: 307–18.

Nightingale RW, McElhaney JH, Camacho DL, Kleinberger M, Winkelstein BA, Myers BS. The dynamic responses of the cervical spine: buckling, end conditions, and tolerance in compressive impacts. *Proc of the 41st Stapp Car Crash Conf.* 1997; 451–71.

Nusholtz GS, Melvin JW, Huelke DF, Alen NM, Blank JG. Response of the cervical spine to superior-inferior head impact. *Proc of the 25th Stapp Car Crash Conf.* 1981; 197-237.

Nusholtz GS, Huelke DF, Lux P, Alem NM, Montalvo F. Cervical spine injury mechanisms. *Proc of the 27th Stapp Car Crash Conf*. 1983; 179-97.

Nusholtz GS, Kaiker PS. Kinematics of the human cadaver cervical spine in response to superior-inferior loading of the head, University of Michigan, Transportation Research Institute, Biosciences Division, UMTRI-86-31. 1986.

Panjabi MM, Cholewicki J, Nibu K, Grauer J, Babat LB, Dvorak J. Critical load of the human cervical spine: an in vitro experimental study. *Clinical Biomechanics*. 1998; 13(1): 11-17.

Paver JG, Friedman D, Carlin F, Bish J, Caplinger J, Rohde D. Rollover crash neck injury replication and injury potential assessment. *IRCOBI Conf Proc.* 2008; 421-4.

Pintar FA, Larson SJ, Harris G, Reinartz J, Sances A, Yoganandan N. Kinematic and Anatomical Analysis of the Human Cervical Spinal Column Under Axial Loading. *Proc of the 33rd Stapp Car Crash Conf.* 1989; 191-214.

Pintar FA, Sances A, Yoganandan N. Biodynamics of the total human cervical spine. *Proc of the 34th Stapp Car Crash Conf.* 1990; 55-72.

Pintar FA, Yoganandan N, Voo L, Cusick JF, Maiman DJ, Sances A. Dynamic Characteristics of the Human Cervical Spine. *Society of Automotive Engineers.* 1995; 195-202.

Pintar FA, Voo LM, Yoganandan N, Cho TH, Maiman DJ. Mechanisms of hyperflexion cervical spine injury. *IRCOBI Conf Proc.* 1998; 249-60.

Raddin J, Cormier J, Smyth B, Croteau J, Cooper E. Compressive neck injury and its relationship to head contact and torso motion during vehicle rollovers. *Society of Automotive Engineers*. 2009.

Ridella SA, Eigen AM, Kerrigan JR, Crandall JR. An analysis of injury type and distribution of belted, non-ejected occupants involved in rollover crashes. *Annals of Advances in Automotive Medicine*. 2009; 53.

Roaf R. A study of the mechanics of spinal injury. *J Bone Joint Surg*. 1960;42B: 810-23.

Robbins, D.H. Anthropometric Specifications for Mid-Sized Male Dummy, Volume 2. Report number UMTRI-83-53-2, University of Michigan Transportation Research Institute, Ann Arbor, MI. 1983.

Ryan MD, Henderson JJ. The epidemiology of fractures and fracture-dislocations of the cervical spine. *Injury: the British Journal of Accident Surgery*. 1992;23(1): 38-40.

Sances AJ, Yoganandan N, Maiman DJ, Myklebust JB, Larson SJ, Pintar F, Myers T. Spinal Injuries with Vertical Impact. *Mechanisms of Head and Spine Injuries*. Aloray Publisher, Goshen, NY. 1986; 305-48.

Shames I. Engineering mechanics: statics and dynamics, 4th ed. Prentice-Hall Inc., Upper Saddle River, N.J., USA. 1999.

Toomey DE, Mason MJ, Hardy WN, Yang KH, Kopacz JM. Exploring the role of lateral bending postures and asymmetric loading on cervical spine compression responses. *Proc of the ASME 2009 International Mechanical Engineering Congress & Exposition*. 2009; 1-8.

Viano DC, Parenteau CS, Analysis of head impacts causing neck compression injury. *Traffic Injury Prevention*. 2008; 9(2):144-52.

White AA, Panjabi MM. *Clinical Biomechanics of the Spine 1st Ed.* JB Lippincott Company, Philadelphia, PA. 1978.

Winkelstein BA, Myers BS, The biomechanics of cervical spine injury and implications of injury prevention, *Medicine and Science in Sports and Exercise*, 29, 7, 246-55, 1997.

Yoganandan N, Sances A, Maiman DJ, Myklebust JB, Pech P, Larson SJ. Experimental Spinal Injuries with Vertical Impact. *Spine*. 1986; 11(9): 855-60.

Yoganandan N, Sances, A, Pintar F. Biomechanical evaluation of the axial compressive responses of the human cadaveric and manakin necks. *J Biomech Eng*. 1989; 111: 250-5.

Yoganandan N, Sances A, Pintar F, Maiman DJ, Reinartz J, Cusick JF, Larson SJ. Injury biomechanics of the human cervical column. *Spine*. 1990; 15(10): 1031-9.

Yoganandan N, Pintar FA, Arnold P, Reinartz J, Cusick JF, Maiman DJ. Continuous motion analysis of the head–neck complex under impact. *J Spinal Disord*. 1994;7: 420–8.

Yoganandan N, Pintar F, Baisden J, Gennarelli T, Maiman D. Injury Biomechanics of C2 Dens Fractures. Annu Proc Assoc Adv Automot Med. 2004; 48: 323–337.

Young D, Grzebieta R, McIntosh A, Bambach M, Frechede B. Diving versus roof intrusion: a review of rollover injury causation. *International Journal of Crashworthiness.*2007;12(6): 609-28.

Appendix A

Injury and Case Information of CIREN Rollover Cases Reviewed in Chapter One

Summary of Cervical Spine Injuries for CIREN Occupants with Commentary

Each case's occupant information, radiology, head contact point (if known), external head trauma (if available), and detailed cervical spine fractures and dislocations are presented.

CIREN Case # 103304

This case involved a 76 year-old male who was involved in a 6 quarter turn rollover. He was located on the near side of the roll. The vehicle tripped in the median, contacted the occupant's roof rail hard, resulting in significant deformation on his side of the vehicle. His injuries are described below:

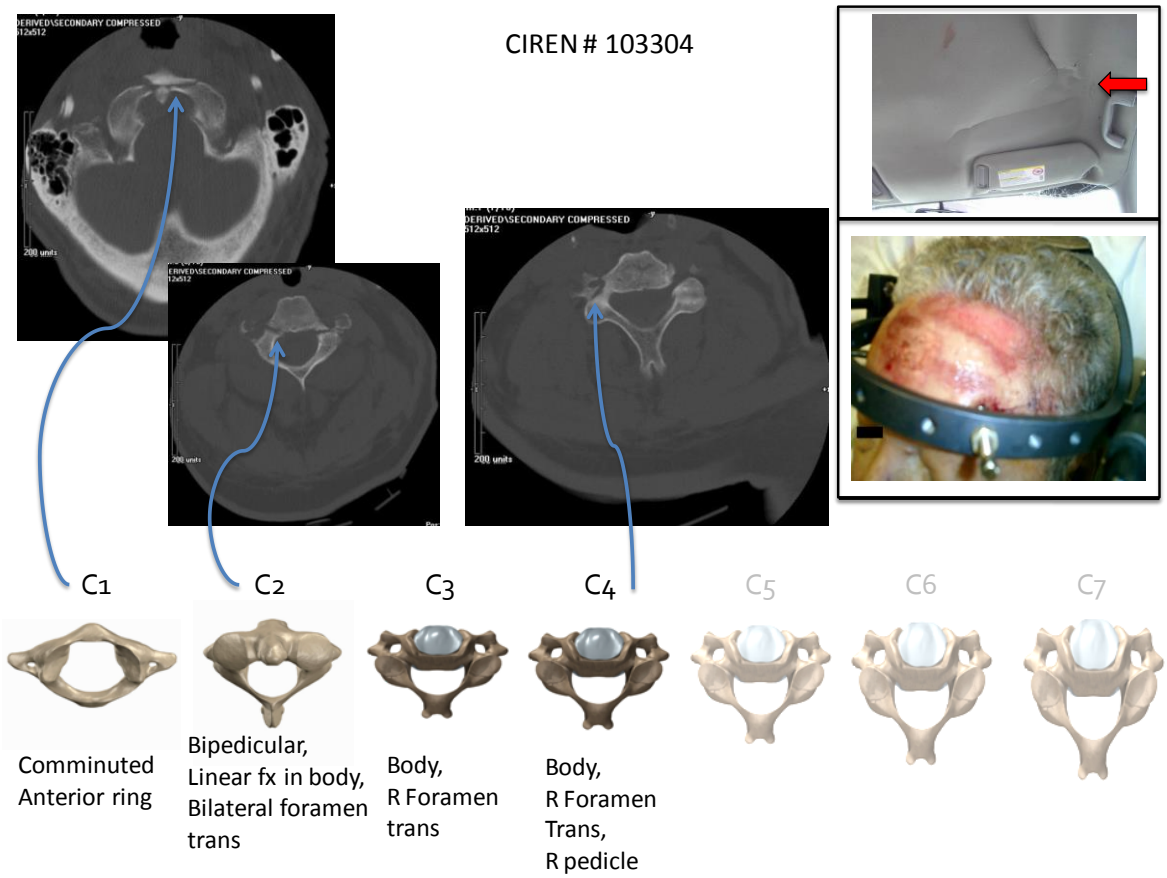

CIREN Case # 160139536

This case involved a 53 year-old male right front passenger involved in a 4 quarter turn rollover. The occupant was on the far side of the roll, following a clockwise yaw and left wheel interaction into sod. There was significant roof intrusion to the right front passenger compartment and A-pillar deformation. The cervical spine injuries are shown below:

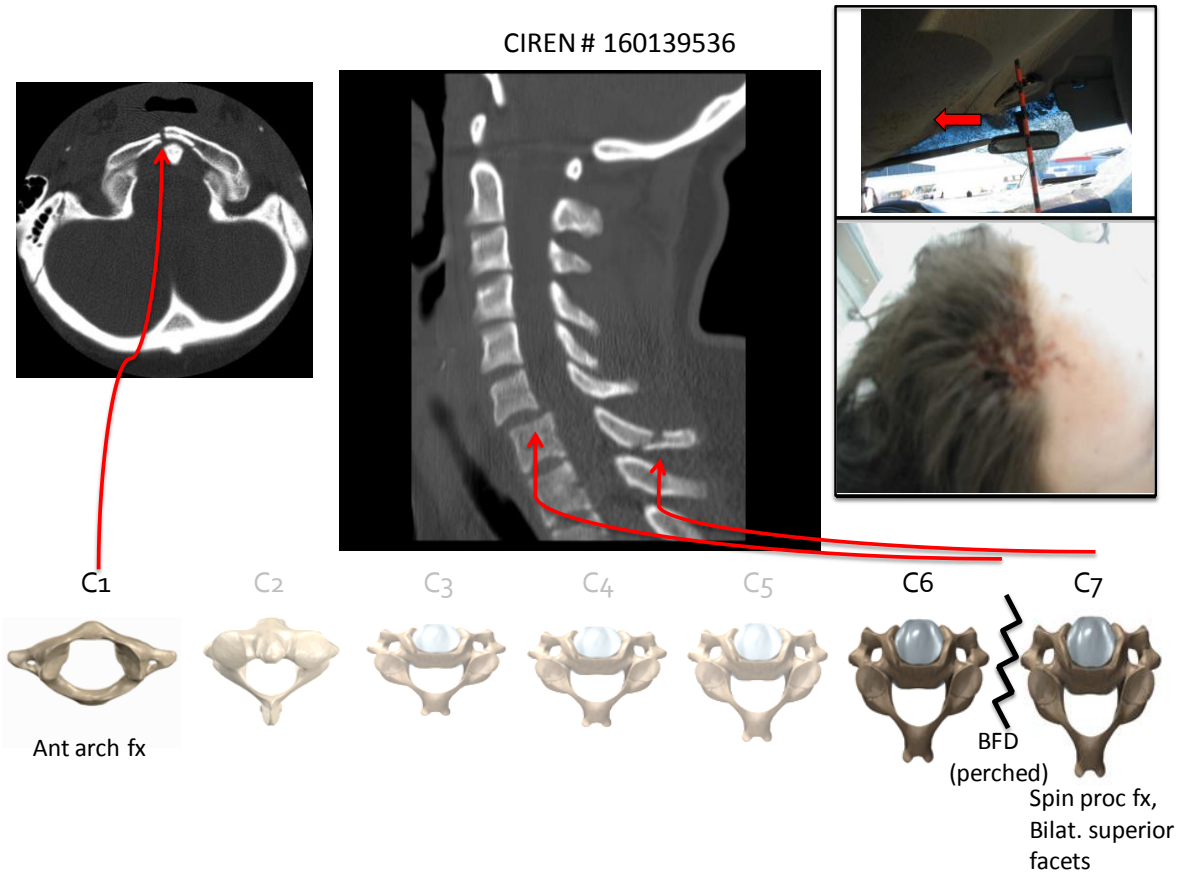

CIREN Case # 163690

This case occupant, a 42 year old male front right passenger, was involved in a 4 quarter turn rollover. He was positioned on the far side of the roll. The vehicle traveled down an embankment and suffered significant intrusion over the passenger seat, A-pillar and B-pillar. His injuries are shown below:

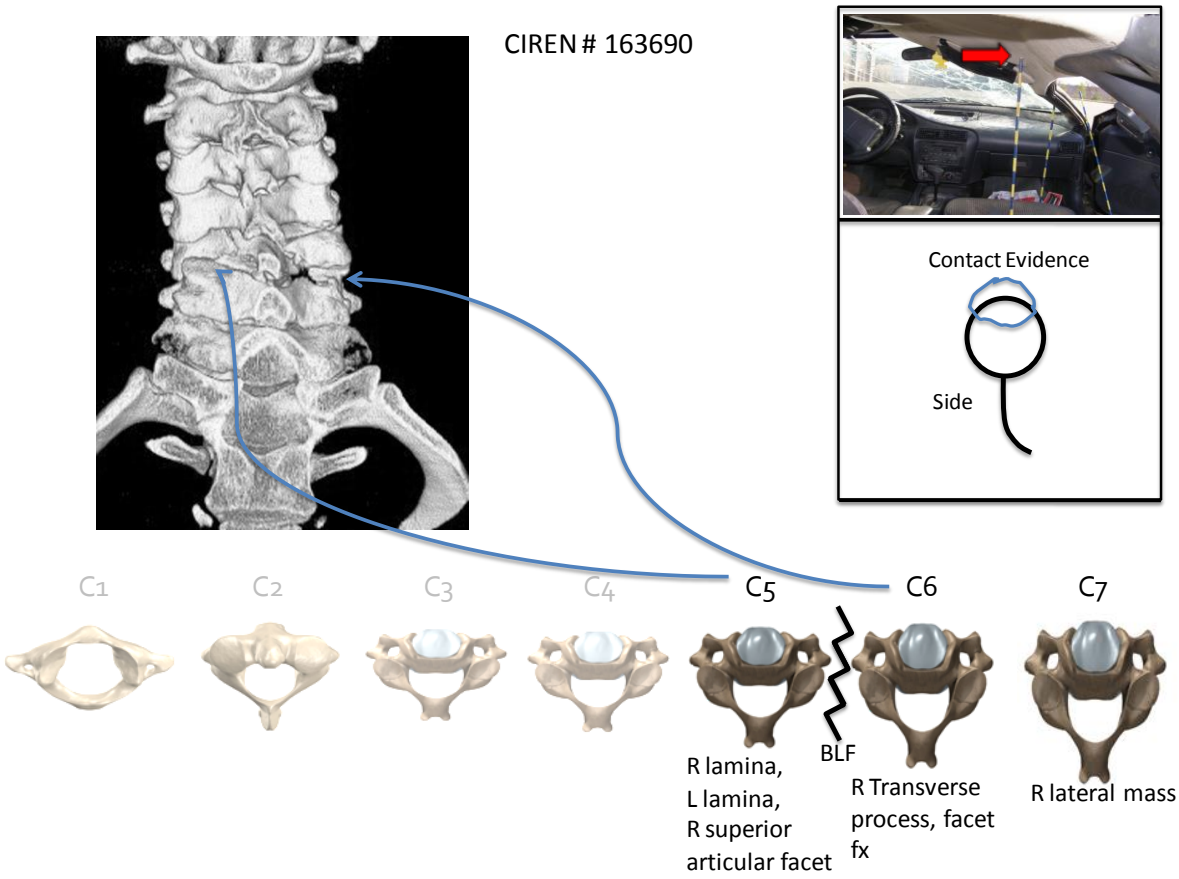

CIREN Case # 537103134

This case involved a 43 year old female front right passenger involved in a 6 quarter turn rollover. She was situated on the far side of the roll that took place after a driver's maneuver resulted in a clockwise yaw. There was severe crush into the right front occupant space, while the driver's side saw little deformation. The case occupant's injuries are described below:

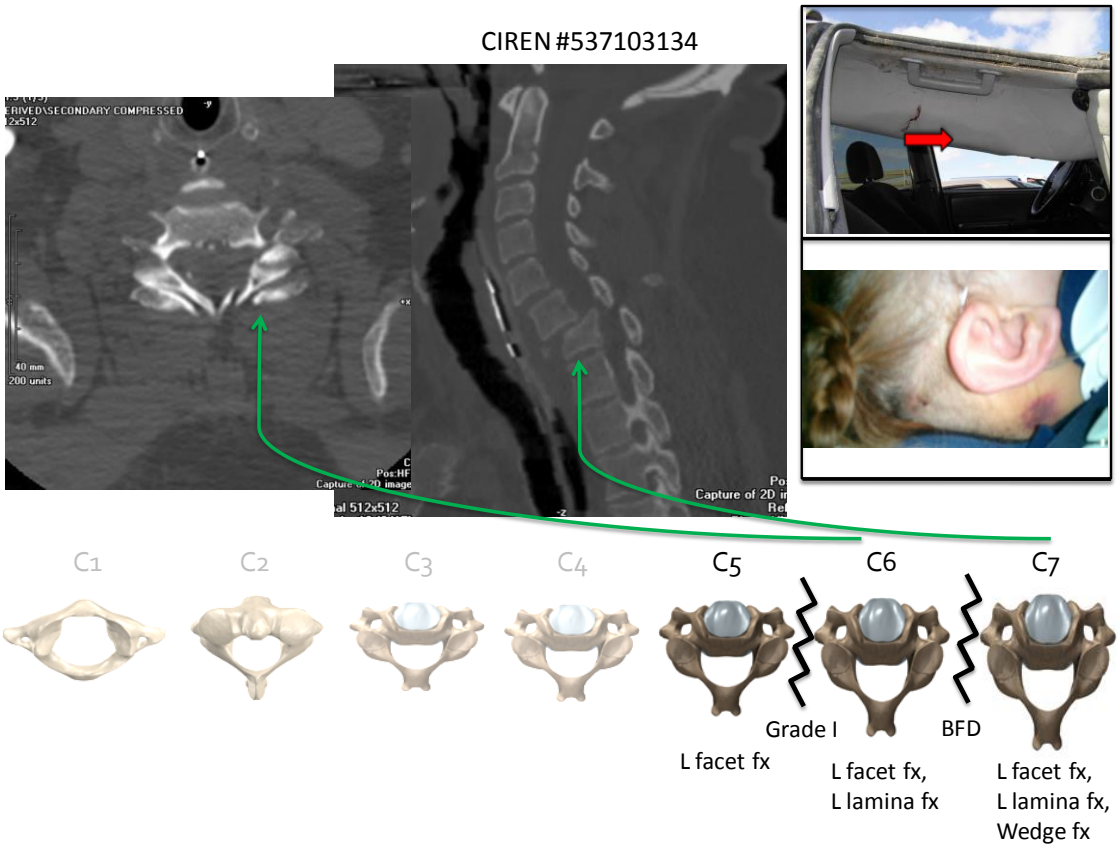

CIREN Case # 160110274

This case involved a 59 year old male driver involved in a 2 quarter turn rollover. After steering to avoid an animal in the road, his vehicle rotated in a counter-clockwise yaw before tripping in the shoulder. He was on the far side of the rollover. The case vehicle was a convertible with the top down. The windshield was flattened downward and the after-market roll bars sustained damage. His injuries are shown below:

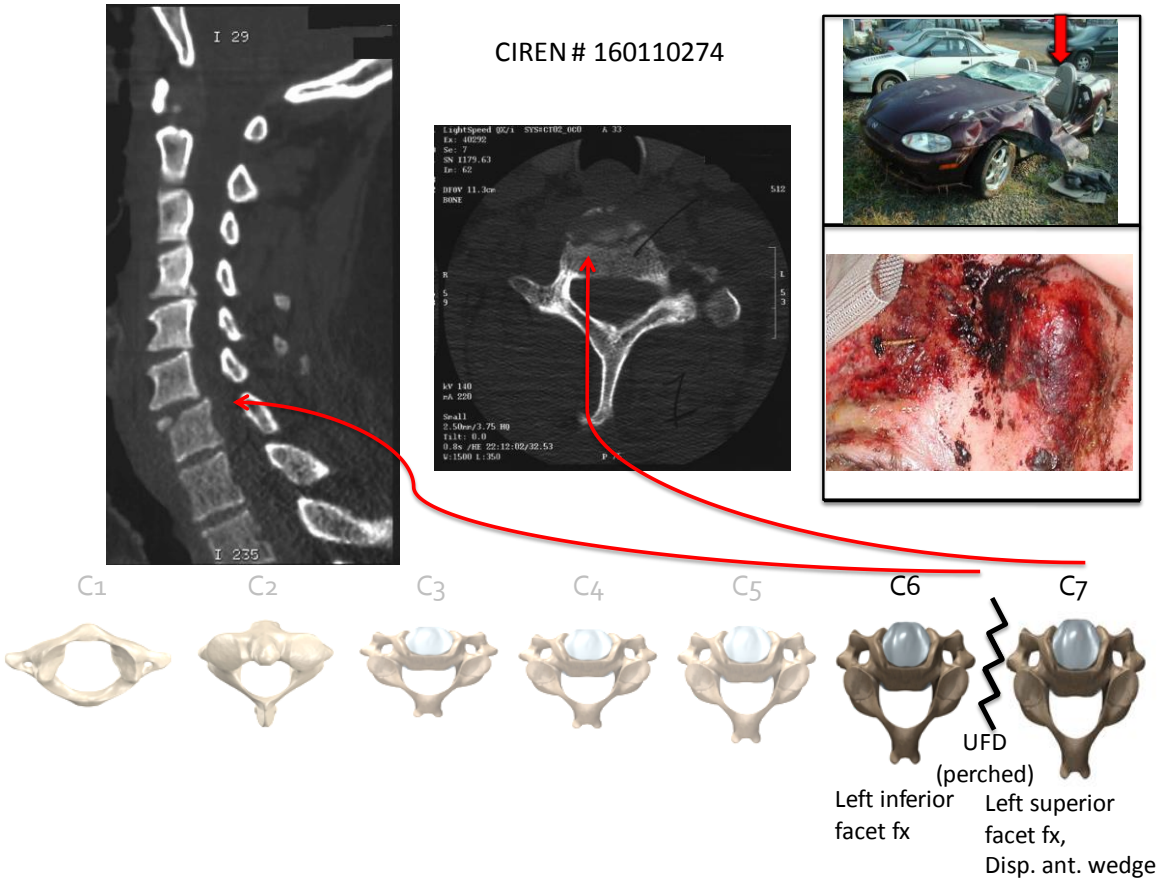

CIREN Case # 558030923

This case involves a 72 year old male right front passenger involved in a 4 quarter turn, right-side leading rollover. After clockwise yaw, the driver's side wheels dug into grass. The rollover resulted in roof damage characteristic of a driver-side leading roll, which more intrusion to the passenger side. The injuries sustained are shown below:

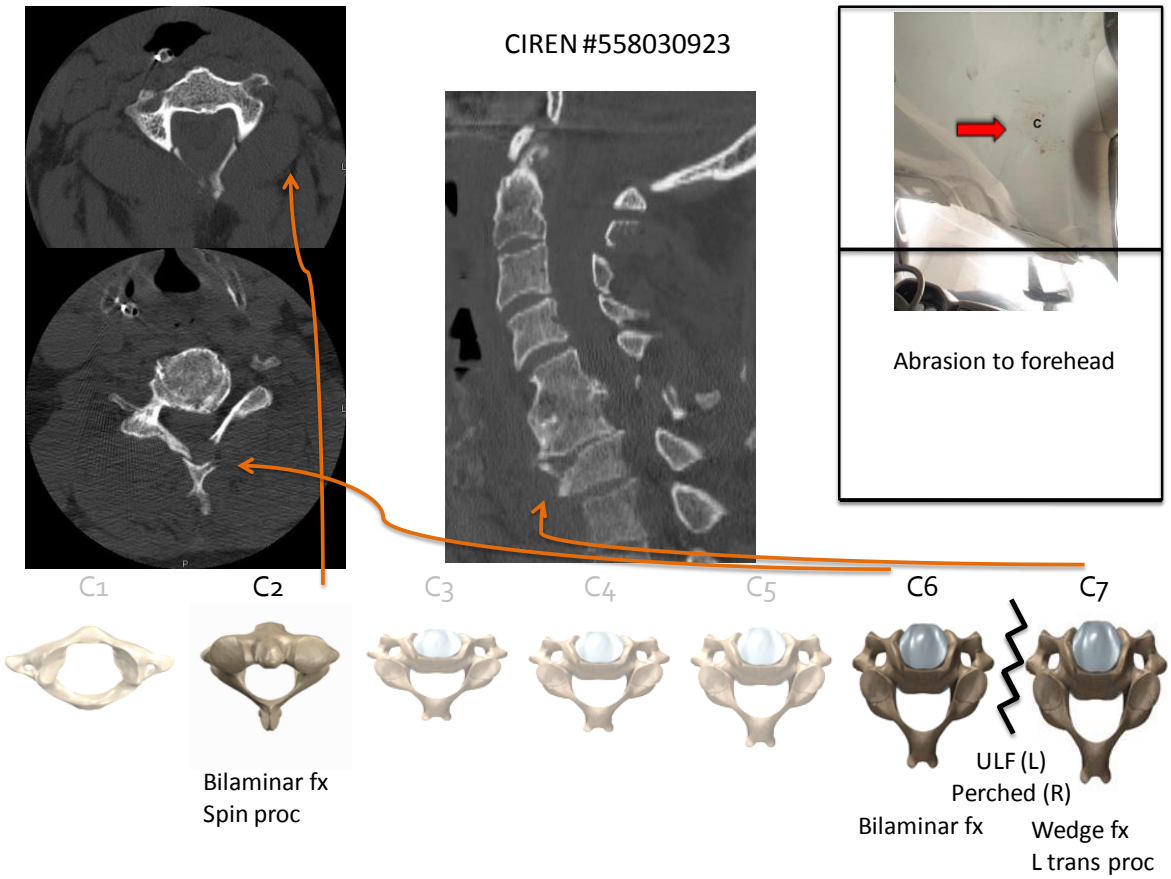

CIREN Case # 163694

This case involves the fatality of a 21 year old female driver who was involved in a 6 quarter turn rollover. After a clockwise yaw and trip, her vehicle went airborne and the roof of the vehicle impacted the ground. There was massive roof deformation with

almost total collapse of the left and right A-pillars, causing the windshield of the convertible (top up) to lay flat.

No radiology was provided due to the fatal nature of this incident.

CIREN Case # 100074514

The 73 year old male case occupant was involved in a 2 quarter turn rollover. While driving, he departed the roadway with right-side leading and the vehicle dropped into a depression and the vehicle tripped. The left pillars were deformed inward laterally. His injuries are shown below (note the T1 vertebral body fracture as well):

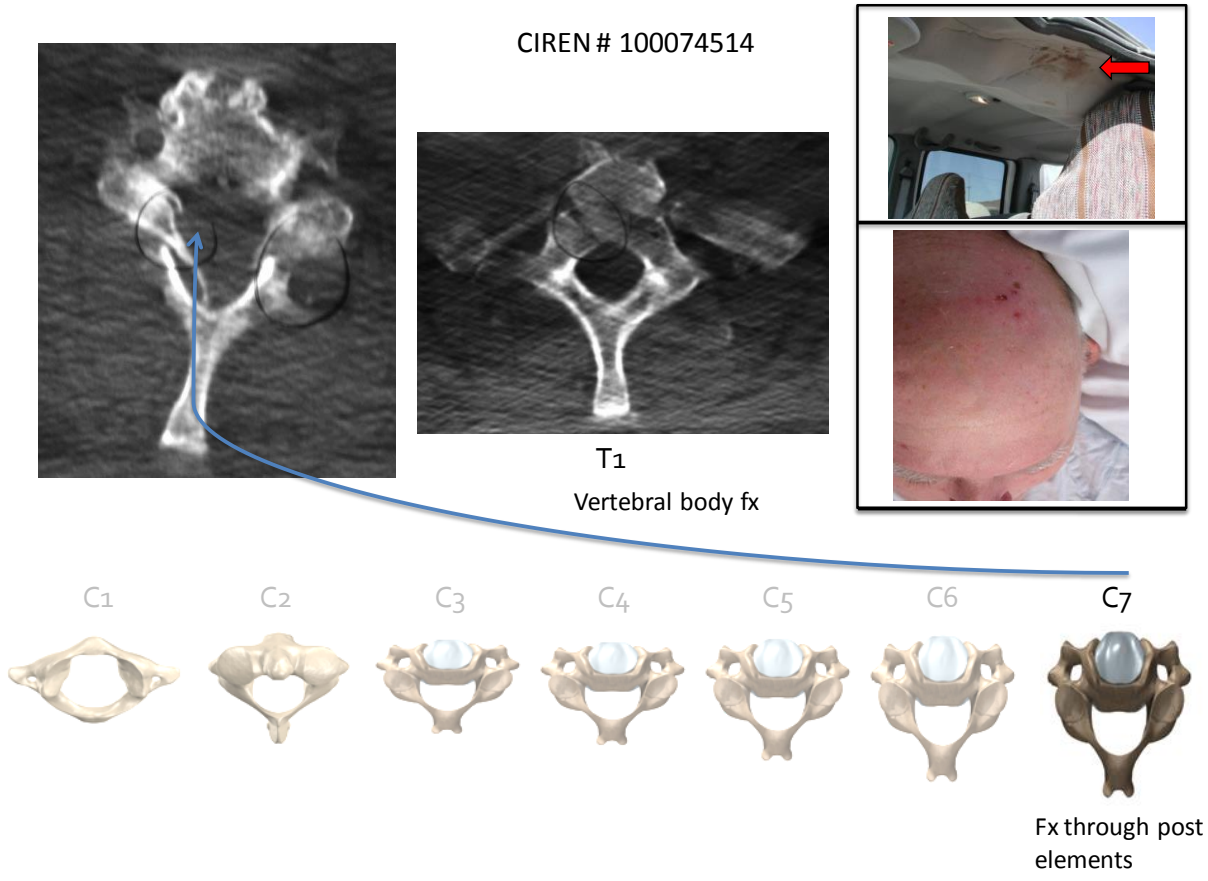

CIREN Case # 125299

The 53 year old male right front passenger was involved in a 4 quarter turn, left-side leading rollover. The vehicle left the right side of the road and its left wheels dug into sod, resulting in a rollover that significantly deformed the passenger side roof and A-pillar.

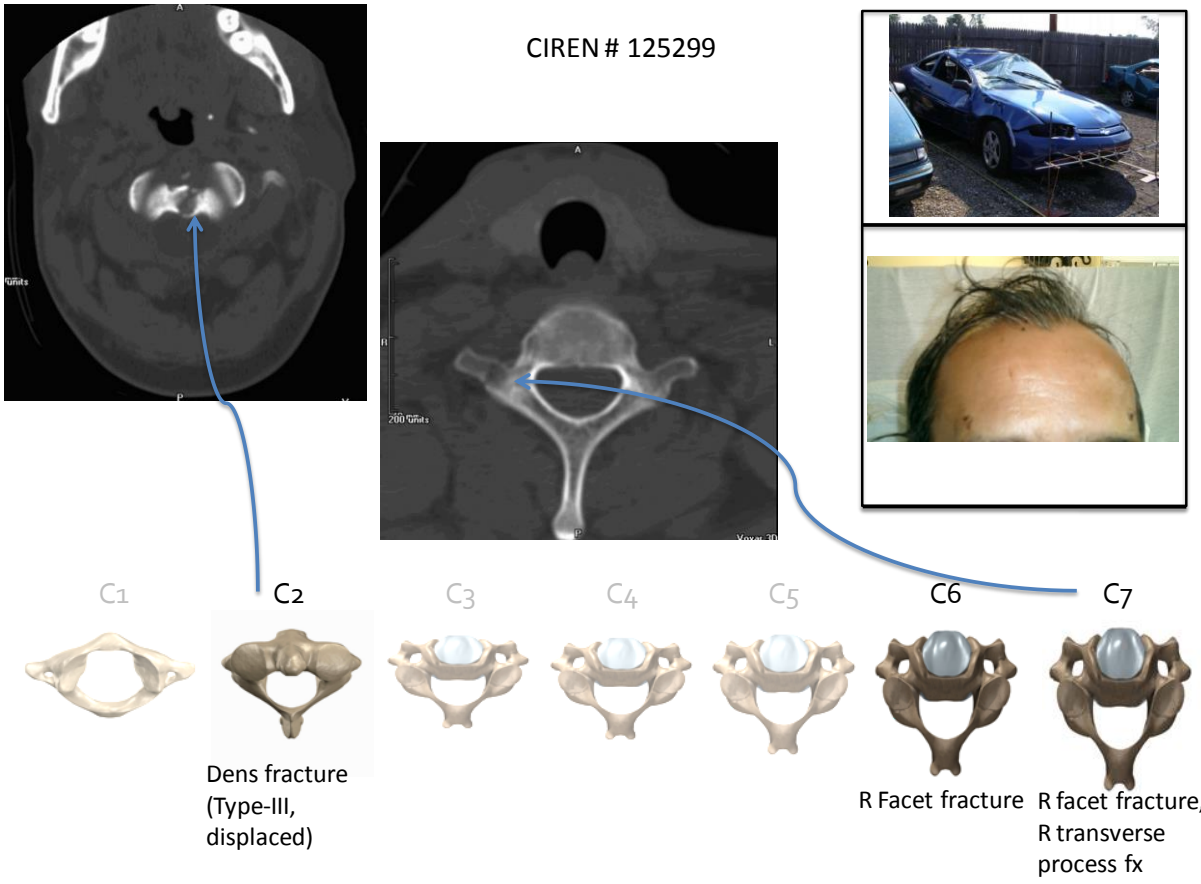

CIREN Case # 100084523

The case occupant is a 33 year old female driver involved in a 8 quarter turn rollover. She was situated at the far side of the roll, after he car was allowed to interact with the bituminous roadway following a counter-clockwise yaw. The left B-pillar was deformed toward the driver's headrest. Her injuries are shown below:

CIREN # 100084523

No radiology available

No head/facial lacerations

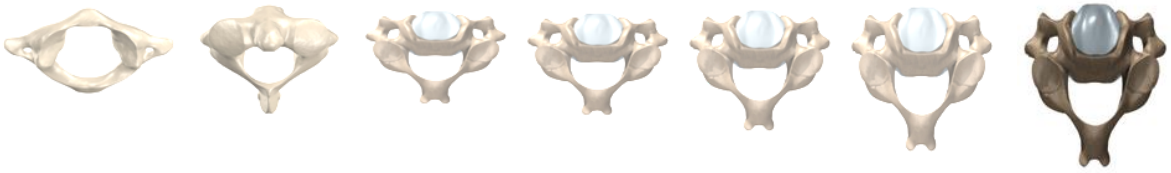

Left superior articular facet

CIREN Case # 100112055

The case occupant is a 34 year old female driver involved in a 8 quarter turn rollover. The vehicle yawed into the grassy median. The roof tented in the middle, which likely resulted from flat landings on both roof rails. There were massive roof and door ground interactions. Her cervical spine injuries are listed below:

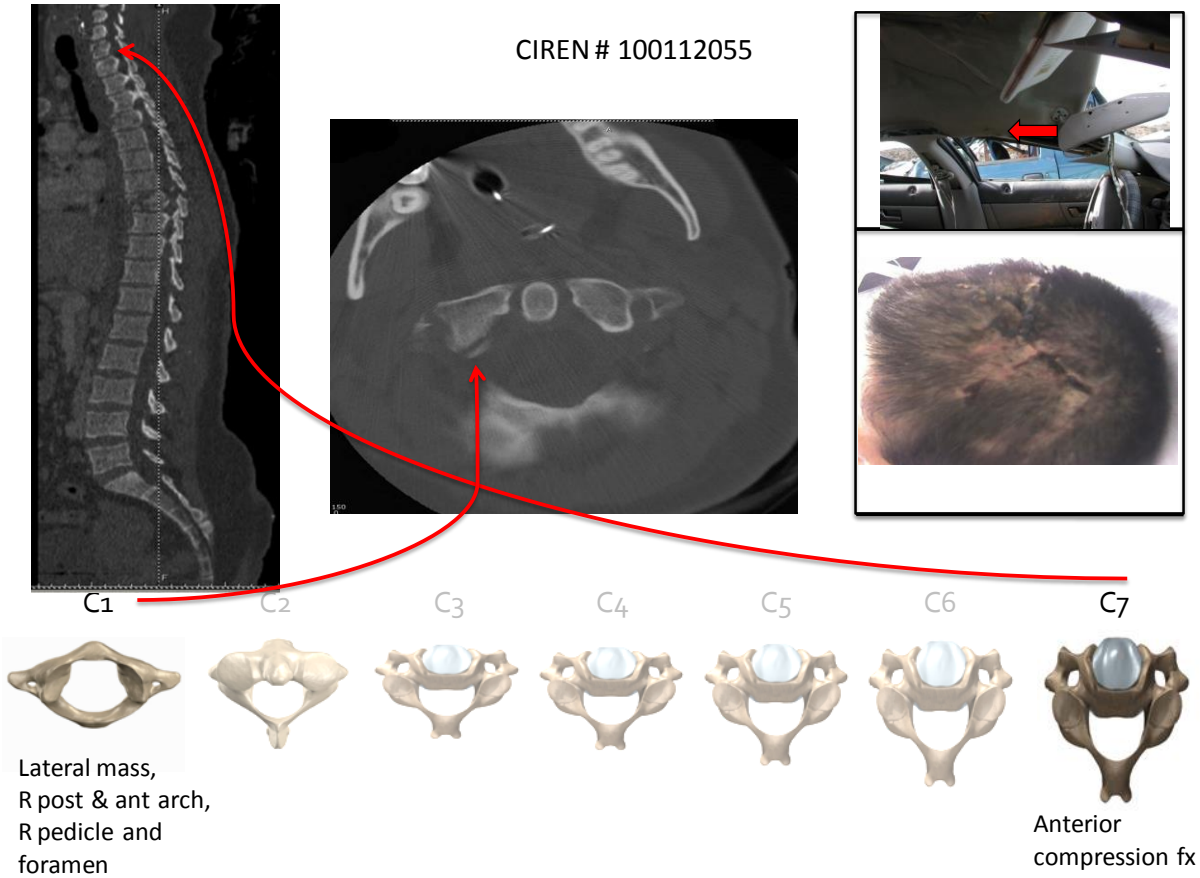

CIREN Case # 590123589

This case involves a 25 year old female driver involved in a 8 quarter turn rollover. After vehicle counter-clockwise yaw and trip in the sandy shoulder, the vehicle rolled, resulting in significant left side roof deformation. The driver A-pillar flattened inward.

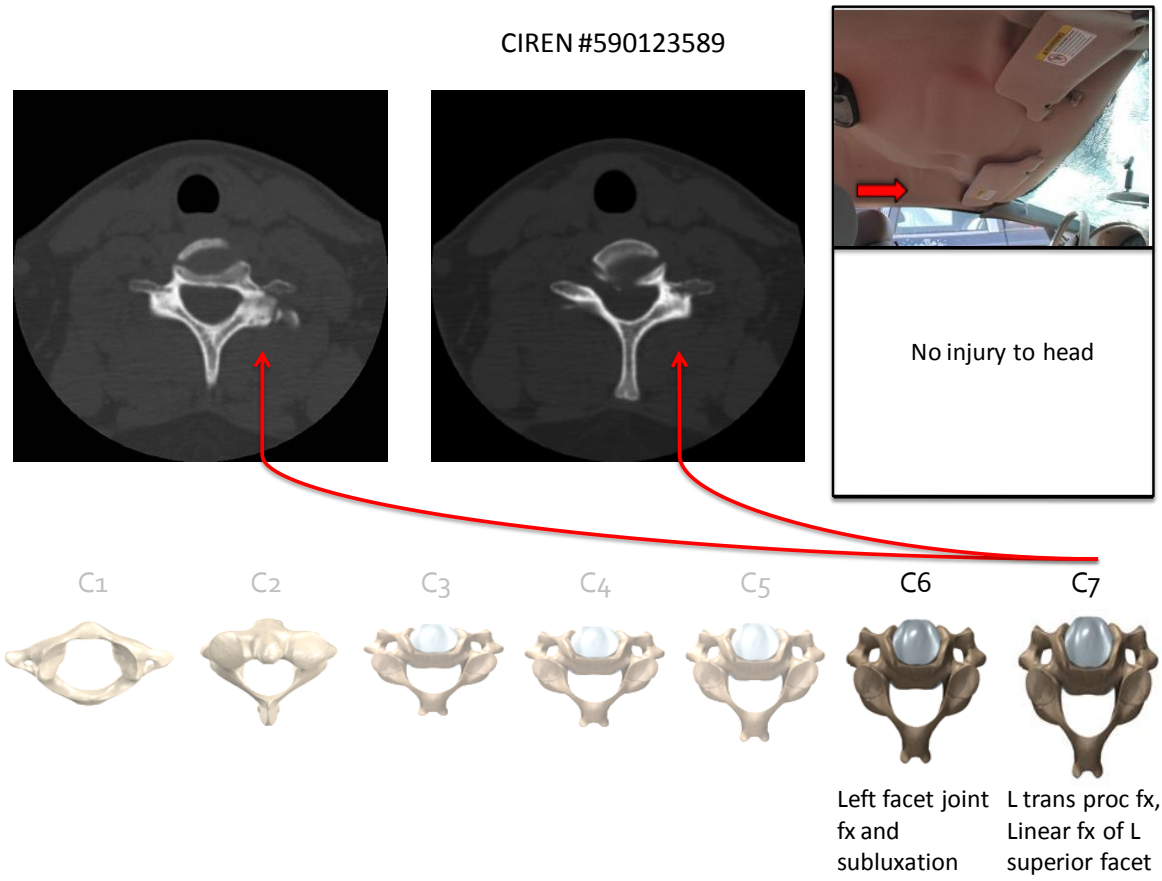

CIREN Case # 551068562

The case occupant, a 21 year old male passenger, was involved in a 4 quarter turn rollover. The vehicle interacted with a large pothole and the vehicle flipped hard to its right side. There was severe crush into the front right occupant space including inward deformation of the A-pillar. His injuries to the cervical spine are shown below:

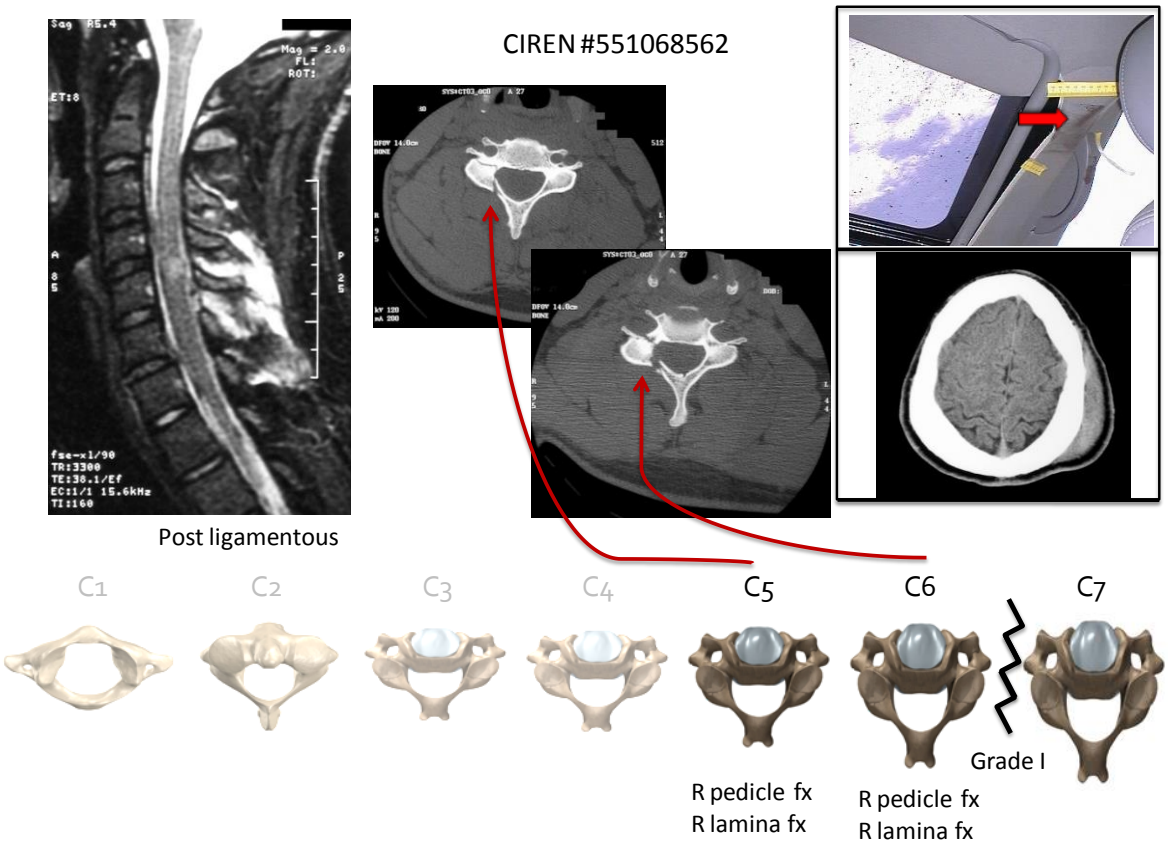

CIREN Case # 590144150

The case occupant, a 26 year old male driver, was involved in a 8 quarter turn right side leading rollover. His vehicle yawed counter-clockwise and tripped on gravel, and the vehicle rolled resulting in a high intrusion deformation to the center of the roof. The vehicle deformation and head contact suggest a far-side roll. His cervical spine injuries are displayed below:

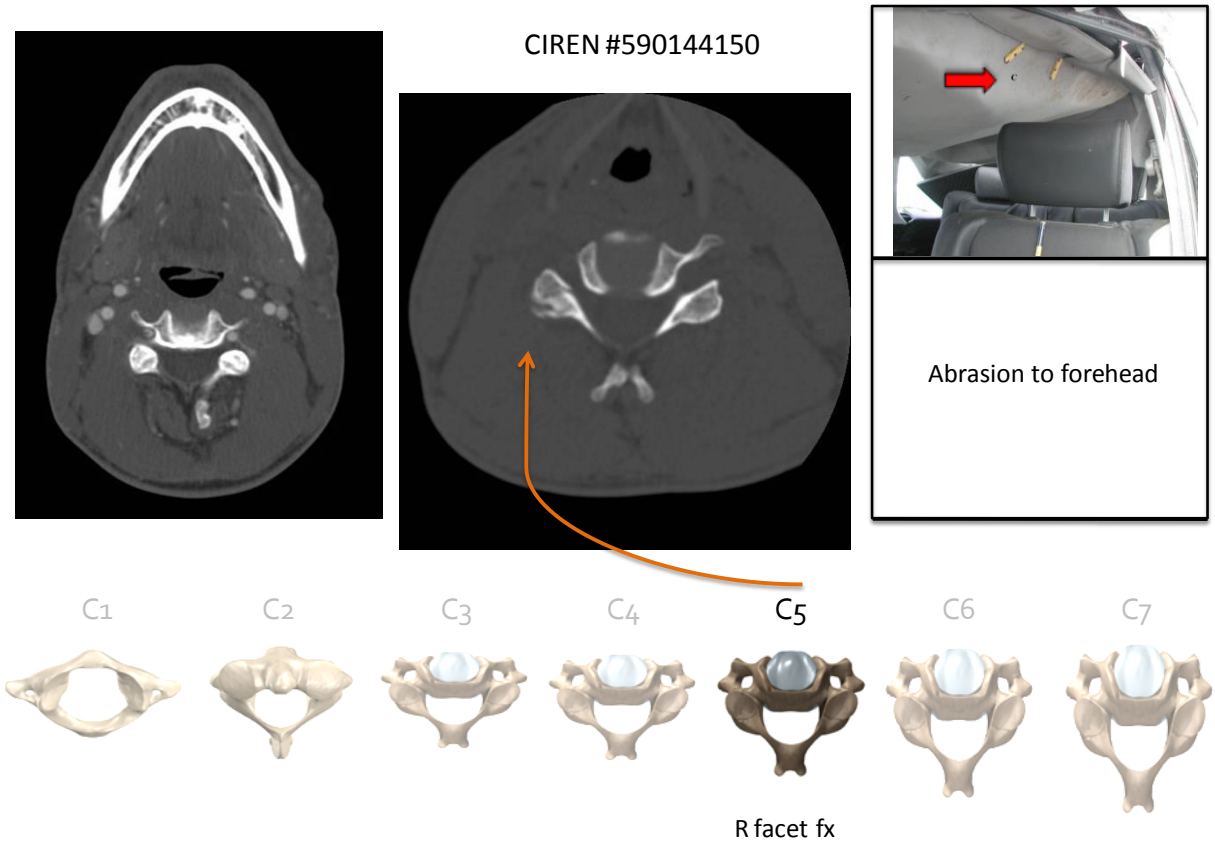

CIREN Case # 781125527

The case occupant, a 50 year old female driver, was positioned on the far side of a 6 quarter turn rollover. The vehicle lost control on ice and rolled over down an embankment, resulting in massive driver-side roof and A-pillar intrusion. The cervical spine injuries suffered are detailed below:

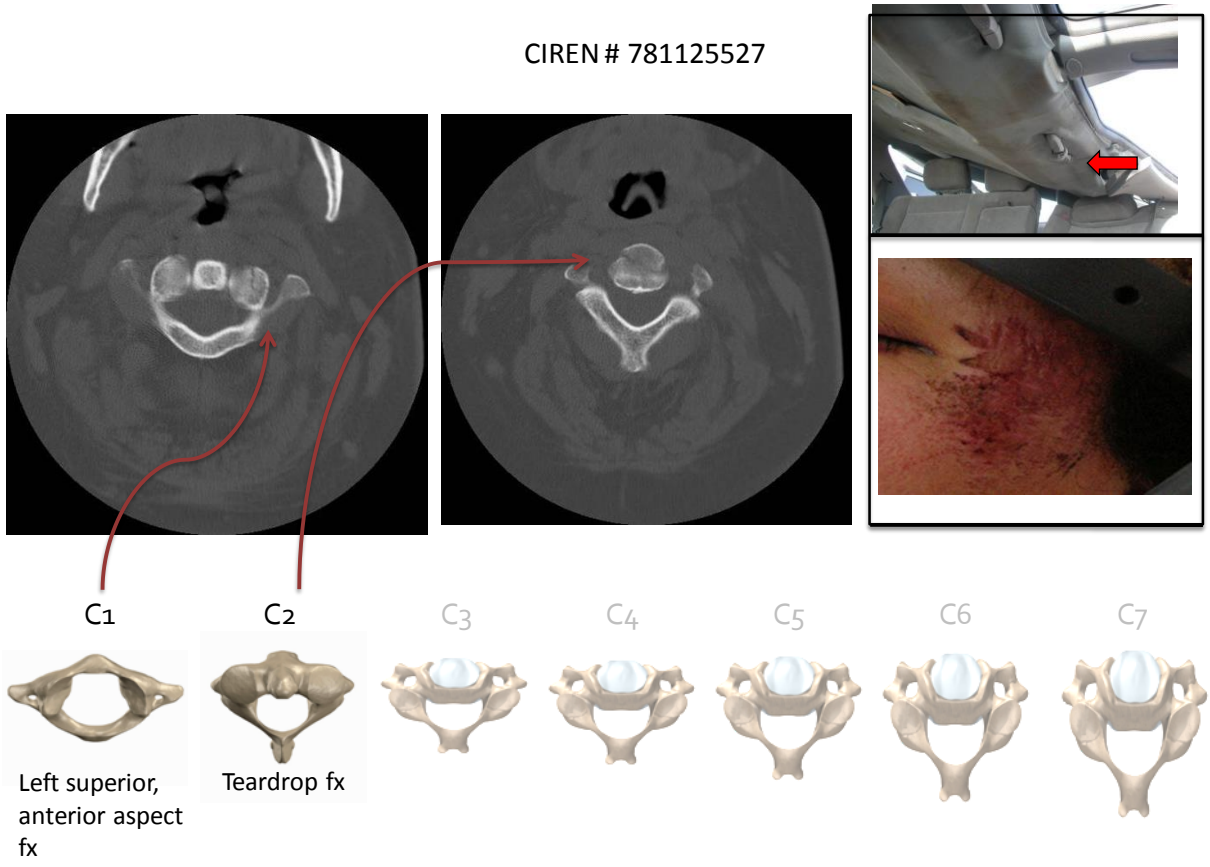

CIREN Case # 852126192

The 50 year old male case occupant was a driver involved in a 4 quarter turn right-side leading rollover. The driver-side roof rail was slated downward toward the front of the Chevrolet Express van and made contact with the driver's headrest. The cervical spine injuries sustained by the driver are illustrated below:

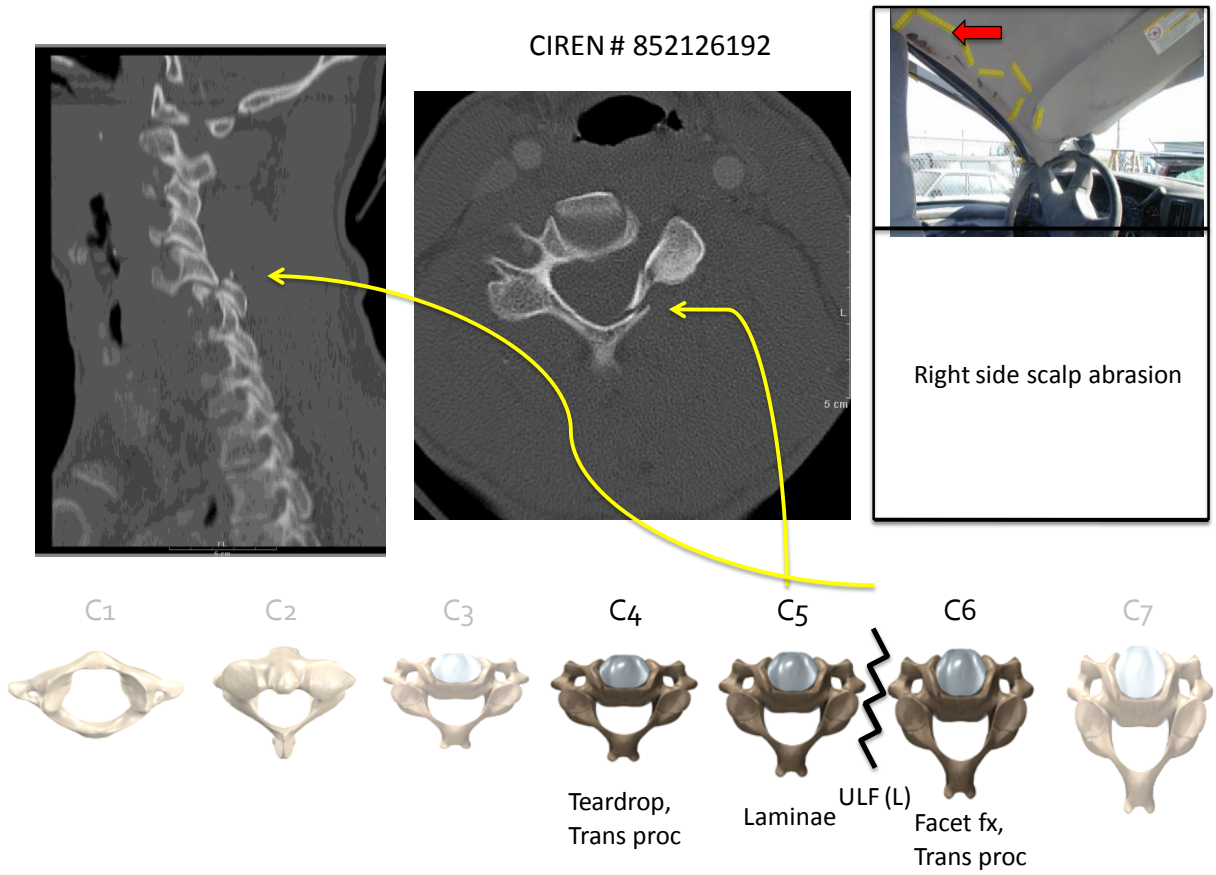

CIREN Case # 852162058

The occupant in this case is a 32 year old male front right passenger in a vehicle involved in a 4 quarter turn rollover. He was positioned on the far side of the roll. The vehicle left the left-side shoulder and travelled into a ditch. The vehicle involved was a BMW Z4 convertible and the convertible top came undone during the roll. The cervical spine injuries sustained by the right front occupant are shown below:

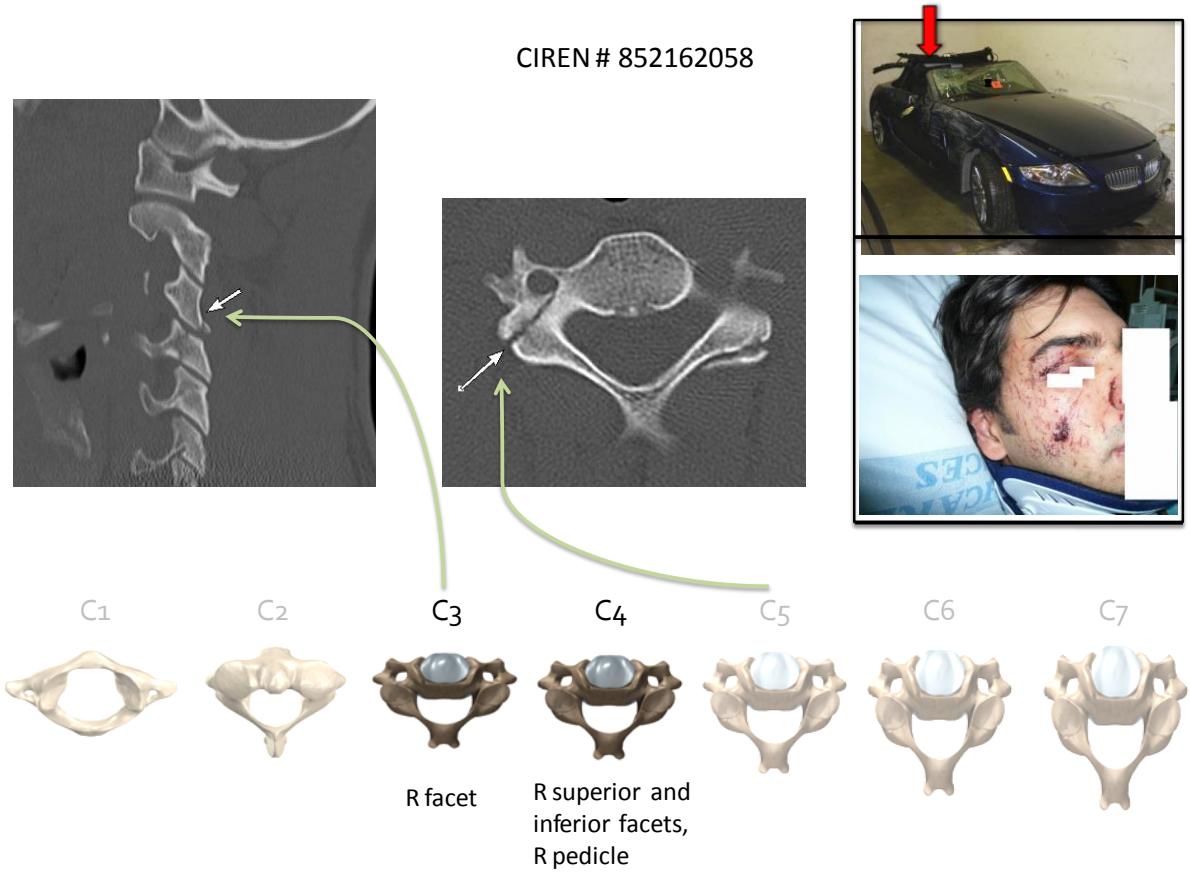

CIREN Case # 852130600

The case occupant is a 78 year old female driver involved in a rollover. The vehicle lost control and began a counter-clockwise yaw leading to a 2 quarter turn rollover into a roadside ditch. The roof of her vehicle was undeformed, as the vehicle's front bumper and trunk suspended the vehicle's roof above the ground at the bottom of the ditch. She still sustained cervical spine injuries:

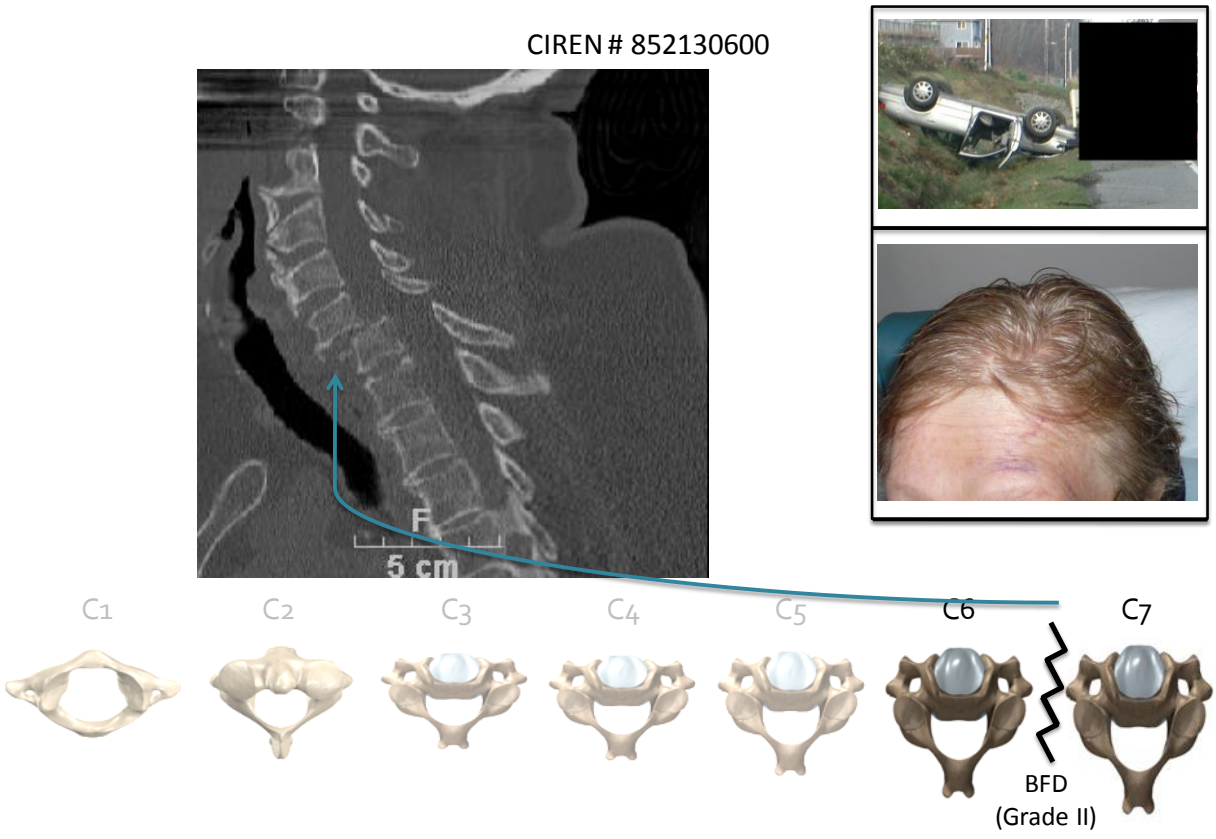

CIREN Case # 852172396

The occupant involved in the rollover crash was a 25 year-old female front right passenger. She was positioned on the near side of the roll, after the vehicle she was seated in lost control and travelled down a sloped median and rolled 8 quarter turns. There was large intrusion on the driver-side and the roof tented in the middle. The sustained cervical spine injuries are as follows:

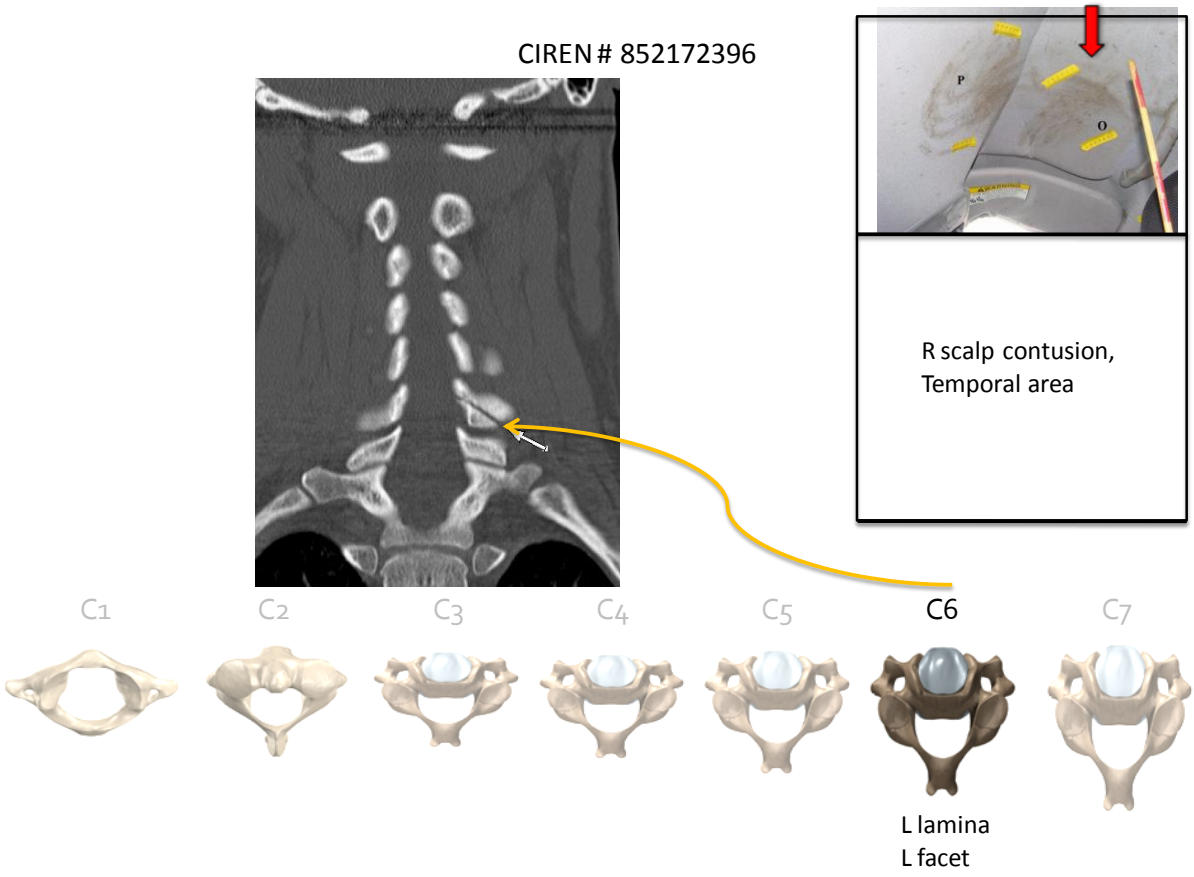

CIREN Case # 852177768

The case occupant is a 28 year old male driver positioned on the far side of a 8 quarter turn rollover. The vehicle rolled on a level grassy area once on the hood and once over the roof. These contacts resulted in shearing deformation to the roof. The driver sustained the following cervical spine injuries:

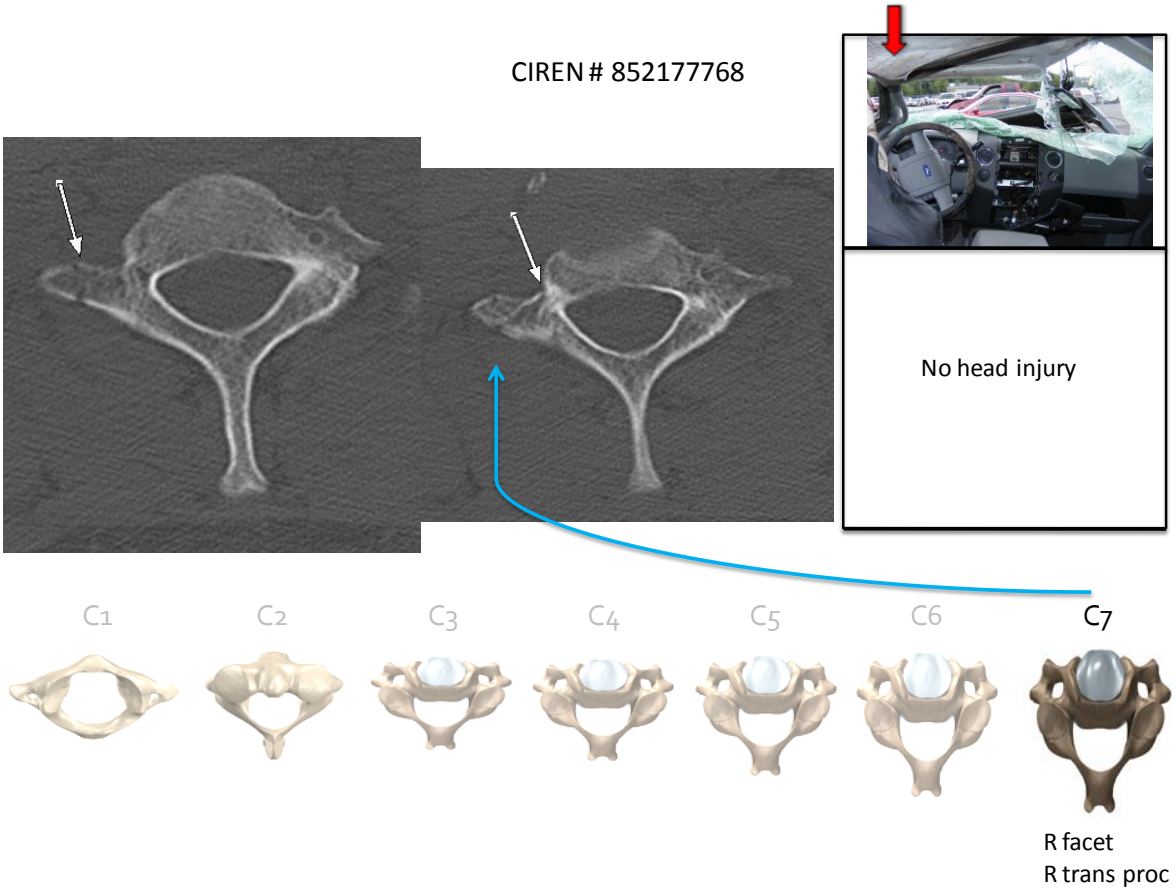

CIREN Case # 857069807

The 44 year old male front right passenger is the case occupant involved in a 8 quarter turn rollover. He was positioned on the far side of the roll, as the driver overcorrected to the right after avoiding an object in the road. The A-pillar on the passenger's side was almost completely flattened, resulting in the following cervical spine injuries:

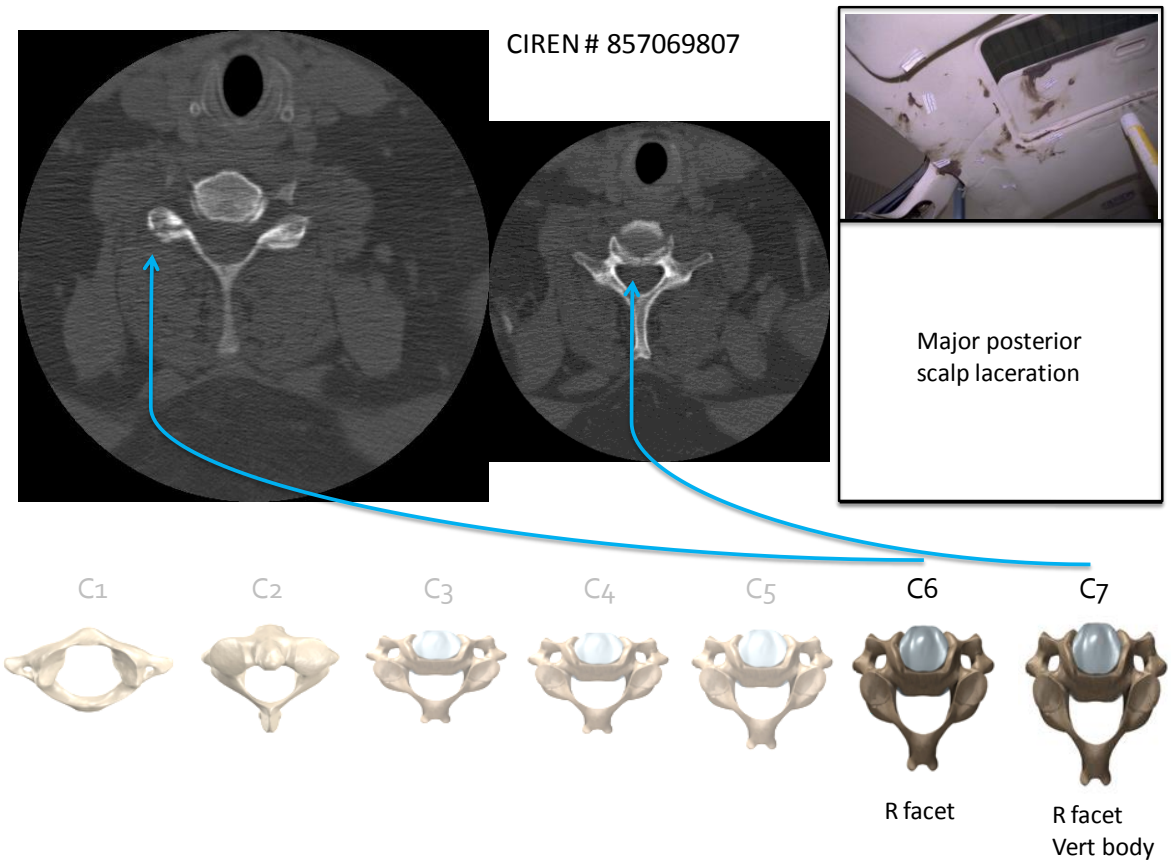

CIREN Case # 857076778

The case occupant is a 24 year old male front right passenger positioned on the far side of a 10 quarter turn rollover. The vehicle rollover took place in a grassy median resulting in severe deformation into the driver's compartment. The passenger's side saw toepan intrusion with less roof intrusion. He sustained the following cervical spine injuries:

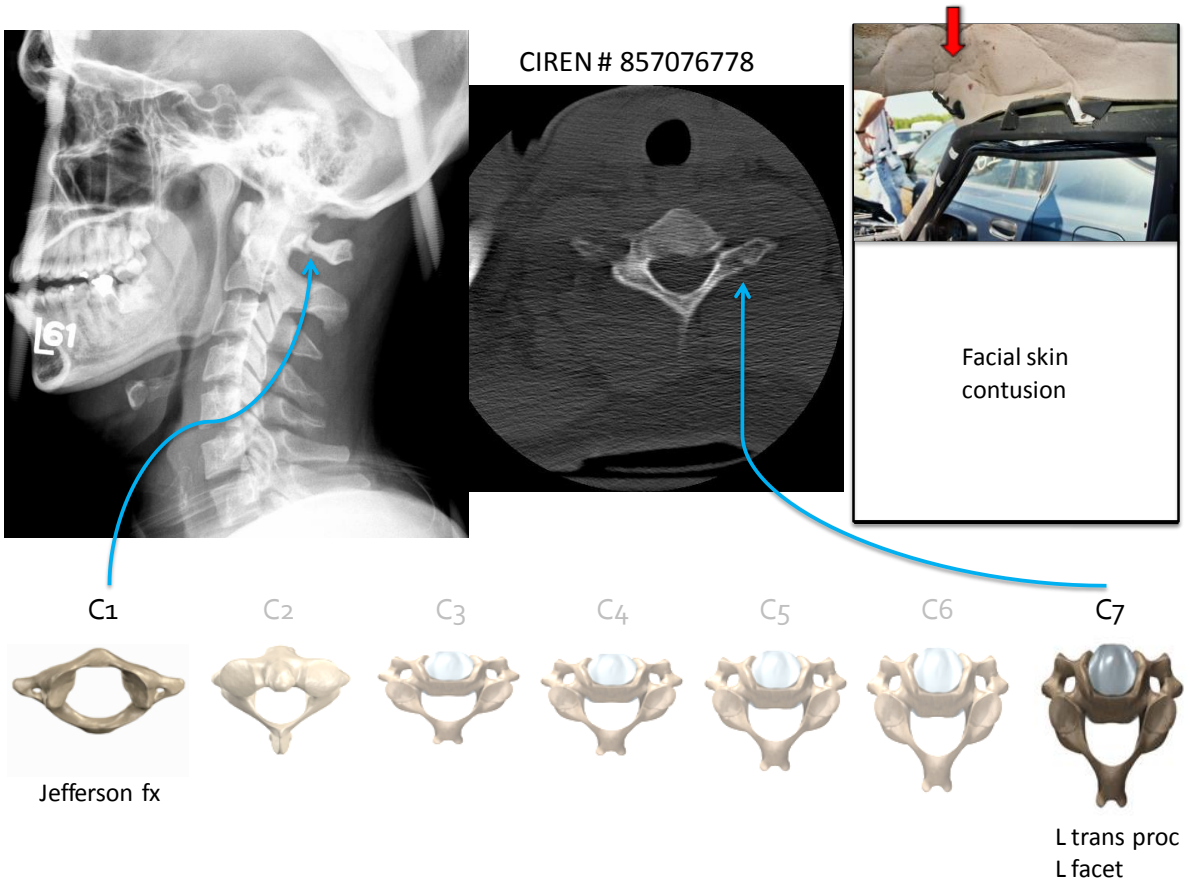

CIREN Case # 965066489

The case occupant, a 18 year old male driver, was involved in a 6 quarter turn rollover. There was significant roof crush into the driver's compartment due to the right-side leading roll. He sustained the following cervical spine fractures:

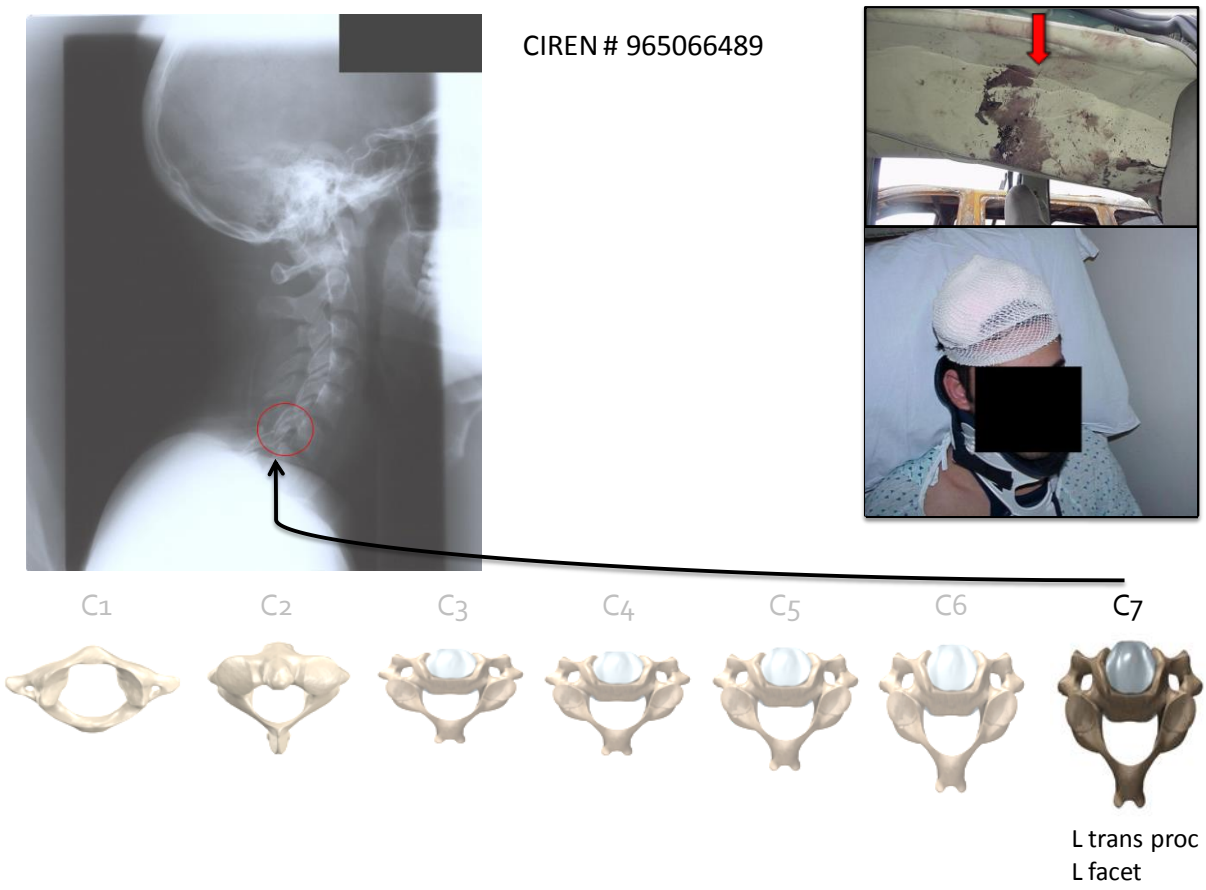

Appendix B

Images, Raw, and Scaled Data of Cadaveric Cervical Spine Compression Tests

Test Method		V700
ASTM D-1667	**Density** (lbs./cu.ft.) (kg/m3)	**7** **112**
ASTM D-2240	**Hardness** (shore 00)	**14**
ASTM D-1667	**Compression Deflection @ 25%** (psi) **kPa**	**0.8** **6**
ASTM D-1667	**Compression Set @ 25%**	**4**
GTP (1)	**Water Absorption** (% by volume)	**1.1**
ASTM D-412	**Tensile Strength** (psi) **kPa**	**25** **173**
ASTM D-412	**Percent Elongation**	**150**
ASTM C-518	**Thermal Conductivity** (k factor) (btu-in.)/(hr.sq.ft.) (°F) **w/mK**	**0.27** **0.039**
	Recommended Service Temperature (°F) (°C)	**-40 - 180** **-40 - 82**
	Recommended Application Temperature (°F) (°C)	**50 - 110** **10 - 45**

Notes:
The length of the rolls vary depending on the thickness of the material. Gaska Tape offers standard length logs, master logs are double the standard length plus 2" and available upon request for quote.

(1) Gaska Tape Procedure

Typical performance properties and characteristics are based on samples tested and are not guaranteed for all samples of this product.

Data is intended as a guide only and is presented without guarantees and without assumption of liabilities resultant from the use of information provided. This data is not to be used for specification purposes.

Figure B1: Material properties of one-inch impact foam.

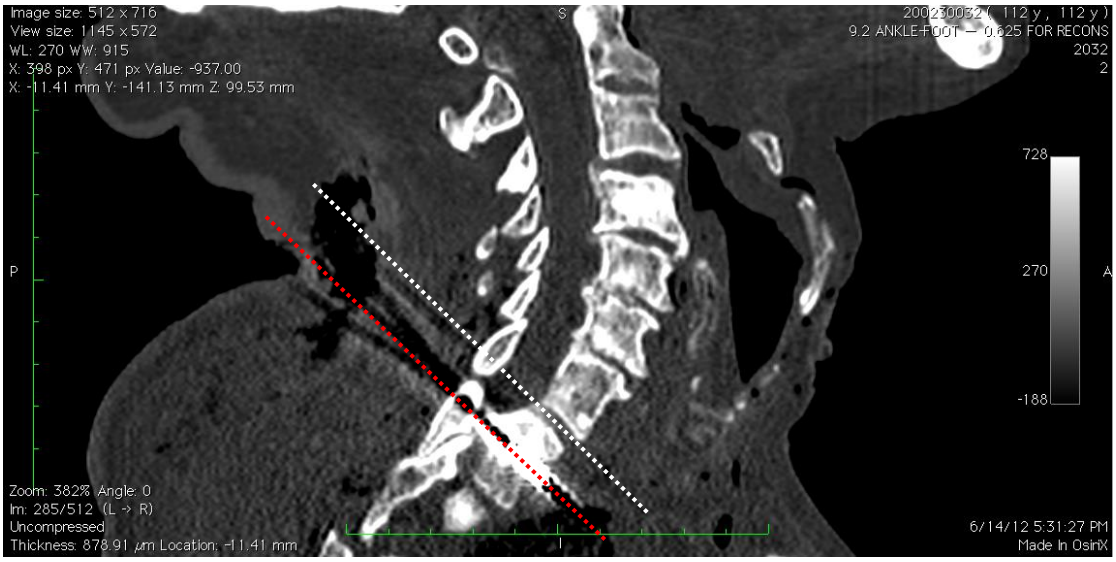

Figure B2: Sagittal CT of Cadaver 552 showing 0-degree angle between T1 mounting screws and the T1 endplate.

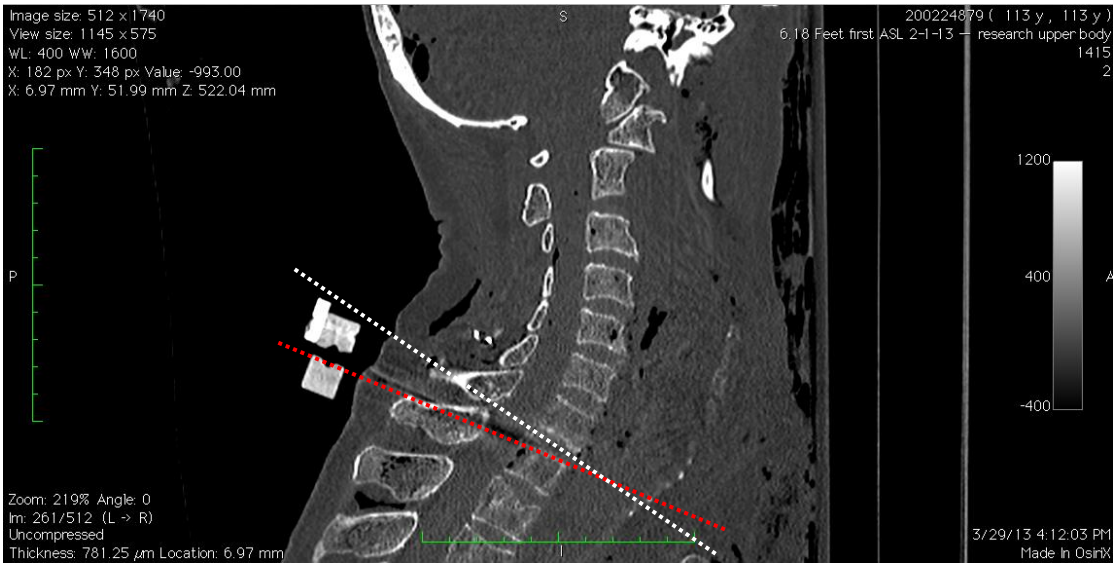

Figure B3: Sagittal CT of Cadaver 553 showing 13-degree angle between T1 mounting screws and the T1 endplate.

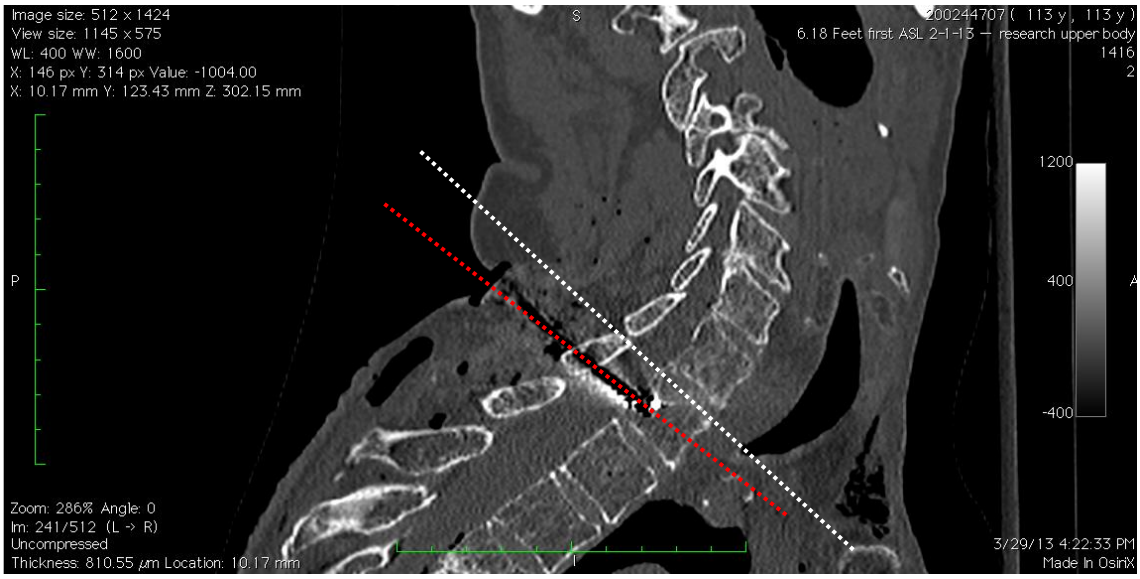

Figure B4: Sagittal CT of Cadaver 631 showing 5-degree angle between T1 mounting screws and the T1 endplate.

Device	*Manufacturer*	*Model*	*S/N*
X-ray tube	Varian	B-180H	H210819
Generator	Quantum Medical	VZW2930RD3-14	AM15991C12
Control Console	Quantum Medical	73662901	J0000984C12

Figure B5: Details on the University of Virginia Center for Applied Biomechanics dynamic x-ray system.

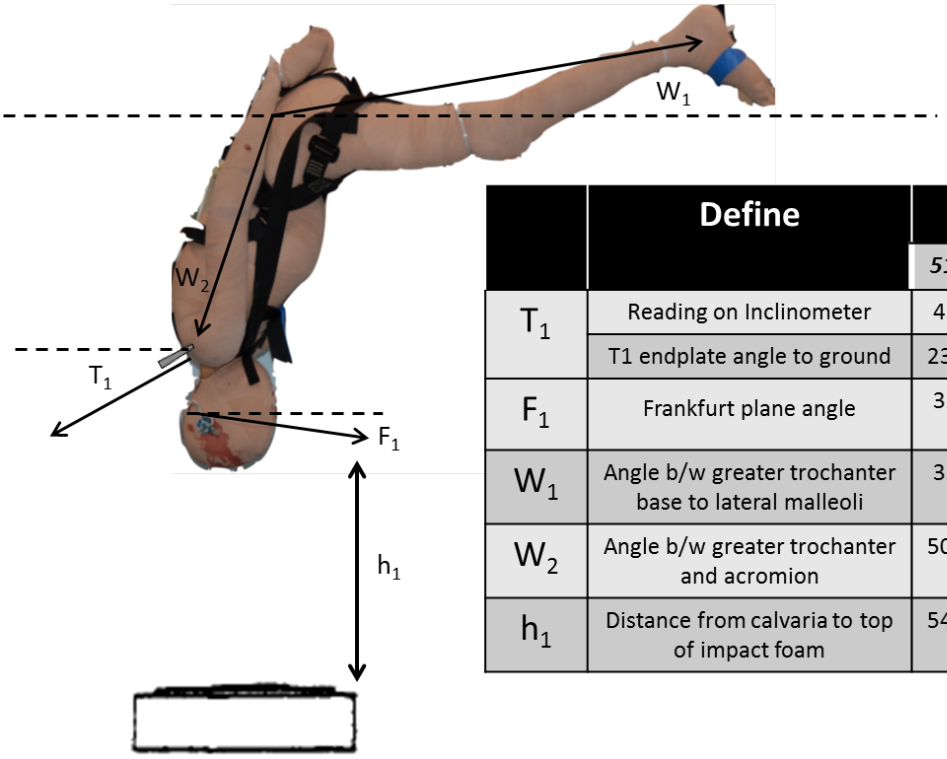

	Define	Degrees or cm			
		516	*552*	*631*	*553*
T_1	Reading on Inclinometer	4.0	23.6	19.1	7.6
	T1 endplate angle to ground	23.0	23.6	24.1	23.6
F_1	Frankfurt plane angle	3.0	2.9	1.5	0.4
W_1	Angle b/w greater trochanter base to lateral malleoli	3.5	1.4	14.3	17.0
W_2	Angle b/w greater trochanter and acromion	50.0	66.0	70.0	66.9
h_1	Distance from calvaria to top of impact foam	54.5	54.5	59.5	59.5

Figure B6: Measurements of anthropometry and pre-positioning were tabulated for each test.

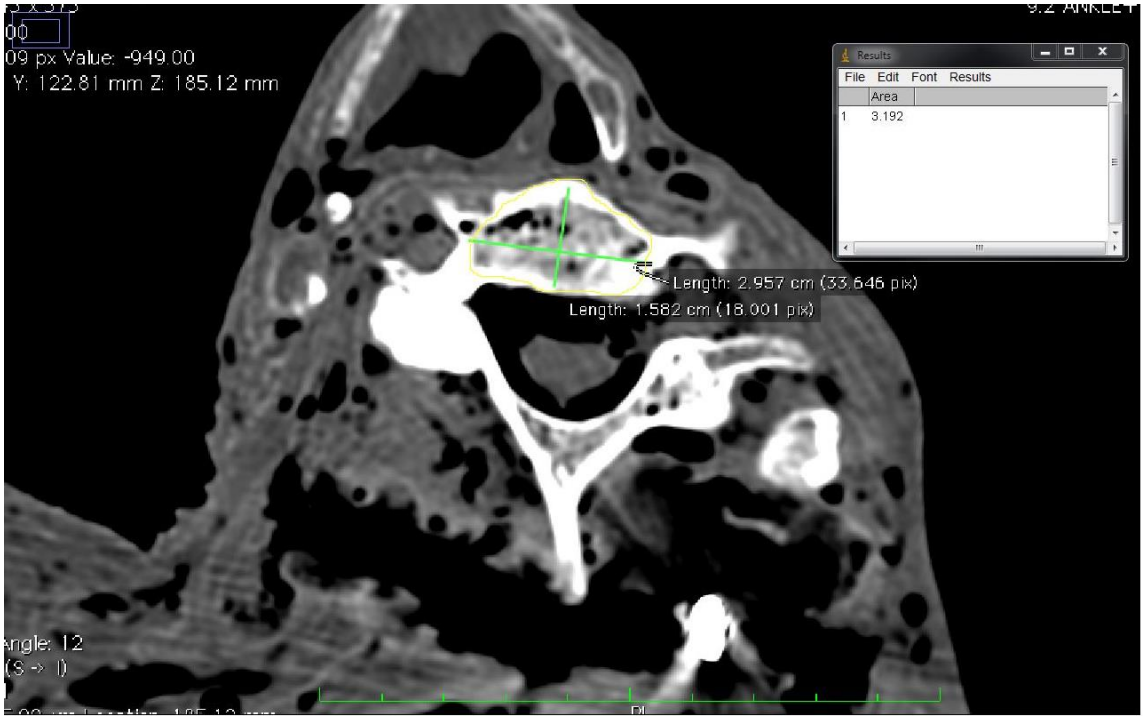

Figure B7: Transverse CT of Cadaver 516 C6 inferior endplate, traced and measured with a cross-sectional area of 3.192 cm^2. Measurements were used to scale kinetics and kinematics data.

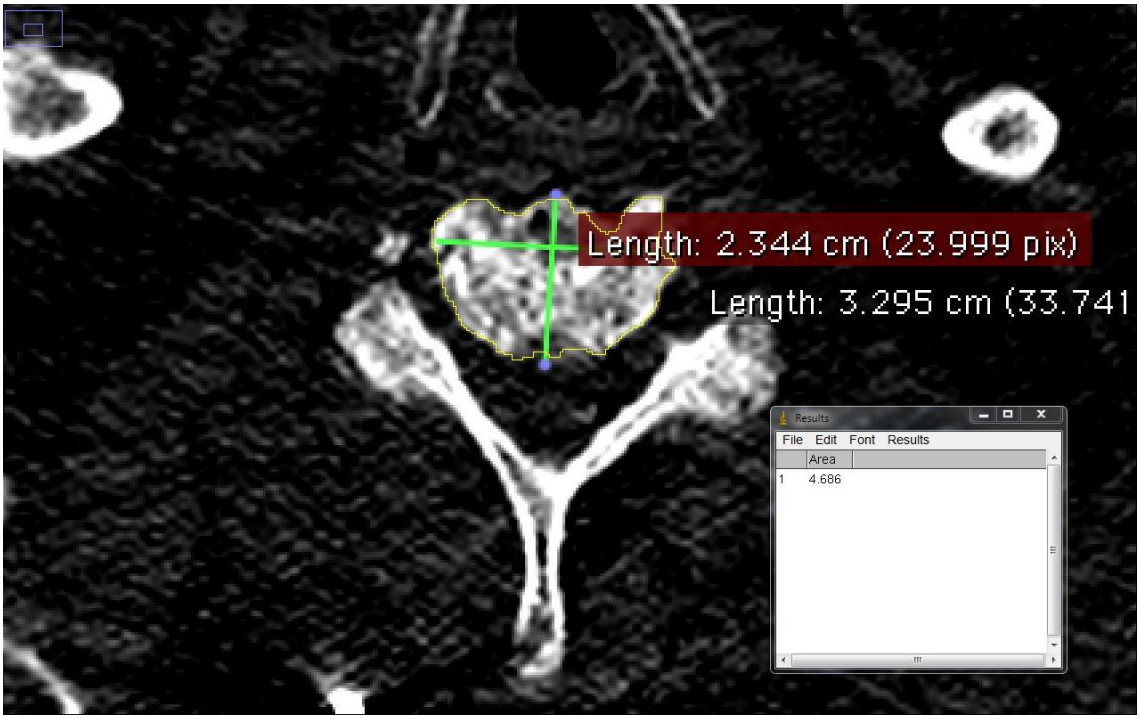

Figure B8: Transverse CT of Cadaver 552 C6 inferior endplate, traced and measured with a cross-sectional area of 4.686 cm^2.

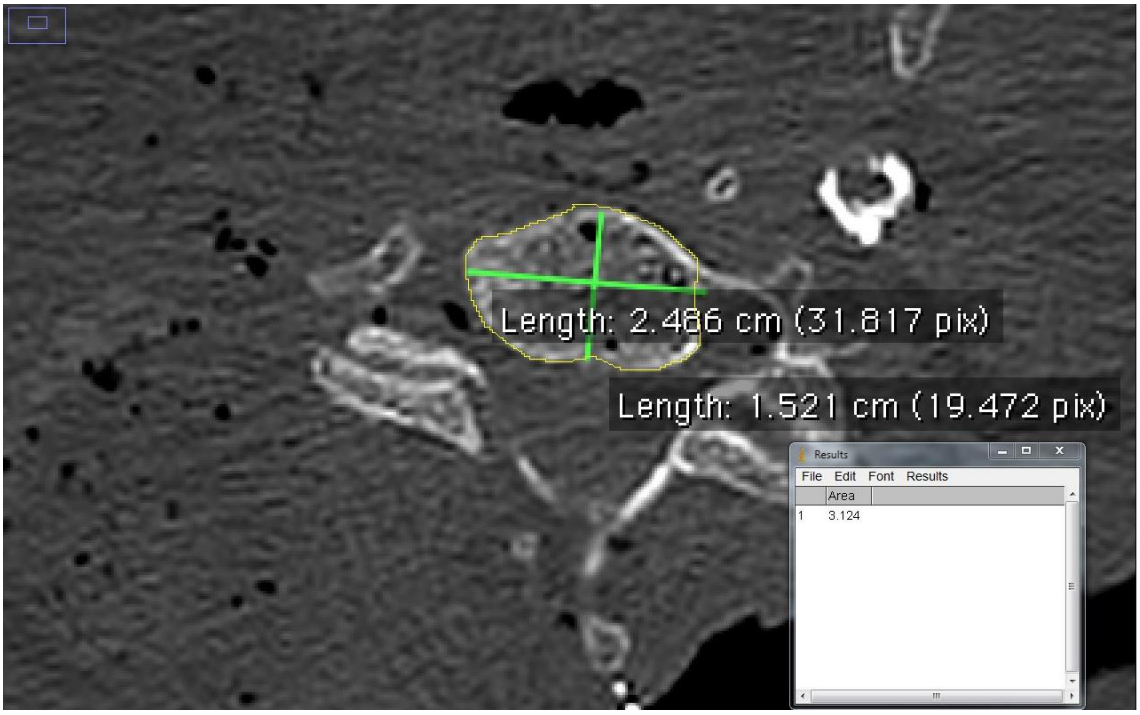

Figure B9: Transverse CT of Cadaver 553 C6 inferior endplate, traced and measured with a cross-sectional area of 3.124 cm^2.

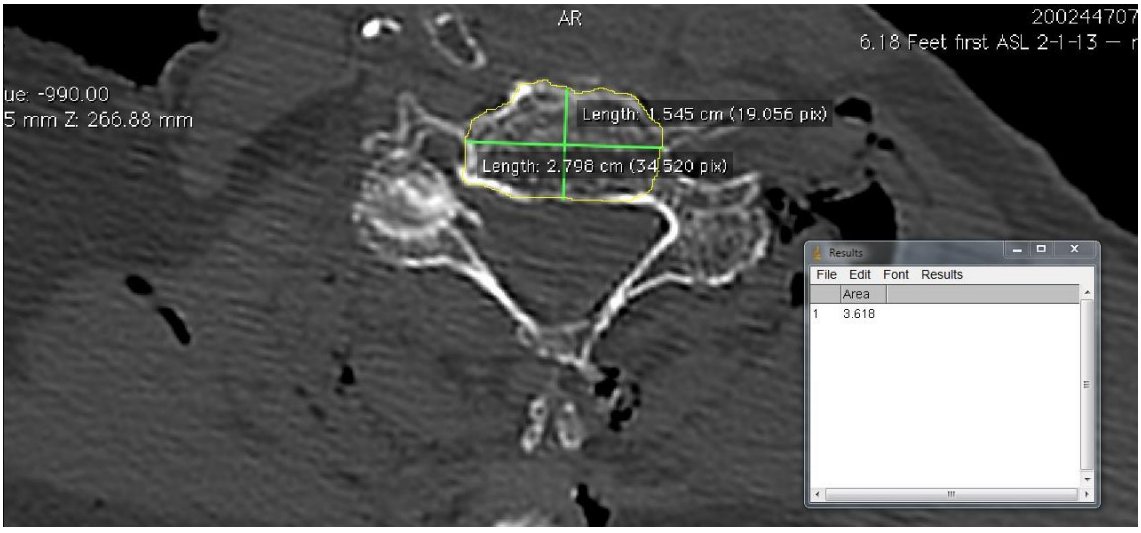

Figure B10: Transverse CT of Cadaver 631 C6 inferior endplate, traced and measured with a cross-sectional area of 3.681 cm^2.

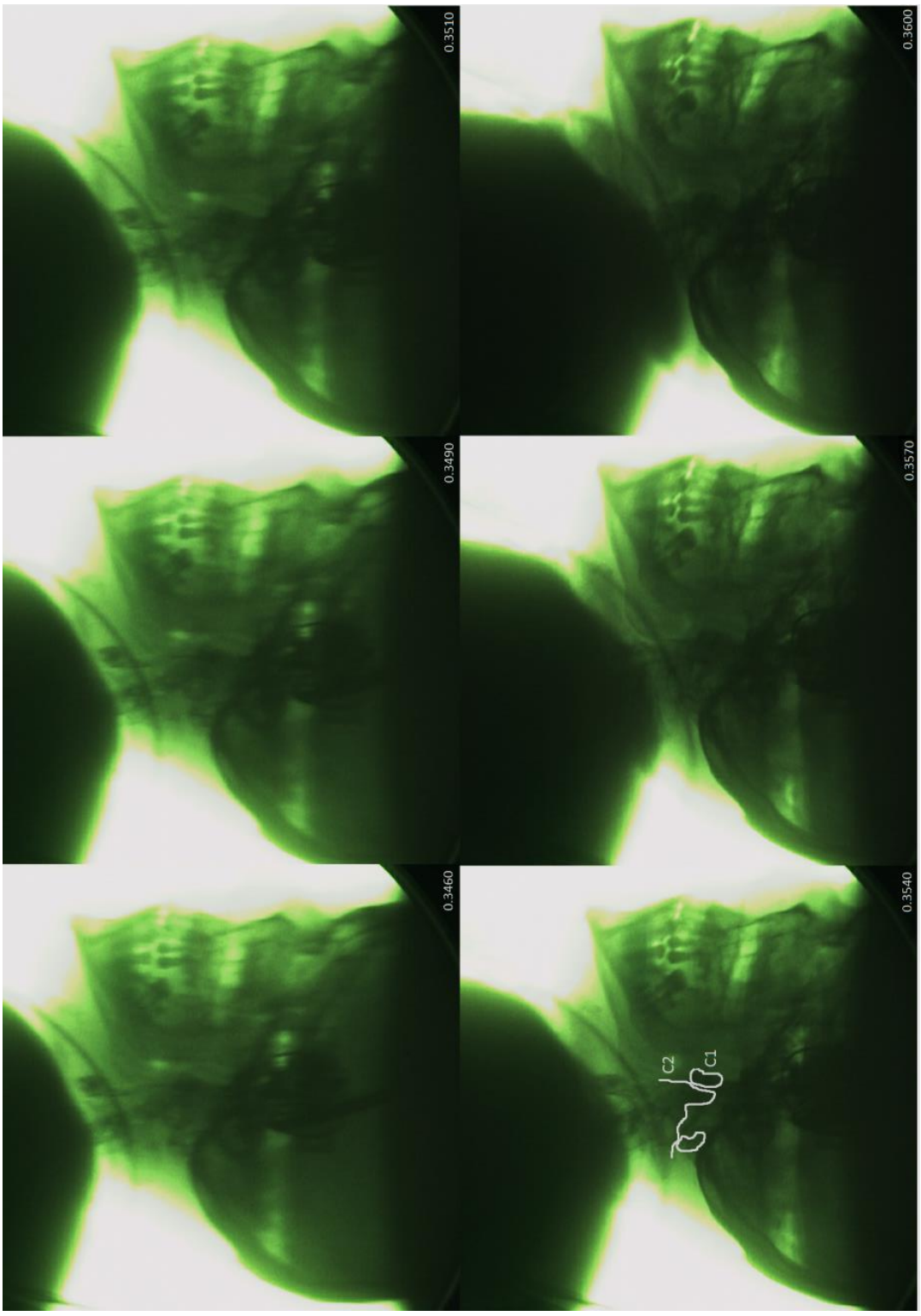

Figure B11: Radiology images of Cadaver 553 during first 15msec of head contact. It is believed that despite the dens contacting the anterior ring of C1 during buckling, the Type-III odontoid fracture occurred after the test was terminated.

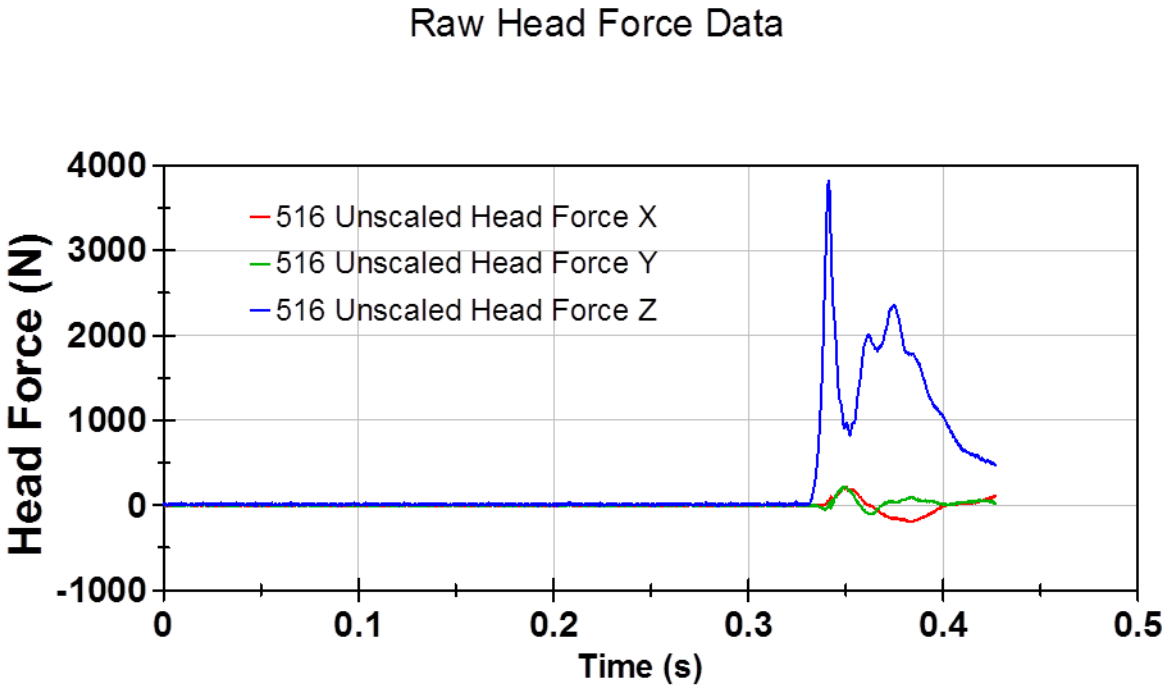
Raw Head Force Data
516 Unscaled Head Force X
516 Unscaled Head Force Y
516 Unscaled Head Force Z
Head Force (N)
Time (s)
4000
3000
2000
1000
0
-1000
0
0.1
0.2
0.3
0.4
0.5

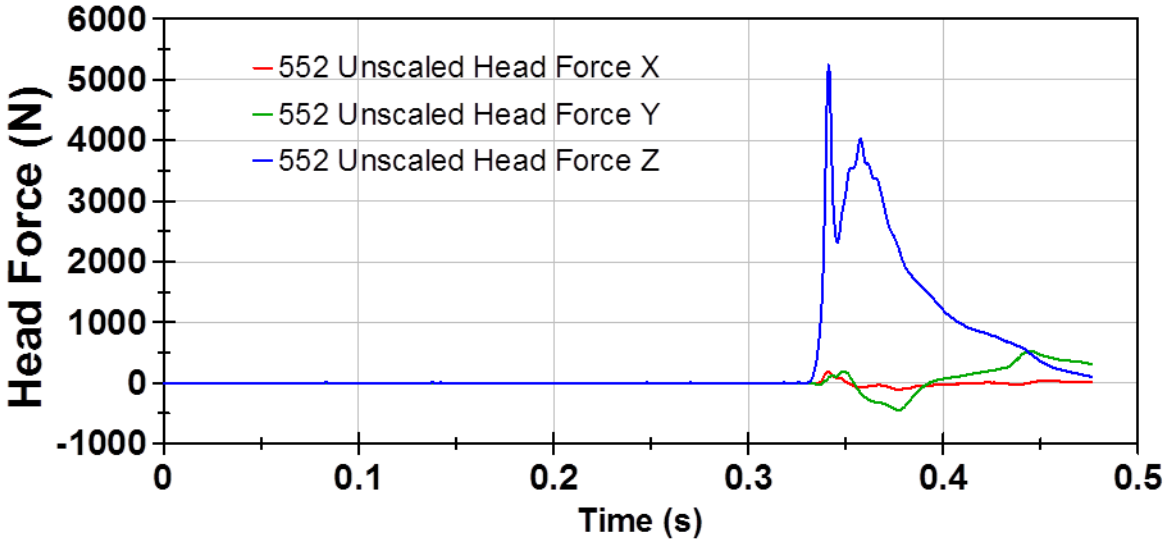
552 Unscaled Head Force X
552 Unscaled Head Force Y
552 Unscaled Head Force Z
Head Force (N)
Time (s)
6000
5000
4000
3000
2000
1000
0
-1000
0
0.1
0.2
0.3
0.4
0.5

Raw Head Force Data

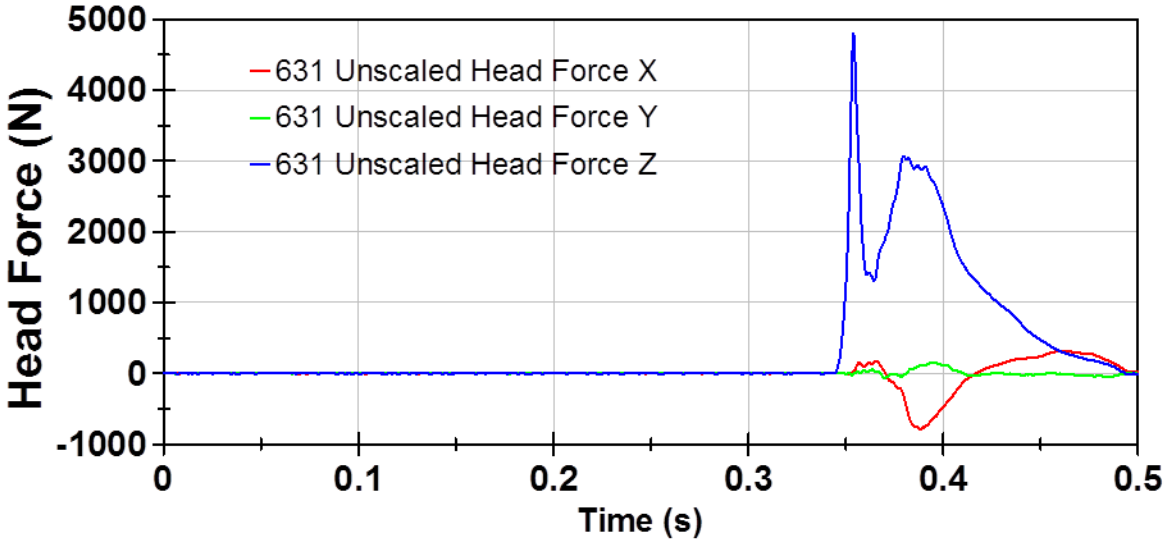

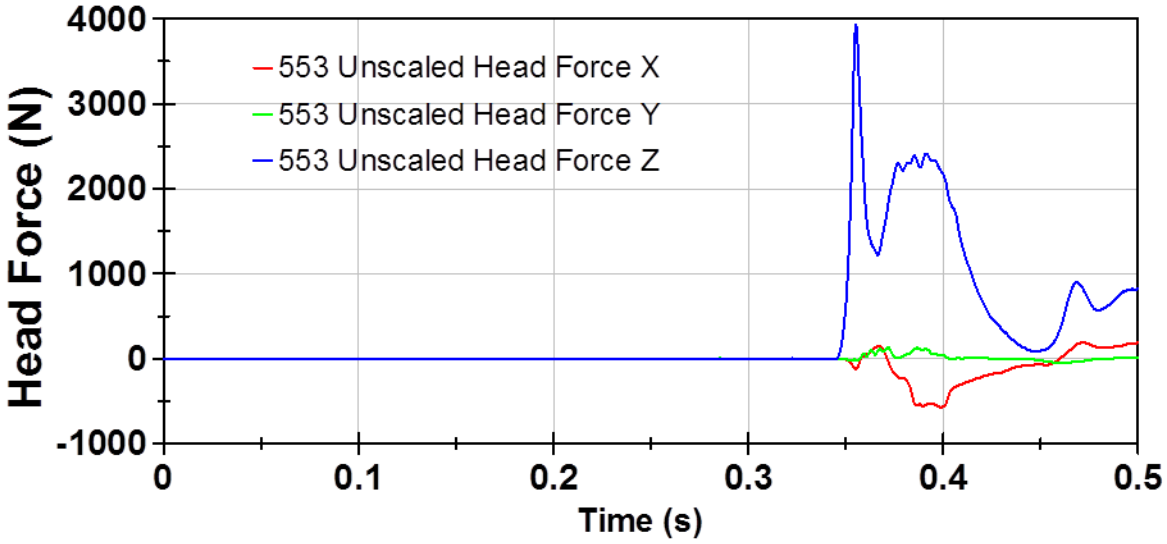

Raw Head CG Acceleration Data

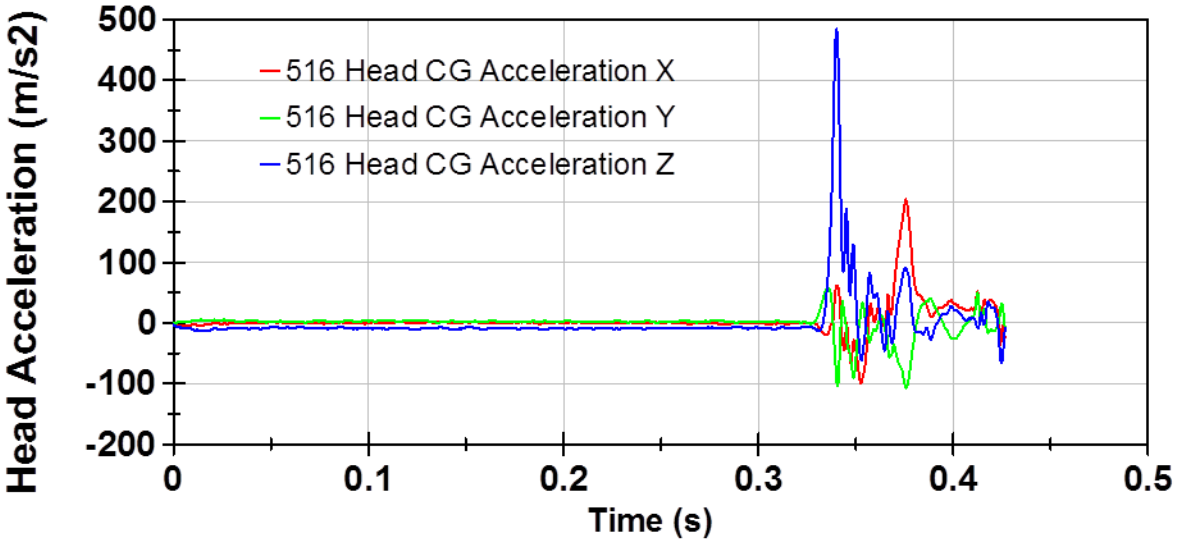

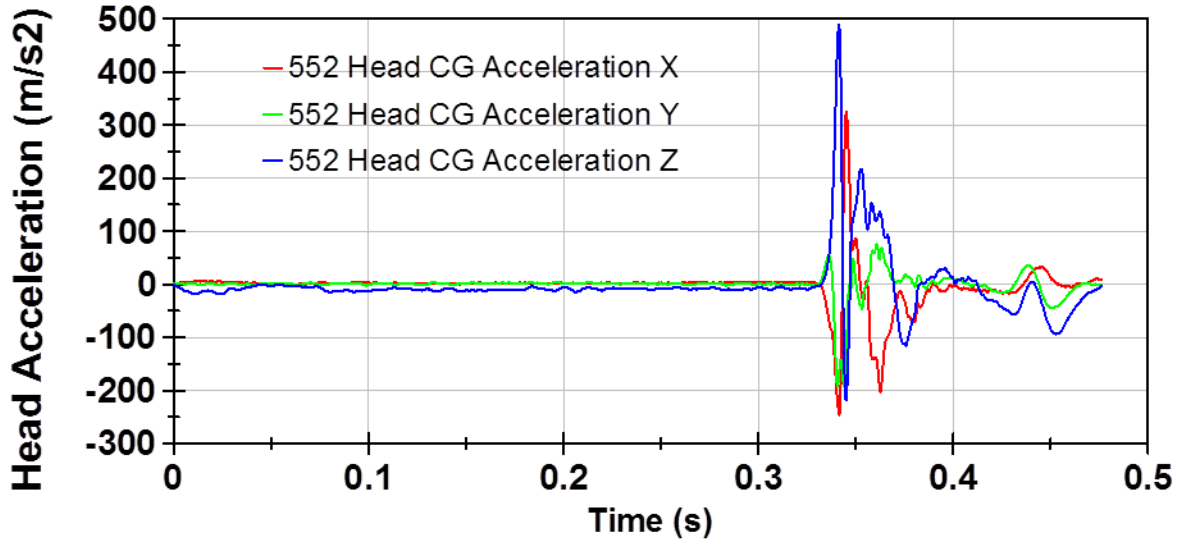

Raw Head CG Acceleration Data

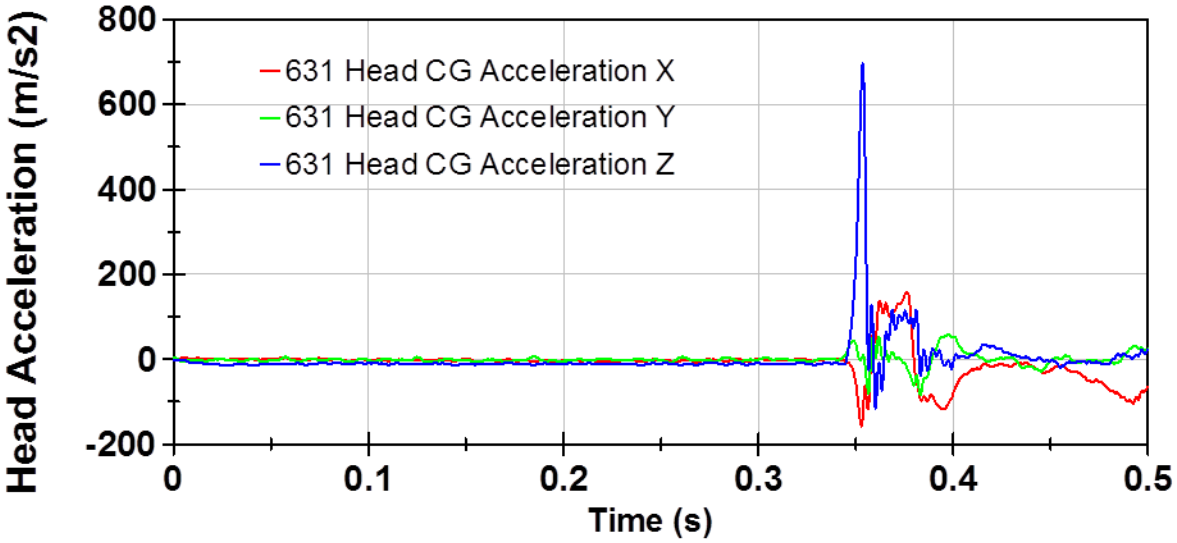

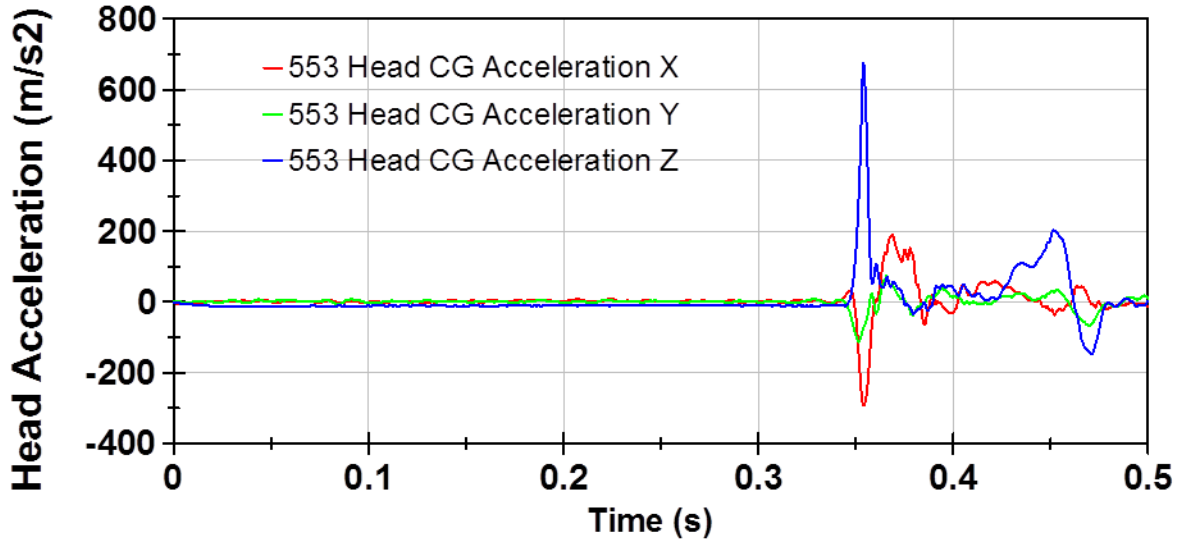

Raw T1 Acceleration Data

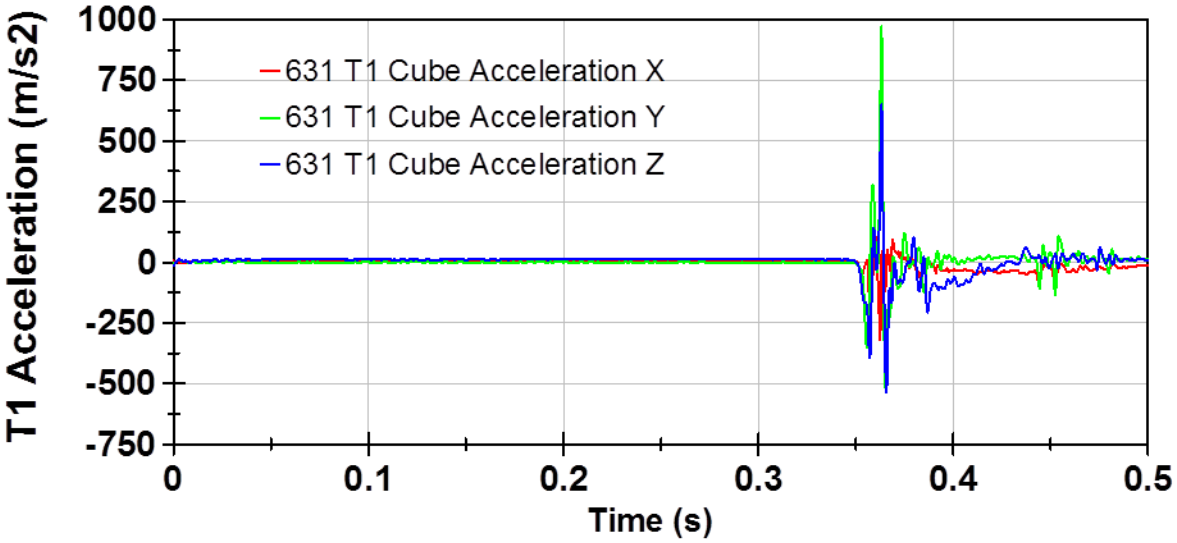

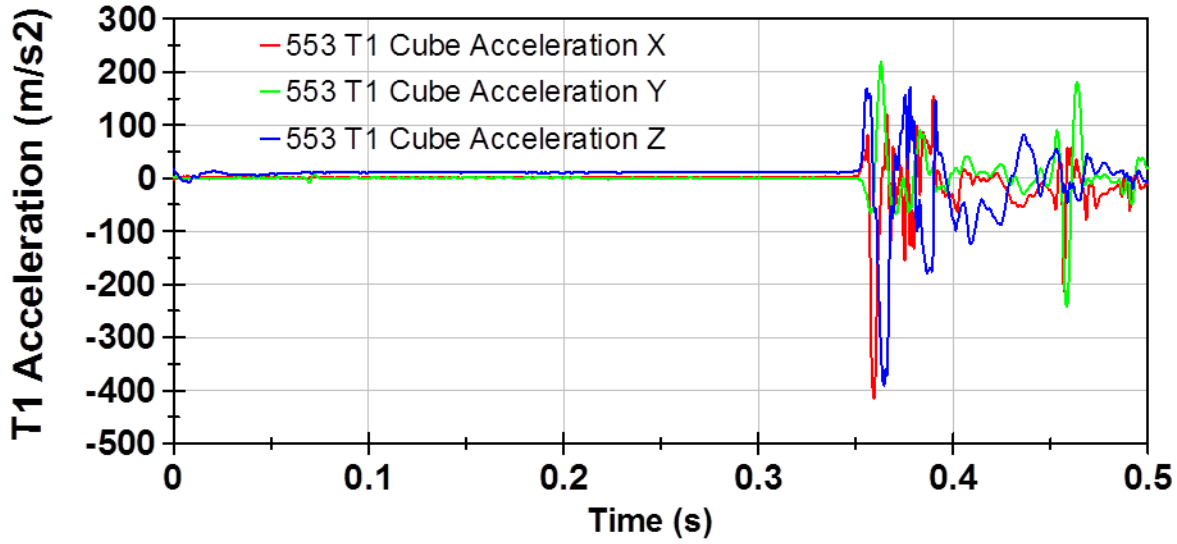

Raw T1 Acceleration Data

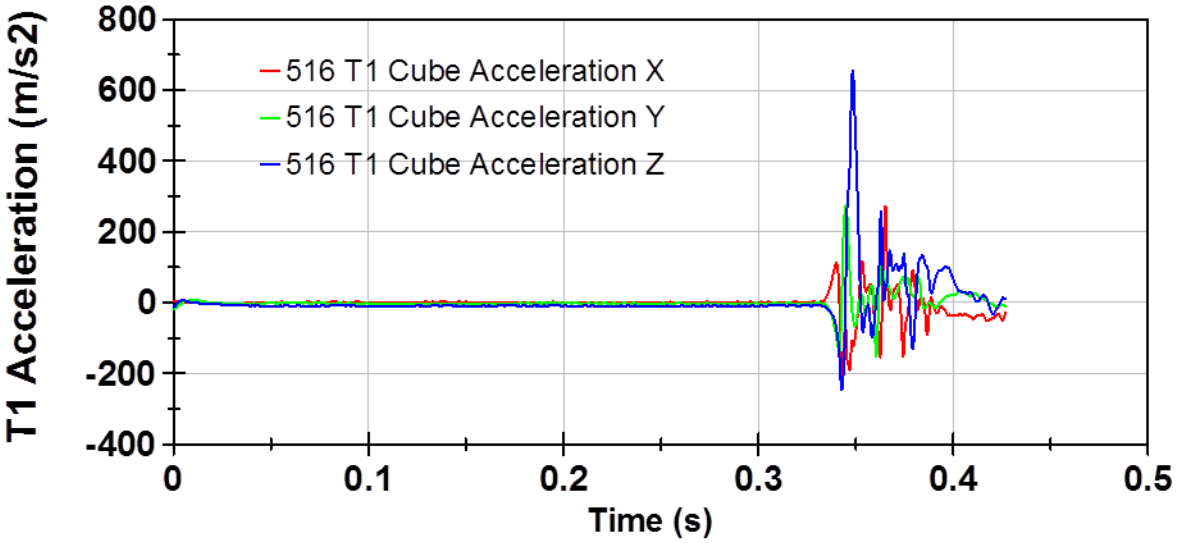

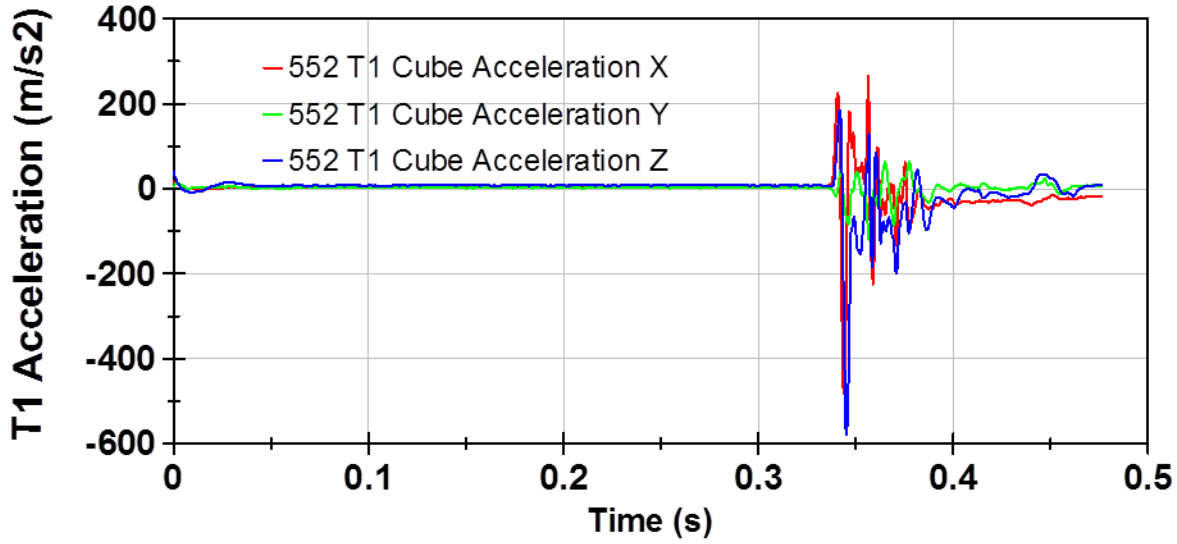

Raw T1 Angular Velocity Data

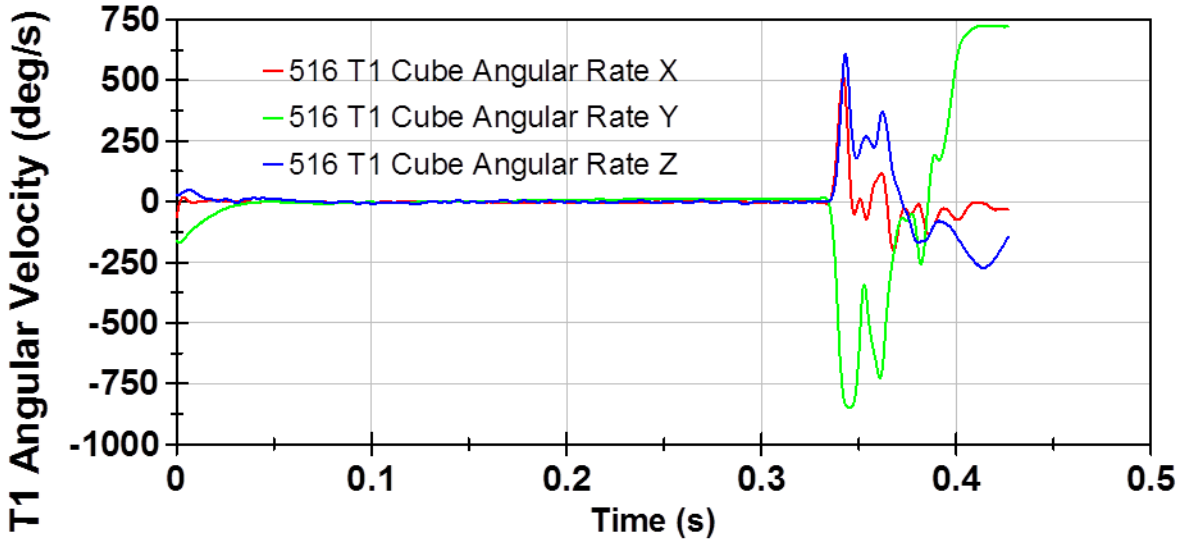

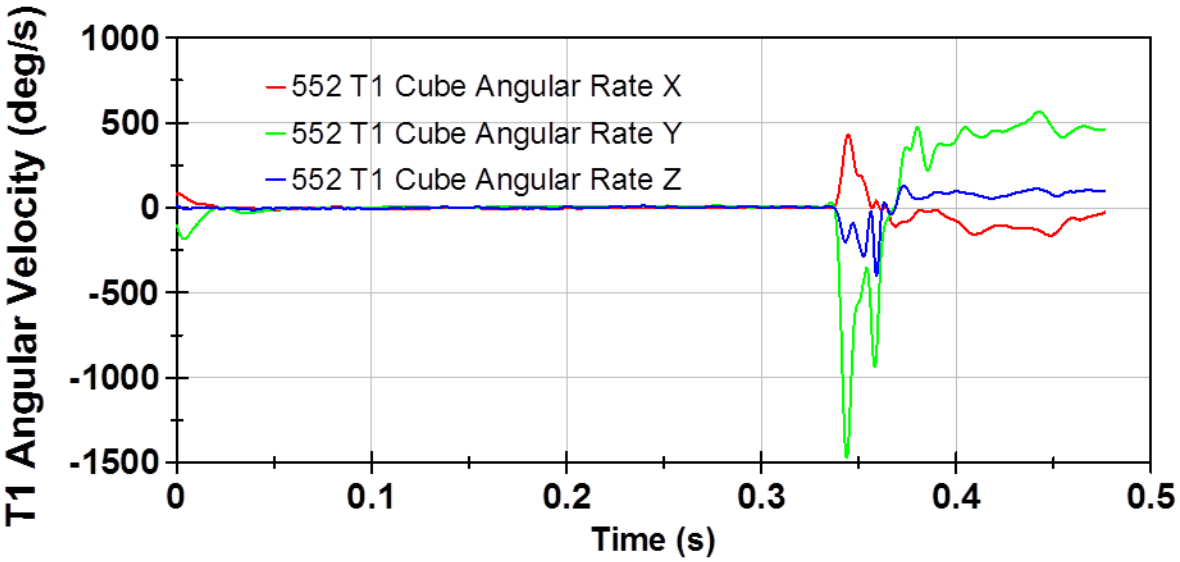

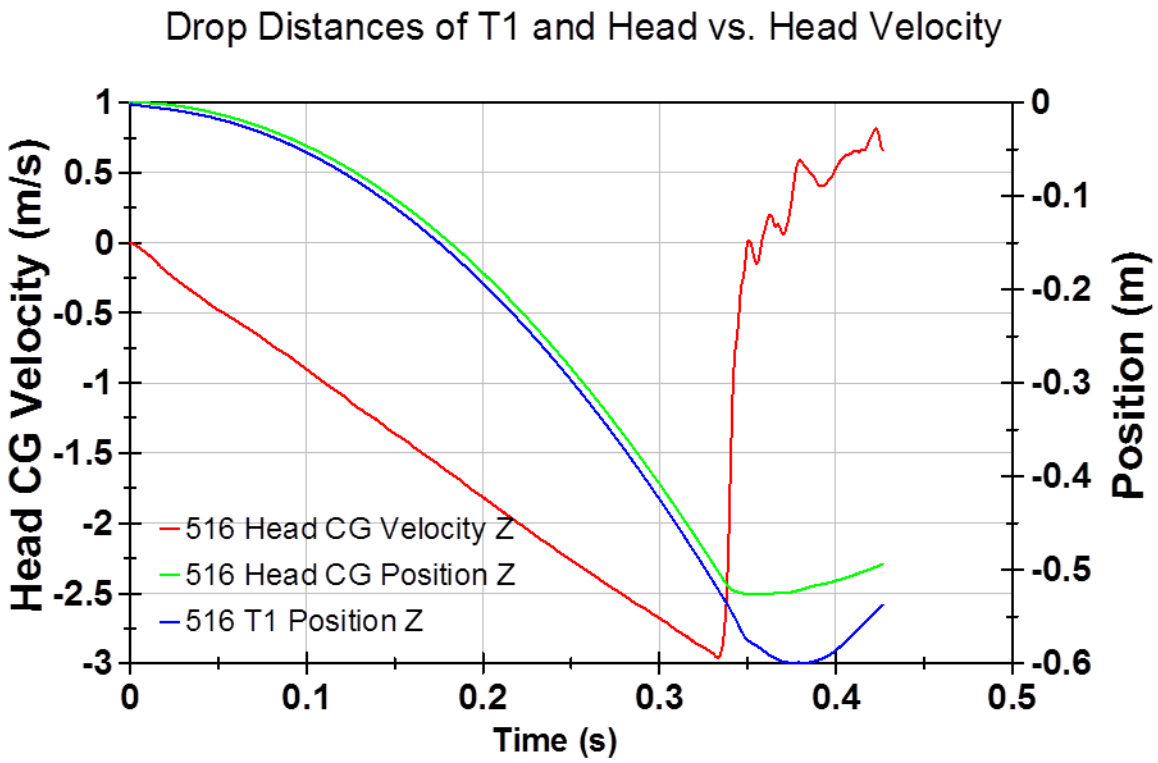
Drop Distances of T1 and Head vs. Head Velocity
Head CG Velocity (m/s)
Position (m)
Time (s)
516 Head CG Velocity Z
516 Head CG Position Z
516 T1 Position Z
1
0.5
0
-0.5
-1
-1.5
-2
-2.5
-3
0
-0.1
-0.2
-0.3
-0.4
-0.5
-0.6
0
0.1
0.2
0.3
0.4
0.5

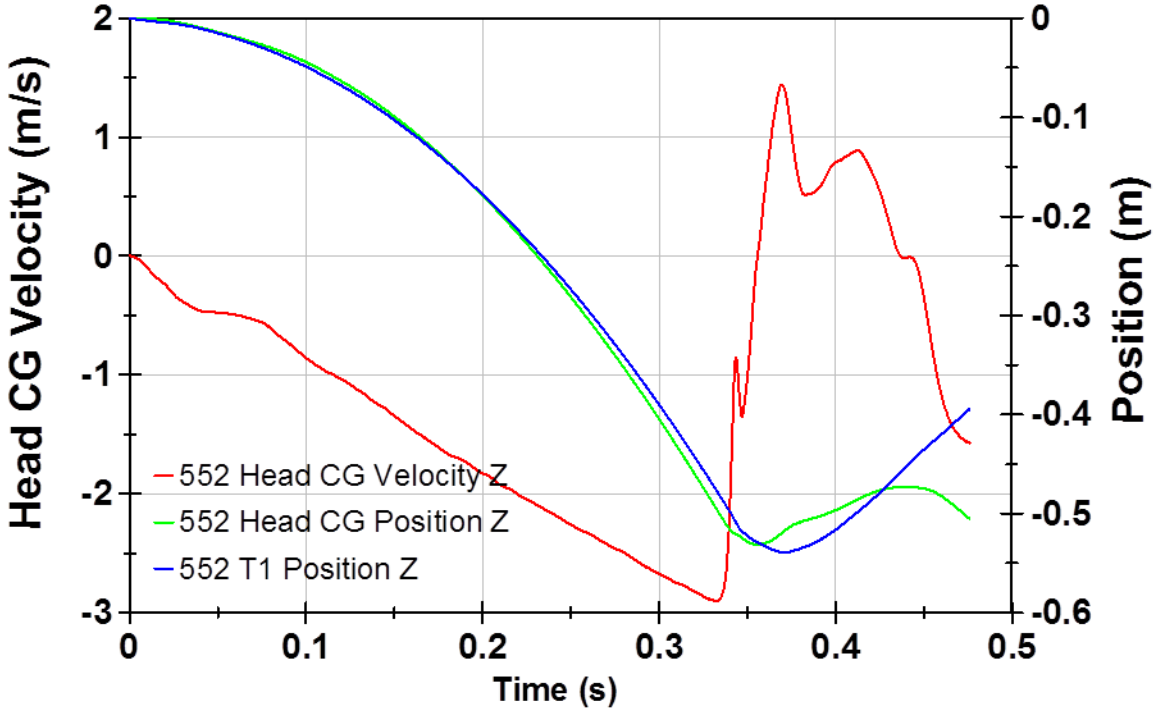
Head CG Velocity (m/s)
Position (m)
Time (s)
552 Head CG Velocity Z
552 Head CG Position Z
552 T1 Position Z
2
1
0
-1
-2
-3
0
-0.1
-0.2
-0.3
-0.4
-0.5
-0.6
0
0.1
0.2
0.3
0.4
0.5

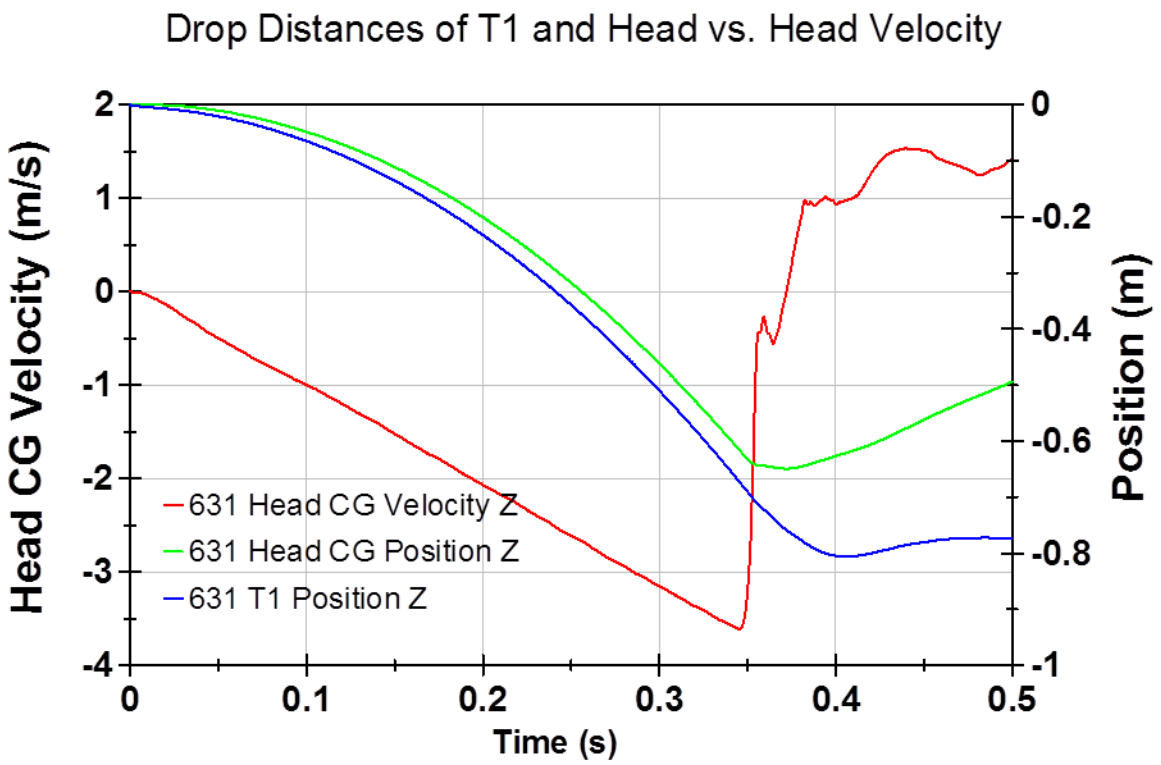
Drop Distances of T1 and Head vs. Head Velocity
Head CG Velocity (m/s)
Position (m)
Time (s)
631 Head CG Velocity Z
631 Head CG Position Z
631 T1 Position Z
2
1
0
-1
-2
-3
-4
0
-0.2
-0.4
-0.6
-0.8
-1
0
0.1
0.2
0.3
0.4
0.5

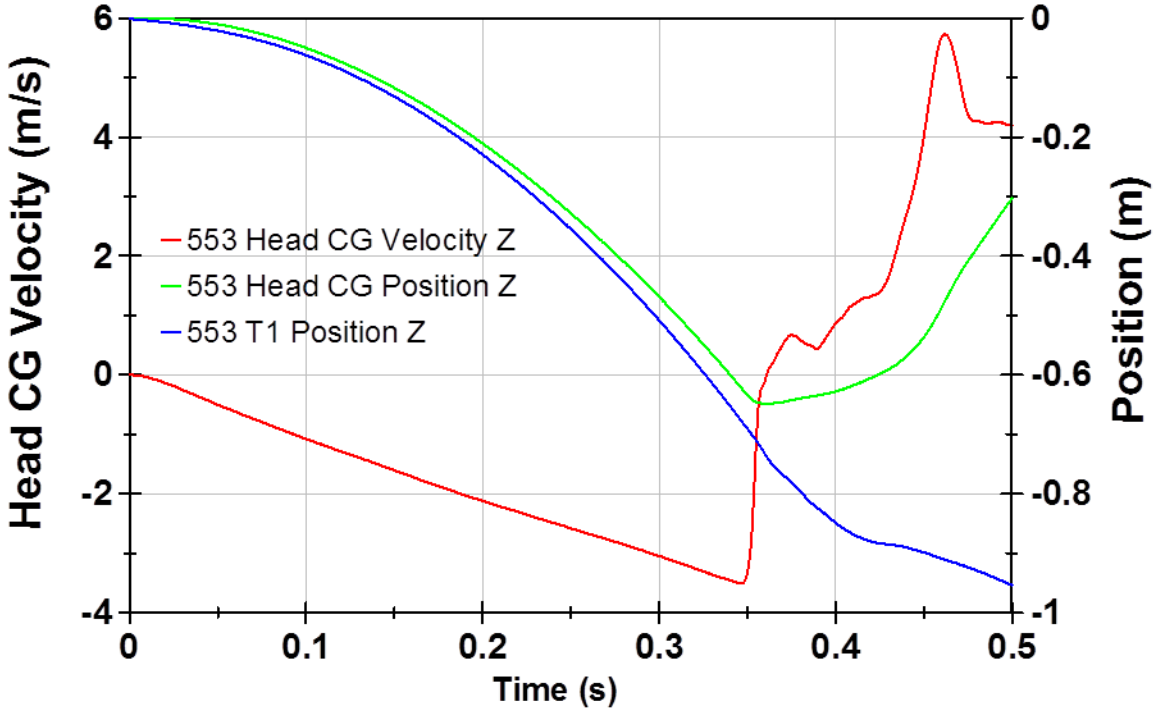
Head CG Velocity (m/s)
Position (m)
Time (s)
553 Head CG Velocity Z
553 Head CG Position Z
553 T1 Position Z
6
4
2
0
-2
-4
0
-0.2
-0.4
-0.6
-0.8
-1
0
0.1
0.2
0.3
0.4
0.5

Scaled Head Force, Upper Neck Force and Head CG Acceleration

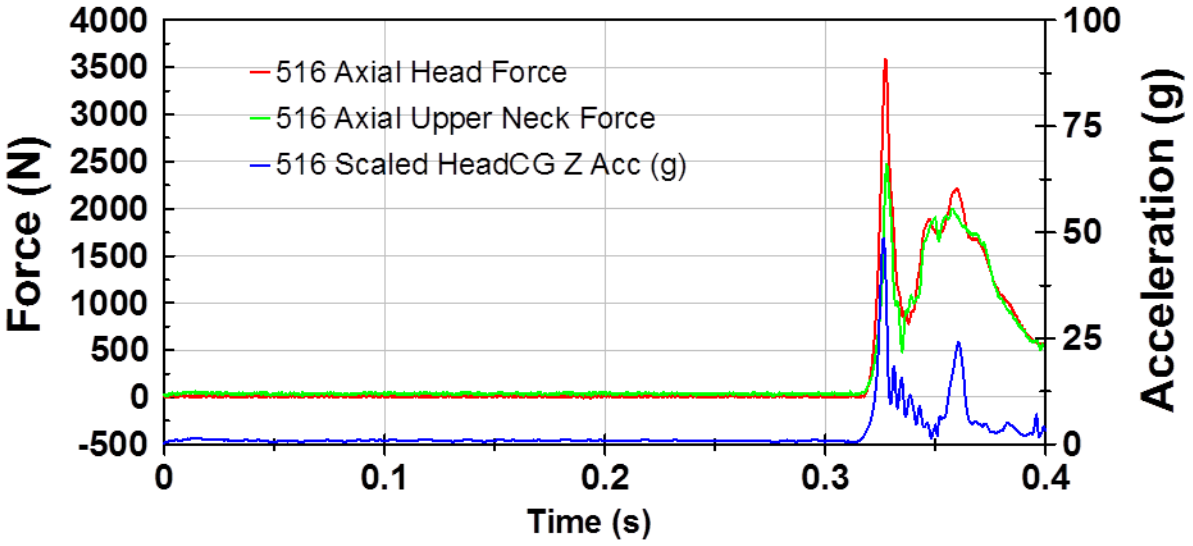

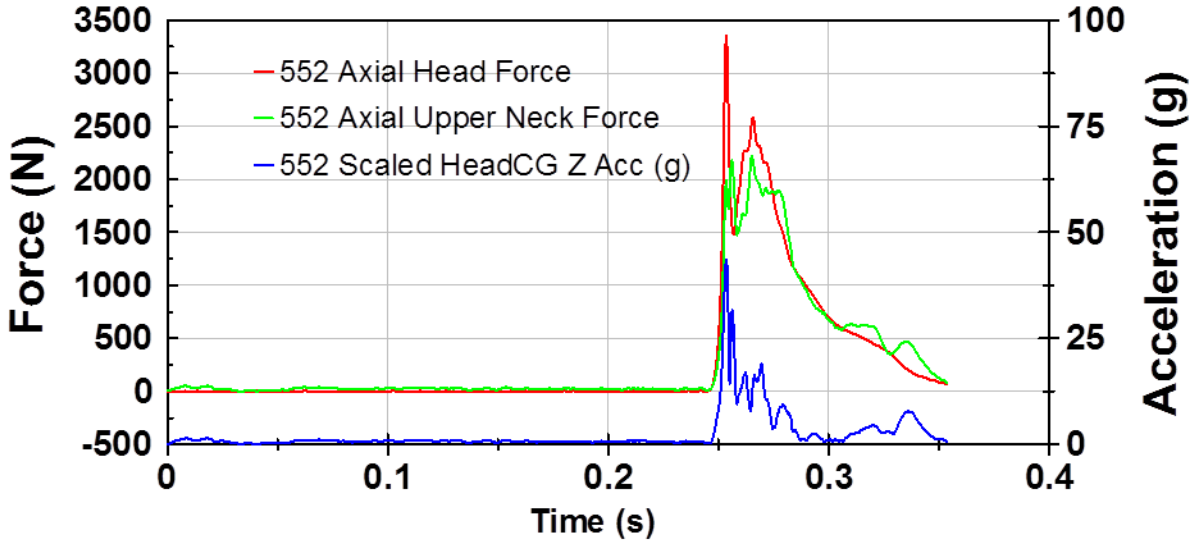

Scaled Head Force, Upper Neck Force and Head CG Acceleration